

Evaluation of concrete armour units used to repair damaged dolos breakwaters

Master of Science Thesis

June 2012

A.M. Vilaplana Domingo

Graduation Committee:

Prof. Dr. Ir. W. Uijtewaal

Prof. Dr. Ir. M.J.F. Stive

Ir. J. van de Bos

Ir. H.J. Verhagen

Ir. D. Phelp



**Council for Scientific and Industrial
Research**



Delft University of Technology
Faculty of Civil Engineering and Geosciences
Section of Hydraulic Engineering

Core-Loc is a registered trademark of the US Army Corps of Engineers, USA

Accropode is a registered trademark of Sogreah Consultants, France

Xbloc is a registered trademark of Delta Marine Consultants, The Netherlands

The use of trademarks in any publication of Delft University of Technology does not imply any endorsement or disapproval of this product by the University

Preface

To acquire the Master of Science degree at Delft University of Technology in the field of Hydraulic Engineering, an evaluation of various repair methods that can be applied on the breakwaters of Richards Bay port has been performed. This study was completely carried out in the hydraulic laboratory facilities of the Council for Scientific and Industrial Research (CSIR) at Stellenbosch, South Africa.

Firstly, I would like to acknowledge my graduation committee for their supervision and support during this research, especially to H.J. Verhagen and D. Phelp, who have given me the opportunity to travel to South Africa and participate in such a challenging project.

Secondly, I would like to thank CSIR staff of the hydraulic laboratory for their help and advice during every stage of this project. I would like to highlight to Kishan, Johan, Marius and Padhraic for their patience and explanations during the whole research and for making me feel like one member more of the team.

This South African adventure would not have been the same without my German gang, especially Julia and Stefan, who have become my family during these months. We have discovered a new place and shared this unforgettable experience.

Besides, prior to the South African adventure, I was living the experience of being in a foreign country. This experience would not be the same without my international friends from TU Delft and other friends that I have met during my stay in The Netherlands. To all of them and particularly to Anna, Raneë, Ellen, Nima and Dan thanks for having been part of this.

Moreover, I would like to thank my Spanish friends, those I have met along my life, from school to university. Gràcies per compartir amb mi molts moments de la meua vida i per mostrar-me que a pesar de la distància sempre tindrè el vostre recolzament. En especial, els meus companys de pis Ernesto, Edu i Cris per convertir l'experiència universitària a València en inoblidable, les meues amigues de la universitat, Elisa, Carme, Susanna i M^a Carmen amb qui he compartit totes les alegries i les penes de treure'ns la carrera, a mis compañeros de fatigas en el departamento de obras hidráulicas por vuestros ánimos durante la realización de mi proyecto final de carrera, i finalment, les meues xiques Anna, Zaira, Paula i Lorena per totes les inoblidables nits que hem viscut juntes i per estar sempre al meu costat.

Por último me gustaría agradecer a mis padres y hermano por sus consejos y apoyo incondicional durante todo este tiempo. Gracias por respetar en todo momento las decisiones que he tomado y por permitir que mis sueños se convirtiesen en realidad. Vosotros me habéis demostrado que el esfuerzo y el trabajo duro tienen su recompensa y gracias a vuestro ejemplo y a la confianza que habéis depositado en mí, he sido capaz de conseguir todo lo que me he propuesto hasta el momento.

Ana Vilaplana

Rotterdam, May 2012

Abstract

Richards Bay Port, located in the East Coast of South Africa, was built during the 1970s. Two rubble mound breakwaters were constructed to protect the deep-water entrance channel and create a sheltered area for the vessels. Since the completion of these breakwaters in 1976, they have withstood several major storms, including cyclones that have caused significant damage to the dolos armour layers. To restore their functionality, two major reparations were carried out in 1987 and 1996, respectively.

In addition, a severe storm that occurred in March 2007 caused relevant damages to the breakwaters of Richards Bay Port. Their damage level was established after the survey conducted in May 2007. This survey concluded that most of the breakwaters sections had an intermediate damage, except from the South Breakwater's roundhead, which was in failure and it required urgent repairs. Since then provisional measures have been adopted to avoid the spread of damage along the breakwater while new repair works are designed.

The main objective of this thesis was to determine the most suitable design for the repair works that should be applied in the roundhead of the South breakwater at Richards Bay Port through a Quasi Three-Dimensional (3D) model testing. This was achieved by reproducing the observed damage at the structure's roundhead in one of CSIR's hydraulic laboratory flumes and testing three repair alternatives. These repair alternatives consisted of covering the damaged structure with new armour units. Dolos, Core-Loc and antifer cubes were the armour units used in this research.

The wave basin used to conduct this research had a length of 32m, a width of 4m and an available height of 1m. A transitional slope of 1:15 that extends about 4.5m long was built inside the basin to connect the deep water with the shallower water close to Richards Bay Port. Thereafter, the seabed profile corresponding to the South East direction was constructed along the next 20m of the basin.

The structure was placed at a distance of 26m from the wavemaker. Graded gravel was used to construct the core, underlayer and toe protection of the roundhead, with a nominal size of 4.2g, 4.8g and 12.2g, respectively. The existing armour layer was built using dolos of 68g and gravel that represented the broken pieces. Above this damaged armour layer, the new armour units were placed with a nominal size of 82g for the dolos, 102g for the Core-Loc and 100g for the antifer cubes. The new armour units were placed trying to replicate the placement conditions at the roundhead.

A total of 8 to 9 tests were conducted per armour unit. Five wave conditions were tested with increasing significant wave heights varying from 7cm to 18cm. Two water levels were set up per wave condition (High Water and Low Water). The tested wave conditions were generated with a JONSWAP spectrum and a duration that corresponded to a 1000 waves approaching the structure.

Prior to and after each test, pictures were taken from three fixed positions perpendicular to the roundhead. These images were visually compared with the Armour Track software developed by CSIR to identify and quantify the movement of the armour units. This software is based on the superposition technique and it is useful to determine the stability of the structure. For each test, the stability number and the measured damage within the reference area were estimated. Generally the

movements of the units occurred along the water line. However for higher wave heights (return periods of 20, 50 and 100 years), the waves overtopped and the damage started to concentrate in an area located between the angles 120 and 150 degrees from the direction of the incident wave, until failing with the overload condition.

From these experiments it followed that the Core-Loc repair alternative does not perform as good as the other two options. Although all the repair options have difficulties to achieve the placement requirements at the roundhead, this phenomenon has a larger impact in the Core-Loc armour layer because it consisted of a single layer and any unit displacement resulted in failure of the structure. Therefore repairs should be undertaken more frequently, which leads to larger maintenance costs. The remaining repair options had a similar performance, even though the resistance mechanism of dolos and antifer cubes is different. The first one resists by the interlocking between the units, whereas the antifer cubes resist by their mass. Both are placed as double armour layers and thus some damage is allowed before carrying new repair works. The main difference between them is the actual feasibility to construct the units. The antifer cubes do not have any size restriction. Therefore heavier units can be manufactured without changing the stability of the unit. However, dolos have a size limitation because of its slenderness, and right now dolos heavier than 30-tonne cannot be built.

Overall it could be concluded that the repair alternative consisting of antifer cubes is the one that should be applied at this particular location due to its performance and its construction feasibility.

Table of contents

Preface	v
Abstract	vii
Table of contents	ix
List of Figures	xiii
List of Tables	xvii
List of symbols	xix
1. Introduction	23
2. Description of Richards Bay problem	25
3. Theoretical background	29
3.1. Introduction.....	29
3.2. Development of armour units	30
3.2.1. Historical overview	30
3.2.2. Classification of armour units	32
3.2.3. Dolos	34
3.2.4. Antifer Cubes.....	35
3.2.5. Accropode	36
3.2.6. Core-Loc.....	37
3.2.7. Accropode II	38
3.2.8. Xbloc	39
3.3. Hydraulic stability.....	40
3.4. Maintenance of coastal structures.....	43
3.4.1. Introduction.....	43
3.4.2. Evaluation of structure condition and response.....	44
3.4.3. Maintenance actions.....	47
4. Description of the repair works approach	49
5. Design of the repair alternatives	51
5.1. Roundhead repair method	51
5.2. Design conditions	51
5.2.1. Seabed profile	52
5.2.2. Design storm	53
5.2.3. Design water levels.....	56
5.3. Design of the repair alternatives	61
5.3.1. Covering alternative	63
5.3.2. Replacement alternative	64

6. Model set-up.....	69
6.1. Principles of physical modelling	69
6.1.1. Principle of similitude	69
6.1.2. Advantages of physical modelling	70
6.1.3. Disadvantages of physical modelling	71
6.2. Physical model design	73
6.2.1. Facilities	73
6.2.2. Model scale selection.....	76
6.2.3. Model design	76
7. Experimental process.....	83
7.1. Probe and wavemaker calibration	83
7.2. Model construction.....	84
7.3. Test program	87
7.4. Data analysis	87
8. Test results.....	89
8.1. Experiment 1: Covering alternative using 36-tonne dolosse.....	89
8.1.1. Test RB-B1	90
8.1.2. Test RB-A1	90
8.1.3. Test RB-B2.....	91
8.1.4. Test RB-A2.....	91
8.1.5. Test RB-B3.....	92
8.1.6. Test RB-A3.....	92
8.1.7. Test RB-A4.....	93
8.1.8. Test RB-B4.....	93
8.2. Experiment 2: Covering alternative using 45-tonne Core-Loc	94
8.2.1. Test RB-B1	95
8.2.2. Test RB-A1	96
8.2.3. Test RB-B2.....	96
8.2.4. Test RB-A2.....	97
8.2.5. Test RB-B3.....	97
8.2.6. Test RB-A3.....	98
8.2.7. Test RB-B4.....	98
8.2.8. Test RB-A4.....	99
8.2.9. Test RB-A5.....	99
8.3. Experiment 3: Covering alternative using 44-tonne antifer cubes.....	100
8.3.1. Test RB-B1	101
8.3.2. Test RB-A1	101

8.3.3.	Test RB-B2	102
8.3.4.	Test RB-A2	102
8.3.5.	Test RB-B3	103
8.3.6.	Test RB-A3	103
8.3.7.	Test RB-B4	104
8.3.8.	Test RB-A4	104
8.3.9.	Test RB-A5	105
9.	Evaluation of the test results	107
9.1.	Evaluation method	107
9.2.	Evaluation of the experiments	107
9.3.	Construction feasibility	111
10.	Conclusions and recommendations	113
10.1.	Conclusions	113
10.2.	Recommendations	115
	References	117

Appendices

Appendix A.	Extreme analysis	121
A.1.	Design storm	121
A.2.	Extreme wind	123
Appendix B.	Material properties	124
Appendix C.	Pictures of the experiments	127
	Experiment 1: Covering alternative with 36-tonne dolosse	127
	Experiment 2: Covering alternative with 45-tonne Core-Loc	135
	Experiment 3: Covering alternative with 44-tonne Antifer cubes	144

List of Figures

Figure 1.1 – Richards Bay location	23
Figure 1.2 – South and North breakwaters and North of Richards Bay Port	23
Figure 3.1 – Conventional cross-section of a rubble mound breakwater	30
Figure 3.2 – Classification of concrete armour units [CHL, 2006]	32
Figure 3.3 – Dolos. Plan and side views	34
Figure 3.4 – Antifer cubes. Oblique, plan views and cross-section	35
Figure 3.5 – Accropode. Oblique view [CLI, 2011]	36
Figure 3.6 – Core-Loc. Top, front and side views [TURK ET AL., 1997]	37
Figure 3.7 – Accropode II. Oblique view [DENECHERE, M., 2011]	38
Figure 3.8 – Xbloc. Plan and side views	39
Figure 3.9 – Wave-induced forces on a stone [VERHAGEN, H.J. ET AL., 2009]	40
Figure 3.10 – Eroded area profile [CHL, 2006]	46
Figure 5.1 – Bathymetry of South Breakwater at Richards Bay	52
Figure 5.2 – Seabed profile from the breakwater to the buoy location	53
Figure 5.3 – Design storm. Wave heights	53
Figure 5.4 – Design storm. Wave periods	54
Figure 5.5 – Wave propagation in the surroundings of South Breakwater Head	55
Figure 5.6 – Estimated wave heights in various locations near the roundhead	56
Figure 5.7 – Water level variation at Durban. Semidiurnal tide	57
Figure 5.8 – Water level components variation at Durban	58
Figure 5.9 – Dolos cover layer alternative	63
Figure 5.10 – Antifer cubes cover layer alternative	63
Figure 5.11 – Core-Loc cover layer alternative	64
Figure 5.12 – Double-layer of 36-tonne dolosse for the replacing alternative	65
Figure 5.13 – Double-layer of 44-tonne antifer cubes for the replacing alternative	65
Figure 5.14 – Single-layer of 45-tonne Core-Loc for the replacing alternative	66
Figure 5.15 – Single-layer of 45-tonne Xbloc for the replacing alternative	67
Figure 6.1 – Wave basin	73
Figure 6.2 – Wavemaker	74
Figure 6.3 – Wave probes	75

Figure 6.4 – Camera equipment.....	75
Figure 6.5 – Seabed profile in the basin.....	76
Figure 6.6 – Model cross-section for covering option using dolos	77
Figure 6.7 – Model cross-section for covering option using Antifer cubes	77
Figure 6.8 – Model cross-section for replacement option using Core-Loc	77
Figure 7.1 – Construction sequence of the roundhead model	85
Figure 7.2 – Roundhead model of the covering alternative with 36-tonne dolosse	85
Figure 7.3 – Roundhead model of the covering alternative with 45-tonne Core-Loc.....	86
Figure 7.4 – Roundhead model of the covering alternative with 44-tonne Antifer cubes.....	86
Figure 8.1 – Images of the roundhead with dolos during test RB-B1	90
Figure 8.2 – Images of the roundhead with dolos during test RB-A1	91
Figure 8.3 – Images of the roundhead with dolos during test RB-B2.....	91
Figure 8.4 – Images of the roundhead with dolos during test RB-A2.....	92
Figure 8.5 – Images of the roundhead with dolos during test RB-B3.....	92
Figure 8.6 – Images of the roundhead with dolos during test RB-A3.....	93
Figure 8.7 – Images of the roundhead with dolos during test RB-A4.....	93
Figure 8.8 – Images of the roundhead with dolos during test RB-B4	94
Figure 8.9 – Images of the roundhead with Core-loc during test RB-B1	95
Figure 8.10 – Images of the roundhead with Core-loc during test RB-A1	96
Figure 8.11 – Images of the roundhead with Core-loc during test RB-B2	96
Figure 8.12 – Images of the roundhead with Core-loc during test RB-A2	97
Figure 8.13 – Images of the roundhead with Core-loc during test RB-B3	97
Figure 8.14 – Images of the roundhead with Core-loc during test RB-A3	98
Figure 8.15 – Images of the roundhead with Core-loc during test RB-B4	98
Figure 8.16 – Images of the roundhead with Core-loc during test RB-A4	99
Figure 8.17 – Images of the roundhead with Core-loc during test RB-A5	99
Figure 8.18 – Images of the roundhead with antifer cubes during test RB-B1	101
Figure 8.19 – Images of the roundhead with antifer cubes during test RB-A1	101
Figure 8.20 – Images of the roundhead with antifer cubes during test RB-B2	102
Figure 8.21 – Images of the roundhead with antifer cubes during test RB-A2	102
Figure 8.22 – Images of the roundhead with antifer cubes during test RB-B3	103
Figure 8.23 – Images of the roundhead with antifer cubes during test RB-A3	103

Figure 8.24 – Images of the roundhead with antifer cubes during test RB-B4	104
Figure 8.25 – Images of the roundhead with antifer cubes during test RB-A4	104
Figure 8.26 – Images of the roundhead with antifer cubes during test RB-A5	105
Figure 9.1 – Relative displacement	109
Figure 9.2 – Reflection coefficient	110
Figure 9.3 – Interannual variation of wave height at Richards Bay	111
Figure A.1 – Long-term analysis combined with Peak-over-Threshold of 3.0m	121
Figure A.2 – Long-term analysis combined with Peak-over-Threshold of 3.5m	121
Figure A.3 – Peak-over-Threshold of 3.0m. Gumbel and inverse Weibull extreme analysis	122
Figure A.4 – Peak-over-Threshold of 3.5m. Gumbel and inverse Weibull extreme analysis	122
Figure A.5 – Design storm. Wave periods	123
Figure B.1 – Toe protection grading curve	125
Figure B.2 – Underlayer grading curve.....	125
Figure B.3 – Core grading curve	126

List of Tables

Table 2.1 – Damage of North Breakwater after May 2011 survey	25
Table 2.2 – Damage of South Breakwater after May 2011 survey.....	26
Table 3.1 - Historical development of concrete armour units	31
Table 3.2 – Classification of armour units by shape, placement method and stability factor	33
Table 3.3 – Comparison of various concrete units [VAN DER MEER, 1999]	33
Table 3.4 – Geometrical characteristics of Dolosse.....	34
Table 3.5 – Geometrical characteristics of Antifer Cubes	35
Table 3.6 – Geometrical characteristics of Accropode	36
Table 3.7 – Geometrical characteristics of Core-Loc.....	37
Table 3.8 – Geometrical characteristics of Accropode II [CLI, 2012]	38
Table 3.9 – Geometrical characteristics of Xbloc	39
Table 3.10 – Hudson’s Stability coefficient values for various concrete armours	41
Table 3.11 – Damage level by N_{od} for antifer cubes	42
Table 3.12 – Evaluation of monitoring data in armoured structures [CIRIA, 2007].....	44
Table 3.13 – Damage level by D for double-layer armour [CHL, 2006].....	46
Table 3.14 – Damage level by S for double-layer armour [CHL, 2006].....	46
Table 5.1 – Initial design conditions	51
Table 5.2 – Design storms	54
Table 5.3 – Design storm at breakwater’s location	55
Table 5.4 – Design water levels relative to Chart Datum	57
Table 5.5 – Design water levels relative to Chart Datum with Sea Level Rise	57
Table 5.6 – Tidal chart at Richards Bay	58
Table 5.7 – Wave set-up estimation [GODA, 2000]	59
Table 5.8 – Pressure set-up estimation.....	59
Table 5.9 – Wind set-up estimation.....	60
Table 5.10 – Storm surge.....	60
Table 5.11 – Sea Level Rise	61
Table 5.12 – Armour unit sizes.....	61
Table 5.13 – Toe design for the covering alternative.....	62
Table 5.14 – Layer thickness, packing density and number of units per area.....	62

Table 5.15 – Required number of antifer cubes and Core-Loc for the covering alternative.....	64
Table 5.16 – Stone size for the underlayer for the double-layer armouring	65
Table 5.17 – Required number of armour units for the double-layer replacement alternative	65
Table 5.18 – Stone size for the underlayer for the single-layer armouring.....	66
Table 5.19 – Required number of armour units for the single-layer replacement alternative	67
Table 6.1 – Armour unit specifications for the model.....	78
Table 6.2 – Graded rock specifications for the underlayer.....	79
Table 6.3 – Graded rock specifications for the toe protection.....	79
Table 6.4 – Graded rock specifications for the core	79
Table 6.5 – Design storms at the model control point.....	80
Table 6.6 – Design water levels for the model in front of the structure	81
Table 7.1 – Wave calibration.....	83
Table 7.2 – Wave characteristics	87
Table 8.1 – Measurements with covering alternative using 36-tonne dolosse	89
Table 8.2 – Damage of the covering alternative using 36-tonne dolosse.....	90
Table 8.3 – Measurements with covering alternative using 45-tonne Core-Loc.....	94
Table 8.4 – Damage of the covering alternative using 45-tonne Core-Loc	95
Table 8.5 – Measurements with covering alternative using 44-tonne antifer cube.....	100
Table 8.6 – Damage of the covering alternative using 45-tonne Core-Loc	100
Table 9.1 – Comparison of stability parameters	108
Table 9.2 – Required number of units and total volume of concrete.....	112
Table A.1 – Gumbel projection.....	122
Table A.2 – Inverse Weibull projection	122
Table A.3 – Extreme wind speeds.....	123
Table B.1 – Graded rock specifications for the toe protection	124
Table B.2 – Graded rock specifications for the underlayer	124
Table B.3 – Graded rock specifications for the core	124
Table B.4 – Percentage of required rock size for the toe protection	125
Table B.5 – Percentage of required rock size for the underlayer	126
Table B.6 – Percentage of required rock size for the core.....	126

List of symbols

a	Antifer Cube bottom width	[m]
A	1. Fluke end width of dolosse	[m]
	2. Core-Loc geometric characteristic	[m]
	3. Surface of armour layer cross-sectional area	[m ²]
A _e	Eroded area	[m ²]
b	Antifer Cube top width	[m]
B	1. Dolosse shank thickness	[m]
	2. Antifer Cube taper angle	[°]
	3. Core-Loc geometric characteristic	[m]
c	Antifer Cube groove depth	[m]
C	1. Length, height and breadth of dolosse	[m]
	2. Core-Loc height	[m]
	3. Pressure constant in pressure set-up equation	[m/mbar]
C ₁	Dolos geometric constant related to the waist ratio	[-]
C _D	air/water drag coefficient	[-]
d	Size of stones	[m]
D	1. Dolosse fillet	[m]
	2. Core-Loc geometric characteristic	[m]
	3. Xbloc height and width	[m]
	4. Relative damage	[%]
D _{n50}	Median stone diameter ($D_{n50}=(W_{50}/\rho_s)^{1/3}$)	[m]
E	Core-Loc geometric characteristic	[m]
E _{JONSWAP}	JONSWAP spectral energy	[m ² /Hz, m ² s]
f	1. Type of coast factor in wind set-up equation	[-]
	2. Frequency in JONSWAP spectrum	[Hz, s ⁻¹]
f _{cc}	Climate Change factor for the increase of extreme wave heights	[-]
f _{peak}	Frequency scale parameter in JONSWAP spectrum	[-]
F	1. Core-Loc geometric characteristic	[m]
	2. Fetch length	[m]
F _r	Froude Number	[-]
g	Acceleration of gravity	[m/s ²]
G	Core-Loc geometric characteristic	[m]
K _D	Damage level in Hudson formula	[-]
K _r	Refraction coefficient	[-]
K _Δ	Layer coefficient	[-]
h	1. Antifer Cube height	[m]
	2. Water depth	[m]
h _t	Water depth above the toe protection	[m]
H	1. Accropode and Accropode II height	[m]
	2. Wave height	[m]
H ₀ '	Significant wave height in near shore	[m]
H _{m0}	Significant wave height from spectrum	[m]

List of symbols

H_{m0}^{CC}	Significant wave height modified by Climate Change	[m]
$H_{pressure}$	Increase of water level due to pressure set-up	[m]
H_s	Significant wave height	[m]
H_s^{buoy}	Significant wave height at buoy location	[m]
H_s^{dw+CC}	Significant wave height in deep water modified by Climate Change	[m]
H_{wave}	Increase of water level due to wave set-up	[m]
H_{wind}	Increase of water level due to wind set-up	[m]
J	Core-Loc geometric characteristic	[m]
l_a	Characteristic length of the armour unit	[m]
L	1. Characteristic length 2. Wave length	[m] [m]
m	Model component	[-]
n	number of layers in which the units are placed	[-]
N	Number of waves in a storm for Van der Meer formula	[-]
N_{od}	Number of displaced units (damage criterion)	[-]
N_{omov}	Number of rocking units	[-]
N_r	Number of units	[-]
p	Prototype component	[-]
P	Notional permeability coefficient in Van der Meer formula	[-]
P_{ave}	Average sea level pressure	[mbar, hPa]
P_{obs}	Observed / forecast sea level pressure	[mbar, hPa]
r	1. Antifer Cube groove radius 2. Xbloc fillet 3. Layer thickness	[m] [m] [m]
Re	Reynolds Number	[-]
s	Antifer Cube corner width	[m]
s_{om}	Wave steepness ($s_{om} = (2 \cdot \pi \cdot H) / (g \cdot T_m^2)$)	[-]
S	Dimensionless damage parameter	[-]
S_d	Design criteria for damage level in Van der Meer formula	[-]
t	Time	[s]
T	1. Accropode and Accropode II thickness 2. Wave period 3. Return period	[m] [s] [year]
T_p	Peak wave period	[s]
u_w	Wind speed	[m/s]
u_w^{CC}	Wind speed modified by Climate Change	[m/s]
U	Flow velocity	[m/s]
u_c	Stone's critical velocity in a turbulent flow	[m/s]
V	Volume of armour units	[m ³]
W	Mass weight	[kg]
W_a	Armour unit weight	[kg]
W_c	Core material unit weight	[kg]
W_m	Model mass weight	[kg]

W_p	Prototype mass weight	[kg]
W_s	Wave set-up factor	[-]
W_u	Underlayer unit weight	[kg]
W_{50}	Median armour stone weight	[kg]
α	1. Angle of breakwater's slope 2. Energy scale parameter	[rad] or [°] [-]
γ	Shape parameter of JONSWAP spectrum	[-]
Δ	Relative mass density ($\Delta = \rho_s / \rho_w - 1$)	[-]
Δ_m	Model relative mass density ($\Delta = \rho_s / \rho_w - 1$) _m	[-]
Δ_p	Prototype relative mass density ($\Delta = \rho_s / \rho_w - 1$) _p	[-]
λ	Scale parameter	[-]
μ	Dynamic coefficient of viscosity	[N·s/ m ²]
ν	Kinematic coefficient of viscosity	[m ² /s]
ξ	Surf similarity parameter, Iribarren number ($\xi = \tan \alpha / \sqrt{H/L_0}$)	[-]
ξ_m	Surf similarity parameter, Iribarren number ($\xi_m = \tan \alpha / \sqrt{H/L_0}$)	[-]
ρ	Mass density	[kg/m ³]
ρ_a	Density of armour units	[kg/m ³]
ρ_{air}	Density of air	[kg/m ³]
ρ_m	Model mass density	[kg/m ³]
ρ_p	Prototype mass density	[kg/m ³]
ρ_s	Density of rock material	[kg/m ³]
ρ_w	Density of water	[kg/m ³]
σ	Shape parameter of JONSWAP spectrum	[-]
Φ	1. Packing density of placement 2. Direction of approximation to the shore	[-] [rad] or [°]
φ	Repose angle of the material	[rad] or [°]

1. Introduction

The port of Richards Bay, located on the East Coast of South Africa (see Figure 1.1), was constructed during the 1970s to accommodate a coal terminal, which after several expansions has become the largest bulk terminal of South Africa in terms of handled cargo volumes.



Figure 1.1 – Richards Bay location

Two rubble mound breakwaters were constructed to protect the deep-water entrance and to create a sheltered area where the vessels can perform their activities safely. These structures were completed in 1976. Since then they have withstood several major storms, including cyclones with significant wave heights close to the design storm wave height, which caused significant damage to the dolos armour layers. To restore the original functional conditions, two major reparation works have been thus carried out (in 1987 and 1996 respectively).

Nowadays, the armouring of the North Breakwater consists of a double layer of 5-tonnes dolosse on trunk and root. The head is constructed with a double layer of 20-tonnes dolosse with a double row of 30-tonnes dolosse deposited in front of its base. The armouring of the South Breakwater comprises a double layer of 5-tonnes dolosse on root, 20-tonnes dolosse on trunk and 30-tonnes dolosse on head. Figure 1.2 shows the breakwaters of Richards Bay port.



Figure 1.2 – South and North breakwaters and North of Richards Bay Port

Since the completion of these breakwaters, their performance has regularly been monitored by visual inspection, aerial photography, profiling techniques and, lately, with more accurate close-up photographs taken by mobile cranes or helicopter. From these monitoring surveys, the cumulative damage of the structure can be determined by means of checking the broken and lost dolosse and localizing the most damaged sections. This information is then used to define the repair works that will restore the structure functionality.

A severe storm that occurred in March 2007 caused relevant damages to the breakwaters of Richards Bay Port. Their damage level was established after the survey performed in May 2007, which concluded that the South Breakwater's roundhead was in failure state and urgent repairs were required. Other sections of the breakwaters were fairly damaged but with no need of urgent repairs. Since then, provisional measures have been adopted to avoid the spread of the damage along the breakwaters while new repair works are designed.

The main objective of this thesis is to determine the most suitable design for the repair works that should be applied in the roundhead of the South breakwater at Richards Bay Port through a Quasi Three-Dimensional (3D) model testing. To achieve this, the observed damage at the breakwater's roundhead has been firstly reproduced in one of CSIR's hydraulic laboratory flumes to understand the system's behaviour after the major storm suffered in 2007. Secondly, several repair alternatives have been tested in the same flume. At the same time, a comparison of the hydraulic stability of various armour units is also performed, which helps in the definition of the optimal repair method.

This thesis outline is as follows. Chapter 2 describes the damage problem of the breakwaters at Richards Bay Port. In chapter 3, an intensive review of the available literature is provided, to gain insight into the current knowledge on breakwaters; special attention is devoted to their structural design, the historical development of armour units, and the repair methods that are applied on damaged breakwaters. A description of the general approach to define the repair works of any rubble mound breakwater is provided in chapter 4. Chapter 5 focuses on the design of several repair alternatives for the head of the South Breakwater at Richards Bay Port. The required theory to set up a hydraulic physical model is discussed in chapter 6; whereas chapter 7 describes the testing process, which comprises the model construction, the testing programme and the procedure for the analysis and evaluation of the experimental results. The results of the experiments are presented in chapter 8 and chapter 9 deals with the evaluation of those results of. Finally, chapter 10 summarizes the conclusions and recommendations derived from the testing.

2. Description of Richards Bay problem

The breakwaters of Richards Bay port have been annually monitored since 1987. Their last survey was held on May 2011 and consisted of taking aerial photographs from a helicopter at pre-marked sections along the length of the breakwater. These aerial pictures are used to record the condition of the above-water part of the breakwaters and to assess the damage in the dolos armour layers. This provides an early warning system of the development of any dangerous change in the condition of the armouring, so that repair measures can be undertaken.

To understand the performance of the breakwaters, the damage estimated through the surveys must be linked to the wave events recorded during the monitoring period. Here only storms whose wave height is larger than 3m are considered.

These breakwaters have withstood various storms since their last repair in 1996. However, in March 2007 a severe storm with a wave height of 8.5m hit them. The wave height of this event was higher than the wave height used in their design. As a result, the breakwaters were significantly damaged, especially the South Breakwater roundhead [CSIR, 2007]. Since then provisional measures, such as placement of extra dolosse, have been applied to prevent the spread of damage while new repair works are designed.

During the last monitoring period (2007-2011), the sea conditions were relatively normal. Therefore, some light damage was added to the severe damage that the breakwaters suffered after the major storm event of March 2007. Table 2.1 and Table 2.2 show the damage assessment after the survey of May 2011 [CSIR, 2011].

Table 2.1 – Damage of North Breakwater after May 2011 survey

Figure number	Station number	Displaced dolosse			Damaged dolosse			New damage ND	Previous damage PD	Cumulative damage CD	Total dolosse N	N _{od}	Cumulative percentage damage	Adjusted damage
		<0.5m (A)	0.5-1.5m (B)	>1.5m (C)	Total D (C)	Broken (E)	Lost (F)							
1	C1P1							0	4	4	125		3.2	
2	C1P2							0	14	14	237		5.9	
3	C1P3		2	1	1			1	10	11	195		5.6	
4	C1P4							0	7	7	240		2.9	
5	C1P5							0	2	2	224		0.9	
6	C2P1	1 + 1P		1	1	1	1	3	23	26	260		10.0	
7	C2P2							0	5	5	281		1.8	
8	C3P1			1	1			1	15	16	391	0.8	4.1	1.2
9	C4P1							0	7	7	290	0.4	1.8	0.5
10	C5P1							0	2	2	378	0.1	0.5	0.2
11	C6P1							0	28	28	379	1.4	7.4	2.2
12	C7P1							0	13	13	370	0.7	3.5	1.0
13	C8P1						1	1	3	4	367	0.2	1.1	0.3

Description of Richards Bay problem

Figure number	Station number	Displaced dolosse			Damaged dolosse			New damage ND	Previous damage PD	Cumulative damage CD	Total dolosse N	N _{od}	Cumulative percentage damage	Adjusted damage
		<0.5m (A)	0.5 - 1.5m (B)	>1.5m (C)	Total D (C)	Broken (E)	Lost (F)							
14	C9P1	1 + 1P		1	1		1 + 2P	2	22	24	384	1.2	6.3	1.8
15	C10P1	3 + 1P					1P	0	15	15	390	0.8	3.8	1.2
16	C11P1			1	1		1	2	16	18	380	0.9	4.7	1.4
17	C12P1							0	5	5	370	0.3	1.4	0.4
18	C13P1							0	6	6	360	0.3	1.7	0.5
19	C14P1							0	4	4	350	0.2	1.1	0.3
20	C15P1							0	2	2	350	0.1	0.6	0.2
21	C16P1							0	3	3	350	0.2	0.9	0.2
TOTAL		5	2	5	5	2	4	10	206	216	6771	0.5	3.2	0.8

Intermediate damage

Failure

According to N_{od} or Percentage

Table 2.2 – Damage of South Breakwater after May 2011 survey

Figure number	Station number	Displaced dolosse			Damaged dolosse			New damage ND	Previous damage PD	Cumulative damage CD	Total dolosse N	N _{od}	Cumulative percentage damage	Adjusted damage
		<0.5m (A)	0.5 - 1.5m (B)	>1.5m (C)	Total D (C)	Broken (E)	Lost (F)							
22	C1P1		1			1		1	9	10	210	0.9	4.8	1.4
23	C1P2	1P					1P	0	11	11	320	1.0	3.4	1.5
24	C1P3			1P			1P	0	14	14	210	1.3	6.7	2.0
25	C1P4	1+2P					2+3P	2	15	17	320	1.6	5.3	2.4
26	C1P5	1P	1P				2+1P	2	9	11	210	1.1	5.2	1.5
27	C2P1							0	10	10	180	0.9	5.6	1.4
28	C2P2		1					0	4	4	280	0.4	1.4	0.6
29	C3P1							0	4	4	160	0.4	2.5	0.6
30	C4P1					1		1	6	7	180	0.7	3.9	1.0
31	C5P1							0	6	6	323	0.5	1.9	0.7
32	C6P1							0	4	4	340	0.3	1.2	0.5
33	C7P1							0	5	5	323	0.4	1.5	0.6
34	C8P1							0	9	9	324	0.7	2.8	1.1
35	C9P1							0	14	14	337	1.1	4.2	1.7
36	C10P1							0	2	2	343	0.2	0.6	0.2
37	C11P1							0	8	8	338	0.7	2.4	1.0
38	C12P1							0	4	4	348	0.3	1.1	0.5
39	C13P1							0	5	5	327	0.4	1.5	0.6
40	C14P1	1				1		1	2	3	323	0.2	0.9	0.4
41	C15P1	1		2	2	2	2	6	10	16	315	1.3	5.1	2.0
42	C16P1	1	1					0	5	5	286	0.4	1.7	0.6
43	C17P1					2		2	6	8	247	0.7	3.2	1.0
TOTAL		4	3	2	2	7	6	15	162	177	6244	0.7	2.8	1.1

Intermediate damage

Failure

According to N_{od} or Percentage

The South Breakwater roundhead is represented by the stations between C1P1 and C1P5, which according to the results of the damage assessment is in bad state, see Table 2.2, even though some provisional measures have been undertaken.

3. Theoretical background

3.1. Introduction

Several types of structures can be found along the coastline, to either protect the coastal area against wave action or to create sheltered areas where vessels can navigate, moor and berth safely. According to the main function of these coastal structures, they can be classified in (1) coastal defence works and (2) harbour defence works [ZWAMBORN, 1976]. However, such structures must not only fulfil the function for which they were built, but also withstand, in most cases, very harsh environmental conditions. Revetments, dikes, and seawalls are few examples of coastal defence works, while breakwaters and caissons are used as defence works of harbours.

This thesis will focus on the repair methods that ensure the hydraulic stability of damaged breakwaters. The main function of such structures is the dissipation of wave energy on the seaside slope. Breakwaters are classified according to their construction material in:

- Mound type: Large embankments of loose elements such as quarry stone, concrete blocks, or gravel.
- Monolithic type: The structure is designed in such a way that behaves as a solid block.
- Composite type: The structure combines monolithic elements with a berm.
- Special type: Other elements, not considered above, are used to dissipate the wave energy.

This research will just consider the rubble mound type of structures since the breakwaters of Richards Bay port are rubble mound type, like most of the breakwaters built all over the world. In general, a rubble mound breakwater is constructed with successive layers of quarry rock and/or concrete elements, whose size is selected in such a way that they are capable of retaining the layer below it, i.e. each one of the layers has to fulfil the filter function. The reasons behind the application of these designs instead of homogeneous ones are: (1) difficulty to obtain large amounts of big blocks to build the whole structure, (2) high construction costs, resulting from the placement of heavy blocks and (3) functionality problems due to the high permeability of large blocks, which allow wave and sediment penetration.

Figure 3.1 shows a typical cross-section of a rubble mound breakwater. The armour layer is usually constructed with heavy stones, however depending on the availability of these rocks it may be required to use concrete blocks instead.

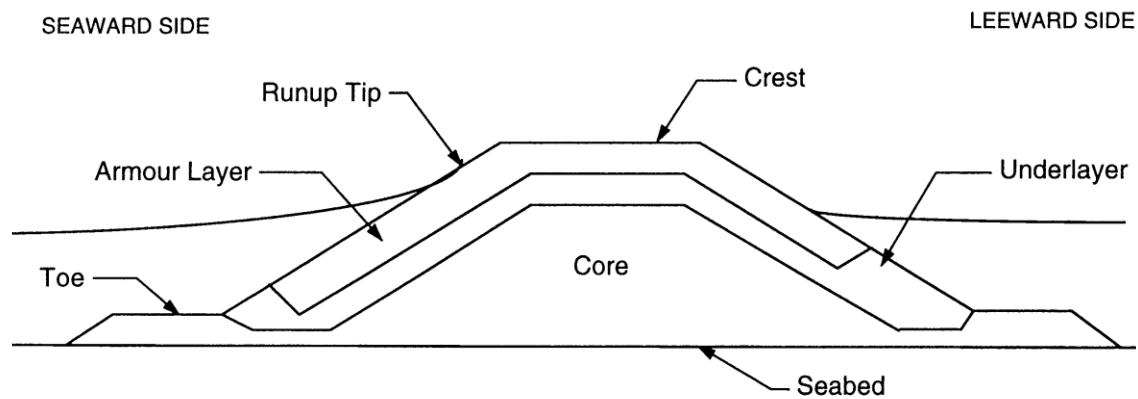


Figure 3.1 – Conventional cross-section of a rubble mound breakwater

Rubble mound breakwaters dissipate the wave energy by absorption; a small part of the wave energy is reflected though. Hence, there is a clear interaction between waves and breakwaters, which should be well understood to perform a good design and guarantee that the structure meets all the functions for which it was built during its lifetime. Several physical processes explain parts of the interaction between waves and rubble mound breakwaters, including wave run-up and run-down along the breakwaters slope, wave reflection and wave absorption within the structure. However, the interaction as a whole is very complex and, nowadays, it cannot be described accurately. As a result, the design of breakwaters is carried out using empirical formulae (discussed in section 3.3), scale models developed in laboratories (which are the basis of this thesis) and knowledge gained from other disciplines.

3.2. Development of armour units

3.2.1. Historical overview

Prior to World War II, breakwater armouring was typically constructed with either rocks or concrete cubes, placed both uniform and randomly. The design of these breakwaters consisted of a gentle slope where a large amount of units were deposited. These units resisted wave loads by their own weight.

Tetrapods were introduced in 1950 by the 'Laboratoire Dauphinois d'Hydraulique' (later on called Sogreah). They are considered as the first interlocking armour units (see Figure 3.2). In comparison to cubes, Tetrapods presented the following advantages: (1) better interlocking and (2) larger porosity of the armour layer, which results in a higher dissipation of wave energy and reduction of wave run-up along the breakwater slope.

Various concrete armour units were developed between 1950s and 1970s and were applied in few local projects. These armour units were designed to be placed in double layers either uniformly or randomly. Their stability lies on the interlocking and own weight. From this period, the more commonly used units are listed in Table 3.1.

The failure of Sines breakwater (Portugal, 1978), which was originally designed with 42-tonnes dolosse, set an end to the concrete armour units' development followed until then. The new designs of armour units aimed to balance hydraulic stability and structural strength. From Sines failure, the following conclusion were drawn: (1) slender armour units, which are designed for maximum interlocking, are not sufficiently stable because they tend to break easily and (2) breakage of armour units may cause progressive damage and reduce the expected life span of the structure.

With the introduction of Accropode in 1981 by Sogreah, a new generation of concrete armour units was developed. They were designed to be placed randomly in a single layer. Accropode became the leading concrete armour unit for the following 20 years because it combined a large hydraulic and structural stability. Further developments of this type of units were Core-Loc, A-Jack and Xbloc. These units present high interlocking and since they are placed in a single layer, more economical breakwaters can be built.

In parallel, a different armour unit concept has been developed from the 1960s. The armour layer consists of hollow blocks placed uniformly in a single layer. The position of each block is linked to the neighbour blocks, which leads to a new mechanism to resist wave loads: friction between blocks. Cob, Shed and Seabee are typical examples of this type of armour units (see Table 3.1).

Table 3.1 - Historical development of concrete armour units

Armour Unit	Country of development	Year
Cube		
Tetrapod	France	1950
Tribar	USA	1958
Modified Cube	USA	1959
Stabit	UK	1961
Akmon	The Netherlands	1962
Tripod	The Netherlands	1962
Dolos	South Africa	1963
Cob	UK	1969
Antifer Cube	France	1973
Seabee	Australia	1978
Accropode	France	1981
Shed	UK	1982
Haro	Belgium	1984
Hollow Cube	Germany	1991
Core-Loc	USA	1996
A-Jack	USA	1998
Diahitis	Ireland	1998
Samoa Block	USA	2002
Xbloc	The Netherlands	2003

3.2.2. Classification of armour units

Breakwater armour units can be classified according to:

- Shape
 - Cubical: Cube, Antifer Cube, Modified Cube, Cob, Shed
 - Double anchor: Dolos, Akmon, Toskane
 - Tetrahedra: Tetrapod, Tetrahedron, Tripod
 - Combined bars:
 - 2-D: Accropode, Core-Loc
 - 3-D: Hexapod, A-Jack
 - L-shape blocks: Bipod
 - Slab type: Tribar, Trilong, Hollow Cube, N-shape Block
 - Others: Stabit, Seabee
- Placement method:
 - Uniform
 - Random
- Stability factor
 - Own weight
 - Interlocking
 - Friction
- Structural strength (see Figure 3.2)
 - Massive or blocky
 - Bulky
 - Slender
 - Multi-hole cubes

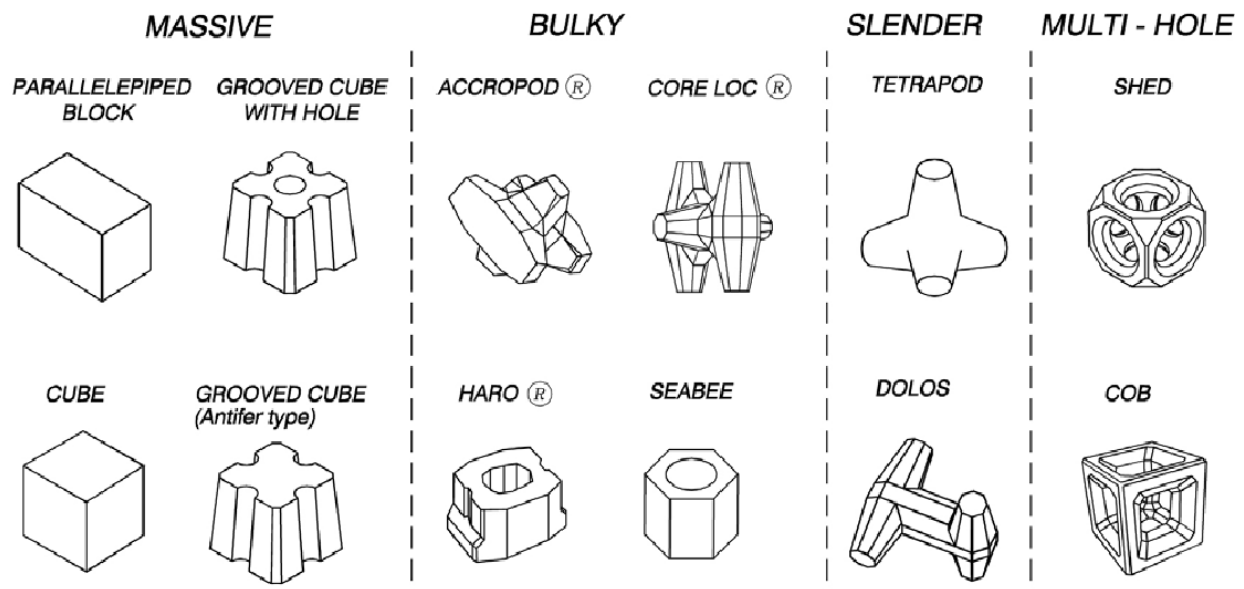


Figure 3.2 – Classification of concrete armour units [CHL, 2006]

A more general classification, which divides the armour units in six categories, consists of the shape, placement method and stability factor (see Table 3.2).

Table 3.2 – Classification of armour units by shape, placement method and stability factor

Placement method	Number of layers	Shape	Stability factor		
			Own weight	Interlocking	Friction
Random	Double layer	Simple	(1) Cube, Antifer Cube, Modified Cube		
		Complex	(2) Tetrapod, Akmon, Tribar, Tripod		
	Single layer	Simple	(5) Cube	(3) Stabit, Dolos	
		Complex		(4) A-Jack, Accropode, Core-Loc, Xbloc	
Uniform	Single layer	Simple			(6) Seabee, Hollow Cube, Diahitis
		Complex			Cob, Shed

Generally, an armour layer consisting of massive units (cubes, antifer cubes) requires more concrete than the rest of armour units, see Table 3.3. Van der Meer made a comparison between different concrete units based on a weight of 30-tonne [VAN DER MEER, 1999]. The stability coefficient (K_D -value) is derived with the Hudson stability formula, which is discussed in section 3.3.

Table 3.3 – Comparison of various concrete units [VAN DER MEER, 1999]

Type of armour unit	Accropode	Core-Loc	Tetrapod	Cube
Number of layers	1	1	2	2
Slope ($\cot\alpha$)	4/3	4/3	1.5	1.5
Stability coefficient (K_D)	12	16	7	7
Damage (N_{od})	0	0	0.5	0.5
Packing density (ϕ)	0.61	0.56	1.04	1.17
Relative volume of concrete	100%	81%	208%	220%

3.2.3. Dolos

Dolos is a concrete unit consisting of three tapered octagonal members; with a complex H-shape where one of its members is turned 90° (see Figure 3.3). Dolosse are used in large amounts to protect coastal structures against wave action. These armour units were developed by Merrifield in 1963 for the repair works at the breakwaters of East London Port (South Africa).

According to the inventor, this armour unit best satisfied the following requirements: (1) high void ratio to increase wave energy dissipation, (2) maximum interlocking and (3) sufficient structural strength. After their first application in East London Port, several laboratory tests have been carried out to determine the dolosse stability on breakwater slopes compared to other armour units.

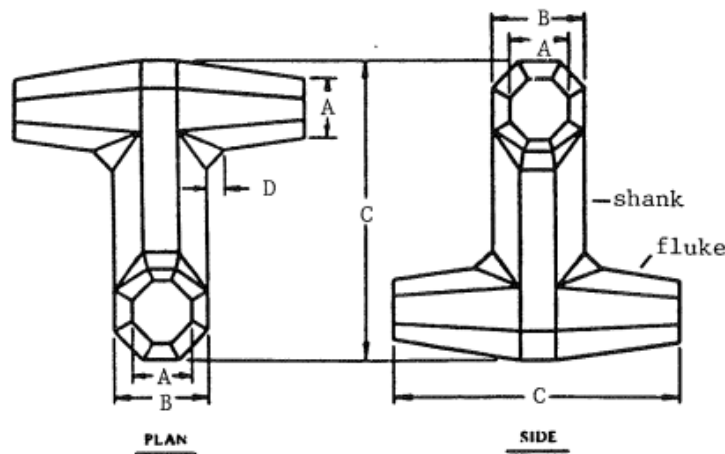


Figure 3.3 – Dolos. Plan and side views

The geometric characteristics of the Dolosse are listed in Table 3.4.

Table 3.4 – Geometrical characteristics of Dolosse

Dimension	Symbol	Expression
Waist ratio	r	$0.34 \cdot \sqrt[6]{W_a/20000}$
Length ¹	C	$\sqrt[3]{V/C_1}$
Breadth ¹	C	$\sqrt[3]{V/C_1}$
Height ¹	C	$\sqrt[3]{V/C_1}$
Fluke end width	A	0.2·C
Shank thickness	B	0.34·C
Fillet	D	0.056·C

¹ Depending on the waist ratio, the following values apply to the constant C₁: For r=0.30, C₁=0.15; r=0.32, C₁=0.16 and r=0.34, C₁=0.17 [ZWAMBORN, 1976].

3.2.4. Antifer Cubes

The Antifer Cube is a massive armour unit that was created by Maquet in 1973 as a result of the laboratory research conducted for the breakwaters of Antifer Harbour (France). Therefore, their first use was on the Antifer Harbour Breakwaters and later they have been used in the repair works of the breakwaters in Sines (Portugal) and Arzew (Algeria).

The blocks have a geometric shape close to a cube, but they present four grooves and a slightly tapered shape, which makes it easier to release them from the moulds (see Figure 3.4). As a result of the hydraulic action and friction of the grooves, the stability of the armour layer was improved compared to plain cubes [FRENS, A.B., 2007].

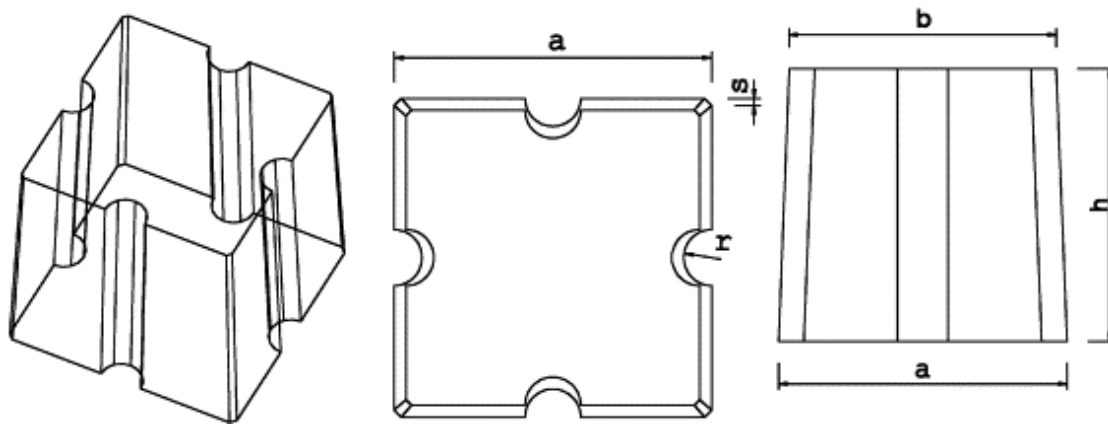


Figure 3.4 – Antifer cubes. Oblique, plan views and cross-section

The geometric characteristics of the Antifer Cubes are summarized in Table 3.5.

Table 3.5 – Geometrical characteristics of Antifer Cubes

Dimension	Symbol	Expression
Bottom width	a	$1.076 \cdot \sqrt[3]{V}$
Top width	b	$0.9254 \cdot a$
Height	h	$0.921 \cdot a$
Groove radius	r	$0.1115 \cdot a$
Groove depth	c	$0.0877 \cdot a$
Corner side width	s	$0.022 \cdot a$
Taper angle	B	87.7°

3.2.5. Accropode

Accropode is an interlocking unit created and patented by Sogreah in 1981. It was the first armour unit that could randomly be placed in a single layer and, thus became the most used unit around the world in the following 20 years [CLI, 2011].

This armour unit has a compact symmetrical shape with flat bases, which provides a better balance between the interlocking capabilities and the structural stability. Figure 3.5 presents a 3D image of the accropode. Since this unit is designed to be placed in a single layer, the placement costs and concrete consumption are reduced.

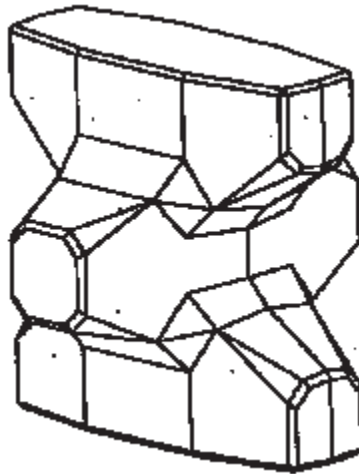


Figure 3.5 – Accropode. Oblique view [CLI, 2011]

Table 3.6 summarizes the geometric characteristics of the Accropode.

Table 3.6 – Geometrical characteristics of Accropode

Dimension	Symbol	Expression
Volume	V	W_a/ρ_a
Height	H	$\sqrt[3]{V/0.34}$
Thickness	T	$1.29 \cdot D_{n50}$

3.2.6. Core-Loc

The Core-Loc is a strong interlocking armour unit developed and patented in 1996 by the US Army Corps of Engineers (USACE). Since its invention, this unit has been worldwide used not only in the construction of new breakwaters but also for the repair works of breakwaters, generally built with dolos.

This unit has a large hydraulic stability due to the interlocking capacity of its symmetrically tapered octagonal members [TURK ET AL., 1997]. Core-Loc consists of three tapered octagonal members, with a complex H-shape where the two outer members are parallel along their longitudinal axis and the third has a longitudinal axis perpendicular to the others (see Figure 3.6).

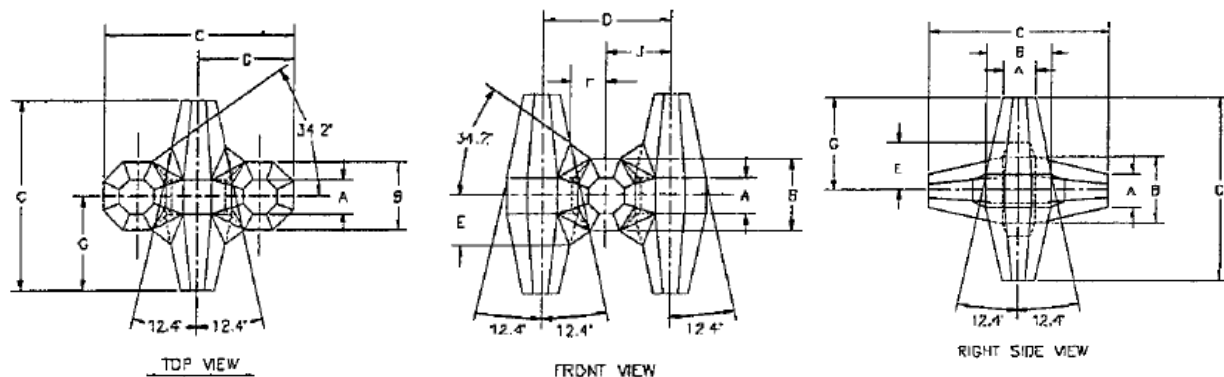


Figure 3.6 – Core-Loc. Top, front and side views [TURK ET AL., 1997]

The geometrical characteristics of the Core-Loc are listed in Table 3.7

Table 3.7 – Geometrical characteristics of Core-Loc

Symbol	Expression
C	$\sqrt[3]{V}/0.2236$
A	$0.179 \cdot C$
B	$0.360 \cdot C$
D	$0.640 \cdot C$
E	$0.248 \cdot C$
F	$0.175 \cdot C$
G	$0.500 \cdot C$
J	$0.320 \cdot C$

3.2.7. Accropode II

Accropode II is an interlocking armour unit invented and patented by Sogreah in 1999. This unit is an improved version of the original accropode, which enhances the hydraulic performance, the structural stability and eases its placement.

The new shape consists of replacing the large flat surfaces and right angles by small surfaces and numerous chamfers. To improve the friction between units, sets of pyramids are included on the unit faces (see Figure 3.7).



Figure 3.7 – Accropode II. Oblique view [DENECHERE, M., 2011]

Table 3.8 summarizes the geometric characteristics of the Accropode II.

Table 3.8 – Geometrical characteristics of Accropode II [CLI, 2012]

Dimension	Symbol	Expression
Volume	V	W_a/ρ_a
Height	H	$\sqrt[3]{V/0.2926}$
Thickness	T	$1.36 \cdot D_{n50}$

3.2.8. Xbloc

Xbloc is an interlocking concrete unit designed and developed by Delta Marine Consultants between 2001 and 2003. The small shore protection at Java (Indonesia) in 2004 was the first project where Xbloc was ever applied.

According to the inventors, Xbloc is an efficient and robust unit with an easier manufacturing process and less restrictive placement regulations. These units have a symmetrical shape that consists of a flat base with four indentations and two cubic noses at both sides of the base (see Figure 3.8). They are designed to be placed randomly in a single layer like Accropode and Core-Loc. Therefore, a reduction of concrete consumption and placement costs are achieved compared to dolosse and Antifer Cubes, which are placed in double layers.

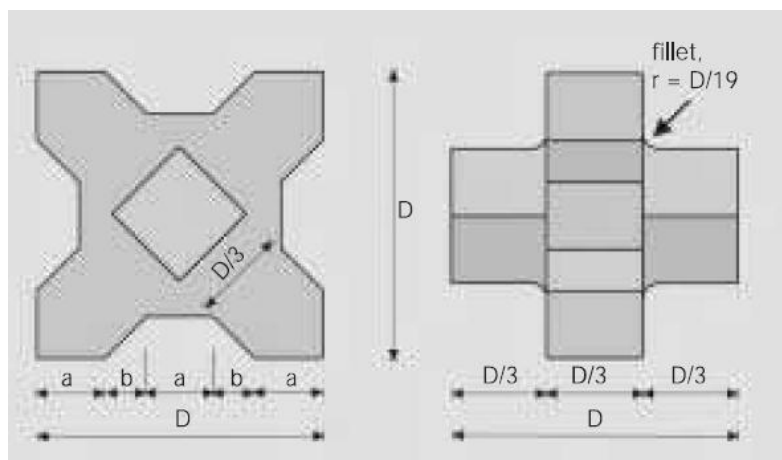


Figure 3.8 – Xbloc. Plan and side views

The geometric characteristics of the Xbloc are presented in Table 3.9.

Dimension	Symbol	Expression
Width	D	$\sqrt[3]{3 \cdot V}$
Height	D	$\sqrt[3]{3 \cdot V}$
Base thickness	-	$1/3 \cdot D$
Fillet	r	$1/19 \cdot D$

3.3. Hydraulic stability

The proper prediction of the size of the armour layer units (D_{n50}) is very important in the design of breakwaters. Since the last half-century, many methods have been proposed to determine the armour unit size. All of these methodologies are based on the same concept: the stability of the units against wave action when they are placed over a slope. Therefore, this section reviews the development of these formulations until present day, focusing on the armour units that are going to be analysed in this research.

To understand how breakwaters behave against wave action, it is necessary to describe the physical processes taking place on that environment. In general, these structures have a permeable core that influences the stability of the armour layer units. The instability of these units is caused by wave forces, which tend to move the stones once a critical value is exceeded. Those wave-generated forces are known as drag, shear and lift forces that are withstood by the friction between stones and their submerged weight (see Figure 3.9). These phenomena can be expressed as:

$$\rho_w \cdot u_c^2 \cdot d^2 \alpha (\rho_s - \rho_w) \cdot g \cdot d^3 \cdot (\tan \varphi \cdot \cos \alpha \pm \sin \alpha) \quad [3.1]$$

Here, the first term defines the wave-induced forces and the second term is the resistance of the armour layer with a correction factor for the slope.

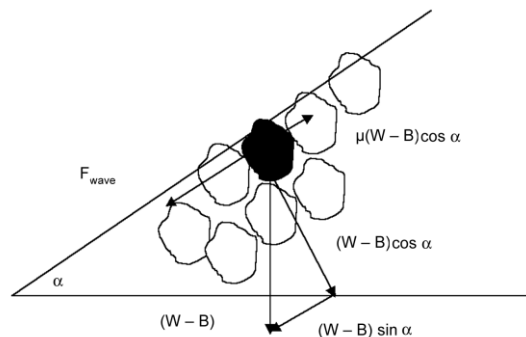


Figure 3.9 – Wave-induced forces on a stone [VERHAGEN, H.J. ET AL., 2009]

By assuming that the velocity of a wave on a slope is proportional to the celerity in shallow water ($u_c = \sqrt{g \cdot H}$), equation [3.1] can be simplified to:

$$\rho_w \cdot g \cdot H \cdot d^2 \alpha (\rho_s - \rho_w) \cdot g \cdot d^3 \cdot (\tan \varphi \cdot \cos \alpha \pm \sin \alpha) \quad [3.2]$$

Equation [3.2] is the starting point for the investigations carried out by Iribarren and later on by Hudson, who performed several laboratory tests to find Iribarren's constants [SCHIERECK, 2001]. These two formulations are not used to design rock armour units anymore, although Hudson's formula is still applied in the design of some concrete armour units, such as Xbloc, Core-Loc and dolos.

$$\frac{H_s}{\Delta \cdot d} = \sqrt[3]{K_D \cdot \cot \alpha} \quad \text{Hudson's stability equation} \quad [3.3]$$

Here, the first term corresponds to the stability parameter and the second is the resistance. In its turn, the second term can be subdivided in a factor that represents the damage level (K_D), see Table 3.10; and a slope correction factor ($\cot \alpha$). This formula can only be applied in a field of regular waves and with a slope range of $1.5 < \cot \alpha < 4$. Besides, extra coefficients must be considered when applying Hudson's equation to other conditions.

Table 3.10 – Hudson's Stability coefficient values for various concrete armours

Breakwater section	Type of wave	Dolos	Antifer cube ²	Core-Loc ³	Xbloc ⁴	Accropode / Accropode II
Trunk	Non-breaking wave	31.8 ¹	7.5	16	16	15 / 16
	Breaking wave	15.8 ¹	6.5	16	16	11.5 / 12.3
Head	Non-breaking wave	16 ²	5	13	13	-
	Breaking wave	8 ²	-	13	13	-

¹ Refers to no damage criteria (<5% of displacement, rocking, etc.); if no rocking (<2%) the K_D is reduced by 50% [SHORE PROTECTION MANUAL, 1984]

² Preliminary design purposes [SHORE PROTECTION MANUAL, 1984]

³ Guidelines for design - Core-Loc .Design Guide Table

⁴ Xbloc. Effective wave protection for breakwaters and shores

To overcome the limitations of Hudson's stability formula, Van der Meer proposed a new formula for rocks, which included a larger number of relevant parameters such as structure permeability, number of waves during the storm and expected damage level at design condition [VAN DER MEER, 1988]. Van der Meer formulae read:

$$\frac{H_s}{\Delta \cdot D_{n50}} = 6.2 \cdot P^{0.18} \cdot \left(\frac{S_d}{\sqrt{N}}\right)^{0.2} \cdot \xi^{-0.5} \quad \text{for plunging waves} \quad [3.4]$$

$$\frac{H_s}{\Delta \cdot D_{n50}} = 1.0 \cdot P^{-0.13} \cdot \left(\frac{S_d}{\sqrt{N}}\right)^{0.2} \cdot \xi^P \cdot \sqrt{\cot \alpha} \quad \text{for surging waves} \quad [3.5]$$

Here, H_s is the wave height, Δ is the relative mass density, D_{n50} is the nominal diameter of the stones, S_d is the design criteria for damage, N is the number of waves in a storm, ξ is the Iribarren number and P is the notional permeability coefficient.

Besides, Van der Meer conducted an extended research on the stability of breakwaters built with concrete armour units, such as cubes, tetrapods and accropodes. As a result several stability formulae were proposed for each concrete unit, which were based on the same governing variables as for rock units. However the research was limited to only one cross-section with a slope of 1:1.5 [VAN DER MEER, 1999]. Van der Meer's stability formula for cubes is expressed as follows:

$$\frac{H_s}{\Delta \cdot D_{n50}} = \left(6.7 \cdot \frac{N_{od}^{0.4}}{N^{0.3}} + 1.0\right) \cdot s_{om}^{-0.1} \quad \text{Stability formula for cubes (displaced units)} \quad [3.6]$$

$$\frac{H_s}{\Delta \cdot D_{n50}} = \left(6.7 \cdot \frac{N_{omov}^{0.4}}{N^{0.3}} + 1.0\right) \cdot s_{om}^{-0.1} - 0.5 \quad \text{Stability formula for cubes (rocking)} \quad [3.7]$$

Here, N_{od} represents the number of displaced units related to a width of one nominal diameter, which is a measurement of the damage (see section 3.4.2.2); N_{omov} stands for the number of units that are

rocking and s_{om} is the wave steepness. Table 3.11 shows the values displaced units to apply in equation [3.6].

	Initial damage	Intermediate damage	Failure
N_{od}	0-0.5	0.5-1.5	>2

More recent research was focused on the stability of antifer cubes, which was carried out by Chegini and Aghtouman. They performed several tests of breakwaters armoured with antifer cubes placed in various slopes (1:1.5 and 1:2). This led to new stability formulae for the antifer cubes that included the effect of the slope [CHEGINI ET AL., 2005].

$$\frac{H_s}{\Delta \cdot D_{n50}} = \left(5.886 \cdot \frac{N_{od}^{0.502}}{N^{0.268}} + 1.449 \right) \cdot \xi_m^{0.065} \quad \text{Stability formula for antifer cubes (displaced units)} \quad [3.8]$$

$$\frac{H_s}{\Delta \cdot D_{n50}} = \left(5.886 \cdot \frac{N_{omov}^{0.502}}{N^{0.268}} + 1.449 \right) \cdot \xi_m^{0.065} \cdot 0.5 \quad \text{Stability formula for antifer cubes (rocking)} \quad [3.9]$$

Here, N_{od} represents the number of displaced units related to a width of one nominal diameter, which is a measurement of the damage; N_{omov} stands for the number of units that are rocking and ξ_m is the surf similarity parameter for mean wave period.

Equations [3.4] to [3.9] are the result of applying a curve-fitting method to a large number of tests results. The physical base of those expressions is still weak and more research needs to be carried out. Firstly, it is necessary to gain a better insight in the relevance of each parameter in the armour units' stability and, secondly, new features might be required to be added in the stability definition, such as wave run-up, angle of incidence of waves, and so on.

Once the size of the armour units is known, the sizes of the material that will be used in the remaining layers of the rubble mound breakwater (toe protection, underlayers and core) can be estimated. These sizes are calculated to fulfil the filter requirements, i.e. the material should be large enough not to be washed out during wave action through the armour layer voids. According to the Coastal Engineering Manual, the following relationships should be applied to ensure the filter requirements [CHL, 2006]:

$$\frac{1}{10} > \frac{W_u}{W_a} > \frac{1}{15} \quad \text{Filter relationship for underlayer material} \quad [3.10]$$

$$\frac{1}{10} > \frac{W_c}{W_u} > \frac{1}{15} \quad \text{Filter relationship for core material} \quad [3.11]$$

The Coastal Engineering Manual recommends using the same material for the toe protection as for the underlayer [CHL, 2006]. However, some research has been conducted to determine the stability of the toe protection by taking into account various parameters that may affect its behaviour, such as water depth in front and above the toe and the allowed damage. As a result, two expressions can be applied to determine the required stone size for the toe protection [CIRIA, 2007].

$$\frac{H_s}{\Delta \cdot D_{n50}} = \left(1.6 + 0.24 \cdot \frac{h_t}{D_{n50}} \right) \cdot N_{od}^{0.15} \quad [3.12]$$

$$\frac{H_s}{\Delta \cdot D_{n50}} = \left(2 + 6.2 \cdot \left(\frac{h_t}{h} \right)^{2.7} \right) \cdot N_{od}^{0.15} \quad [3.13]$$

Here, h_t corresponds to the water depth above the toe's berm.

These equations can be used when the ratios of h_t/h and h_t/D_{n50} are between 0.4-0.9 and 3 to 25, respectively. However, it should be noted that equation [3.12] is based on tests with h_t/h ratio between 0.7 and 0.9 and can give unrealistic results if h_t/H_s is smaller than 2.

3.4. Maintenance of coastal structures

3.4.1. Introduction

Structures armoured with rock or concrete units require regular maintenance to ensure their functionality. However, these structures can typically be designed either for high-performance with minimal maintenance (developed countries) or low-capital cost with regular maintenance (developing countries). The breakwaters at Richards Bay Port are an example of the latest type of design.

Maintenance is defined as all the required activities to keep an object's technical state or to revert it back to its original state. Such state is considered necessary to carry out the structure's expected functions.

The maintenance methods can be classified in curative and preventive methods. The first method comprises the failure-based maintenance, which defines and undertakes the repair works once the structure or part of it has failed. The latest method is divided in: (1) periodic maintenance, which establishes the structure deterioration by using a known time function; (2) use-based maintenance that considers that the structure is degraded after being used a certain number of times; (3) load-based maintenance, where the deterioration of the structure is caused by heavy loads, such as storms; and (4) condition-based maintenance which depends on the physical condition of the structure after conducting inspections.

A combination of two or more maintenance methods is used in hydraulic engineering projects. Generally, a preventive method such as the condition-based maintenance is combined with the failure-based maintenance method to define the repair works.

The maintenance process consists of:

- Management strategy: defines safety aspects and establishes a basic guidance of operation, maintenance and monitoring activities to maintain the functionality of the structure during its lifetime. It should allow for continuous adjustment and refinement to evaluate the structure performance and effectiveness of the plan.
- Monitoring process of environmental conditions and structure response: comprises the observation and measurement of the structure performance related to design objectives, environmental conditions and the expected response. The external loads that affect the structure, such as water levels, wave and wind climates, bathymetry, etc. are also measured.

The applied monitoring techniques should be repeatable according to predefined specifications. Photographic and profile surveys, visual inspections and underwater surveys are examples of monitoring techniques used in breakwaters.

- Evaluation of structure condition and response: consists of quantifying the inspections and surveys with regard to specific condition and performance criteria. These monitoring and evaluation systems allow tracking of structure response over time. During the evaluation of surveys and inspections, some degree of deterioration is permitted to armoured structures unless the structure suffers significant loss of functionality. The armour condition assessment for breakwaters will be further discussed in section 3.4.2.
- Maintenance actions: the outcome of monitoring evaluation is used to design several options of repair and rehabilitation. These options are analysed either to provide recommendations about maintenance actions, which can vary between doing nothing and complete structure removal, or to require additional inspections (see section 3.4.3). Coastal structures ought to be repaired or rehabilitated once they do not fulfil the intended functions or their state is critical.
- Economic analysis of the possible responses: the manager decides about the maintenance alternative to be applied after a careful study of all possible actions and their implementation cost.
- Rehabilitation or repair works: the chosen maintenance action is further developed to enable the construction at the site where damage or deterioration is localised.

3.4.2. Evaluation of structure condition and response

Several techniques exist to inspect the state of coastal structures, as they have been stated in the previous section. The simplest method consists of visual inspection, which despite the subjectivity of the observer's opinion, is still applied in the diagnosis of structure condition. The techniques based on surveys offer lots of information that are used to provide meaningful measure of damage, cumulative damage and risk of failure.

Typical features to evaluate the structure condition are listed in Table 3.12, where it is identified the changing condition for various spatial levels.

Table 3.12 – Evaluation of monitoring data in armoured structures [CIRIA, 2007]

Structure spatial level	Aspect measured	Evaluation
Level I: location	Settlement of foundation Change in alignment	
Level II: geometry	Consolidation of structure Comparison of slope profiles	Damage assessment
Level III: composition	Loss or movement of armour units	Damage assessment
Level IV: element composition	State of deterioration of armour units	Review of design conditions Damage assessment

The damage concept for designing and monitoring breakwaters is defined in section 3.4.2.1, while section 3.4.2.2 deals with the worldwide-applied damage classification.

3.4.2.1. Concept of damage

The concept of damage has been introduced in stability formulations of breakwaters by means of various parameters, such as K_D (Hudson's formula) and S (Van der Meer's equations). However, its definition is not so clear in Hudson's expression, because K_D parameter contains other influencing variables. Hence, to use a valid value of K_D , the damage level should be smaller than 5%. Moreover, in Van der Meer's formulae, the damage level is described with more physical sense by applying Broderick damage expression [CHL, 2006].

The damage to armour layers is related to the specific conditions and duration of a sea state. It can be characterized by two different methods: (1) counting the number of displaced units or (2) measuring the eroded surface profile of the armour slope.

A classification of the movements of the armour units is required in the counting method. Such a classification is based on the number of units that:

- Do not move.
- Show some rocking.
- Are displaced a certain minimum distance, which is generally related to the length of the armour unit nominal diameter (D_{n50}).

The damage can be expressed in terms of a relative displacement D , which is defined as the ratio between the number of displaced units and the total number of units within a specific zone (complete armour layer area or area between a bandwidth around Still Water Level).

$$D = \frac{\text{Number of displaced units}}{\text{Total number of units within a specified zone}} \cdot 100 \quad [3.14]$$

The second method of damage characterization is based on the eroded area profile. Figure 3.10 shows a scheme of how the eroded area profile should be estimated. Broderick defined the dimensionless damage as the relation between the eroded surface profile and the squared of the nominal stone diameter [CHL, 2006]. This expression is independent of the slope length and only considers the vertical settlements.

$$S = \frac{A_e}{D_{n50}^2} \quad [3.15]$$

Here, S represents the dimensionless damage parameter, A_e is the eroded surface and D_{n50} is the stone nominal diameter.

The damage parameter S is appropriate in the damage assessment of armour layers built with rocks and concrete cubes. However, when the shape of the armour units is complex, such as the case of dolosse, it may be difficult to estimate the eroded area (A_e).

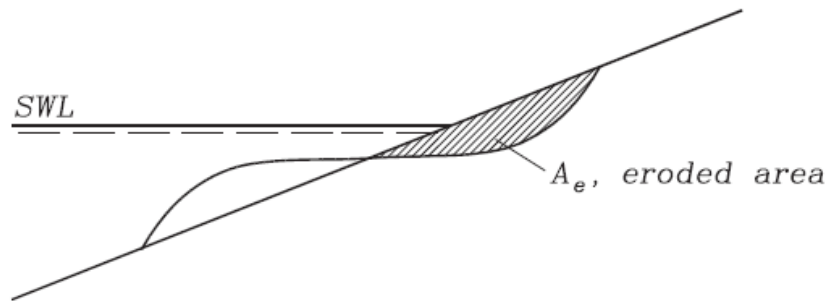


Figure 3.10 – Eroded area profile [CHL, 2006]

3.4.2.2. Damage classification

Once the damage level has been estimated according to one of the methods described in the previous section, the structure damage should be classified in:

- **No damage:** there are no units displaced, but settlement can occur.
- **Initial damage:** Few units are displaced.
- **Intermediate damage:** Units are displaced but the filter layer is not exposed to wave action.
- **Failure:** The filter layer is exposed to wave action.

Table 3.13 and Table 3.14 present the damage level associated to the structure damage classification for the relative displacement D and relative eroded area, respectively.

Table 3.13 – Damage level by D for double-layer armour [CHL, 2006]

Unit	Slope	Initial damage	Intermediate damage	Failure
Rock ¹	1:2-1:3	0-5%	5-10%	≥20%
Cube ²	1:1.5-1:2	-	4%	-
Dolosse ²	1:1.5	0-2%	-	≥15%
Accropode ^{2,3}	1:1.33	0%	1-5%	≥10%

¹ D is defined as percentage of eroded volume.

² D is defined as percentage of units moved more than D_{n50} within the following level restricted areas: For rock see definition under initial damage, for cube $SWL \pm 6D_{n50}$, for Dolosse $SWL \pm 6D_{n50}$, for Accropodes between levels $SWL +5D_{n50}$ and $-9D_{n50}$.

³ One-layer armour cover layer.

Table 3.14 – Damage level by S for double-layer armour [CHL, 2006]

Unit	Slope	Initial damage	Intermediate damage	Failure
Rock	1:1.5	2	3-5	8
Rock	1: 2	2	4-6	8
Rock	1:3	2	6-9	12
Rock	1:4-1:6	3	8-12	17

3.4.3. Maintenance actions

3.4.3.1. Introduction

Structure managers should choose one or more maintenance actions after the completion of the monitoring evaluations. However, these actions must be applied when there are repair indications or rehabilitation needs on the structure. Such needs are identified by: progressive degradation that reduces the structure functionality, damage after storms or other events, chronic damage due to underestimated design loads or unplanned structure performance.

The considered maintenance actions in coastal structures are [CIRIA, 2007]:

- No repair or replacement work and await next monitoring report.
- No repair or rehabilitation work but prompt additional future monitoring of the structure state and/or environmental conditions.
- Carry out further detailed inspection before making a decision.
- Undertake temporary or emergency repair or replacement works.
- Carry out permanent repair or rehabilitation works.
- Instigate development of a new structure.
- Promote abandonment or removal of the structure.

3.4.3.2. Maintenance considerations

Basic maintenance guidance does not exist because the damage and degradation are often localised and specific to the considered structure. However, there are some maintenance features that are applicable to all armoured structures:

- Review original design criteria: as-built drawings are handy to identify changes between the constructed and the original designed structure.
- Cause of the problem: monitoring data provides valuable information to determine the structure condition and to identify what caused the damage. Generally, a combination of circumstances leads to structural damage or failure, which should be properly identified to ensure good repair or rehabilitation works.
- Changes to the design conditions: they usually remain unchanged from the time of the original design to the time when repairs are needed, unless the exposure to wave climate or bathymetry has been altered.
- Condition of armour material: the state of the armour units is analysed to determine whether they can be reused or new units are required.
- Solution for the problem: several solutions with an estimation of their cost are proposed. The structural manager should decide which the chosen solution is.
- Design of the repair or rehabilitation works: the chosen alternative is further developed to ensure its implementation.

3.4.3.3. *Repair and rehabilitation of armoured structures*

Repairs of rubble mound breakwater consist of rebuilding the structure with the existing material or replacing the armour units with new material. The following aspects have to be taken into account when designing repair works: repairs take place on an existing rubble mound structure; the armour slope is difficult to be changed to meet design parameters; the construction of the new toe on an existing structure is more complicated than when it is built for a new structure; transitions between repaired and non-repaired slopes should be accomplished without weakening the existing structure; some armour units should be removed before starting repair works.

The extent of damage or degradation defines the type of repair and rehabilitation option to be applied. Four general categories of armour layer repairs are distinguished:

- Localised replacement of broken or displaced armour units: when the displacement of units represents less than 5%, the repair of the armour layer consists of placing a combination of new and used units in the locations where armour units have been lost. The required size of the units can be the same or larger than the existing depending on how the damage has been originated.
- Overlaying existing armour units: the structure damage occurs in large sections, where the armour units are displaced or move out the slope. The repair works involve the addition of a single or double layer above the existing structure with similar or different armour units.
- Replacing of armour layer: the damage is extended over an important part of the structure's armour layer. Thus, the repair comprises the replacement and reconstruction of the damaged armour layer. Since the structure is rebuilt, the design of the repair works will follow the specifications of any new structure and larger armour units will generally be used.
- Reconstruction of the structure: the whole structure will be rebuilt, when its integrity is seriously compromised due to a catastrophic event. If the structure needs to be reconstructed at the same location, the first step will be its complete removal. The design of the reconstruction will follow the same specifications as a new structure.

4. Description of the repair works approach

This section describes the generic steps followed to define the repair works to be carried out in any coastal structure. The main focus will be centred on rubble mound breakwaters, which are the topic of this research. Besides, the authorities in charge of these structures must have some maintenance policies, which comprise from periodic monitoring to the construction of the chosen repair alternative.

Firstly, the monitoring process of the structure should be specified. This involves visual inspections, photographic surveys and profile surveys that take place periodically. Generally, these monitoring actions are annually conducted at the Breakwaters of Richards Bay Port. The analysis of the information gathered during this process provides an early-warning system of the structure state due to the estimation of its damage. However, the estimated damage should be linked to the wave conditions recorded during the period between surveys to identify the causes of damage. Finally, the Port Authority decides whether any maintenance action should be carried out when the structure develops a potential harmful change in its state.

According to section 3.4.3, the maintenance actions to be applied vary from doing nothing to the complete removal and construction of a new structure. However, since the breakwaters performance is periodically checked, the last maintenance action can be avoided because the repair works will be undertaken before reaching such a state. Hence, the feasible repair plans can be divided in:

- Doing nothing. If the port has future expansion plans in the short term (less than 5 years), this can be the maintenance action to be applied. However it should be noticed that future repair works will be more expensive due to the cumulative damage in the structure.
- Addition of extra new units in the damaged areas. This is a maintenance action that can be used when the future expansion plan of the port would be undertaken in about 10 years. The repair of the armour layer consists of placing a combination of new and used units, which can either have the same size or larger, in the locations where the units have been lost. The structure damage usually represents less than 5%.
- Repair works comprising new design of the armour layer. This maintenance action is applied when the structure damage is larger than 5% or the structure is going to be used more than 20 years before the port expansion plans are carried out.

Taking into account the possible repair plans, the Port Authority decides the lifetime for which the structures should be operational. As a result, one of the above maintenance actions is applied. In the case of the breakwaters at Richards Bay Port, there are no future expansion plans in the short or mid-term and the quantified damage is larger than 5% in some of their sections (see Table 2.1 and Table 2.2). Therefore, the repair works will comprise a new design of the armour layer.

Prior to the design of the repair works, a review of the original design conditions is conducted. This covers the analysis of the original design wave conditions, water levels, seabed profile and the comparison of the as-built cross-sections with the profiles obtained during the surveys. If it is necessary, new design conditions are determined according to the structure lifetime specified by the Port Authority. Besides, the properties of several armour units are discussed to apply the most suitable ones in the design of the repair alternatives (see section 3.2).

Once the design conditions (water level and design storm) are specified, various repair methods can be discussed. These methods are classified in: (1) covering alternative that consists of overlaying new armour units above the damaged armour layer, and (2) replacement alternative, which comprises the removal of the damaged armour layer and its substitution by a new armour layer.

The first repair method is based on placing new armour units above the existing armour layer. In case of armour units whose stability depends on the interlocking between units, this feature should be considered when deciding the type of armour units to be used in the repair works. For instance, the roundhead of the South Breakwater at Richards Bay Port was built with dolos, thus it should be covered with interlocking units such as dolos or Core-Loc to keep this resistance mechanism. However, depending on the degree of damage and the capability of re-profiling the slope, other armour units can be placed on top of the existing armour layer, such as antifer cubes.

The second repair method consists of removing the damaged armour layer and placing a new one. In the design of the new armour layer, it should be discussed whether to use armour units that are placed in double or single layers and whether an extra filter layer is needed between the existing filter layer and the new armour layer.

Several alternatives can be designed from each repair method. Their design covers the estimation of the required size for various armour units, underlayer and toe protection (see equations in section 3.3), determination of required number of units to construct the structure and definition of the structure geometrical shape.

Thereafter, the alternatives can be compared by means of an economic analysis that takes into account all the costs involved in the construction of each repair option. This includes the costs of manufacturing the required units, storage costs of units, site preparation costs, cost of the equipment used in the construction and placement costs of units. Besides, it should be noted that the replacement alternative requires the removal of the damaged armour layer. This may be difficult to be undertaken in some locations due to wave climate, availability of equipment, etc. As a result, one of the described repair methods cannot be feasible.

Moreover, after the design of various alternatives and rejection of some due to their cost, the remaining alternatives are tested in a physical model to check their performance and get better insight in the mechanisms causing the damage. The obtained results are used to choose the appropriate repair alternative and improve its design. Finally, the construction process of the chosen alternative is specified so that contractors can easily carry out the repairs.

5. Design of the repair alternatives

As it has been discussed in the previous section, several repair methods can be applied in a damaged structure according to the degree of observed damage. Paragraph 5.1 deals with the repair method considered for the roundhead of the South Breakwater at Richards Bay Port, while section 5.2 focuses on the new design conditions. In section 5.3, several repair alternatives are proposed.

5.1. Roundhead repair method

The roundhead of the South Breakwater at Richards Bay Port is in a bad state according to the analysis performed to the monitoring survey of May 2011. Most of the roundhead sections present an intermediate level of damage, see Table 2.2. However the most exposed sections to storms are in failure. Several dolosse have been lost, while others have been broken and their pieces are lying on the slope, causing a change in shape of the roundhead. Although the state of the roundhead is classified as damaged, the core material is not visible on the survey pictures. Moreover, in future storms, the pieces of dolos can easily move away due to loss of interlocking and damage other units unless repair works are carried out soon.

Various repair methods can be considered, which vary from doing nothing to rebuild the whole structure (see section 3.4.3.3 and 4). Nevertheless, since the extent of the damage covers a large section of the breakwater roundhead, the repair method to be implemented will consist of either overlaying new armour units above the existing ones or replacing the actual armour layer with new units. Therefore, different structural designs and concrete armour units will be studied for the repair works of the new roundhead.

5.2. Design conditions

The initial design of the breakwaters at Richards Bay Port was based on the wave data collected during February 1968 and May 1972. A prediction of the wave conditions was made using such data for a design lifetime of 50 years. However, this design procedure does not take into account the risk of the structure failure due to an extreme event occurring during its lifetime. This means that the design storm has a high probability of happening and therefore, repair works should frequently be undertaken on this structure. This design practice is commonly applied in developing countries. Table 5.1 presents the results obtained for the initial design [NATIONAL RESEARCH INSTITUTE FOR OCEANOLOGY, 1974].

Table 5.1 – Initial design conditions

Wave direction	Occurrence	Deep sea		Entrance area		Wave direction	Occurrence	Deep sea		Entrance area	
		1/10 year	1/50 year	1/10 year	1/50 year			1/10 year	1/50 year		
[-]	[%]	[m]	[m]	[m]	[m]	[-]	[%]	[m]	[m]	[m]	[m]
NE	0.22	-	-	-	-	S	22.56	5.7	6.5	5.1	5.8
ENE	3.91	4.7	5.4	3.4	3.9	SSW	8.72	6.8	7.8	4.7	5.4
E	8.09	4.0	4.5	3.6	4.0	SW	0.97	4.2	4.8	1.1	1.3
ESE	10.10	3.5	4.0	3.4	3.9	Combined	100.0	6.8	7.8	6.3	7.2
SE	26.66	4.9	5.6	4.8	5.4						

As it has been observed during these years, the initial design conditions underestimated the wave climate at Richards Bay location. Due to the limited available wave data at that time (4 years of wave measurements), these extreme wave estimates are considered unreliable. Therefore, a new analysis of the wave climate has been performed in this research to estimate the design conditions for the repair works.

The new analysis consists of determining the seabed profile around the structure from bathymetry surveys, estimating the extreme storm event and the corresponding water elevation at the South Breakwater toe for different return periods. The bathymetry close to the structure location is presented in section 5.2.1. Section 5.2.2 describes the process followed to determine the wave characteristics of the design storm (extreme wave height and peak period), while the estimation of the water levels will be discussed in section 5.2.3.

5.2.1. Seabed profile

A bathymetry survey was performed to provide accurate information about the current state of the sea bottom in the surroundings of the South Breakwater at Richards Bay. The collected data was processed and a map with the depth-contour lines was drawn, see Figure 5.1.

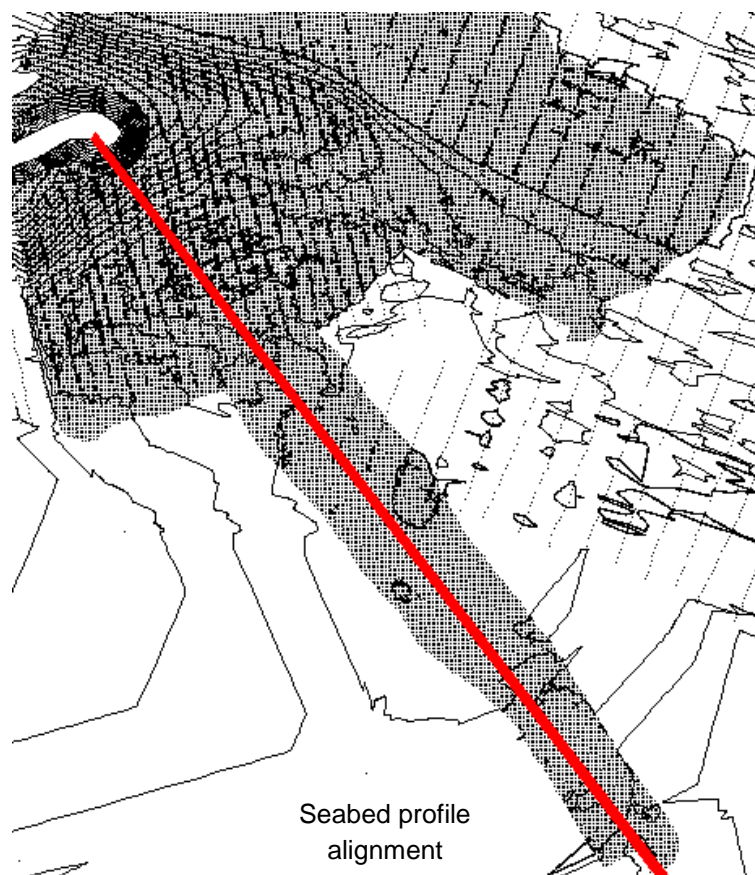


Figure 5.1 – Bathymetry of South Breakwater at Richards Bay

Various seabed profiles can be plotted from the depth-contour map shown in Figure 5.1. However, due to the characteristics of wave propagation, the South Easterly profile has been considered in this research. Figure 5.2 presents the South Easterly profile, which also connects the breakwater with the buoy location.

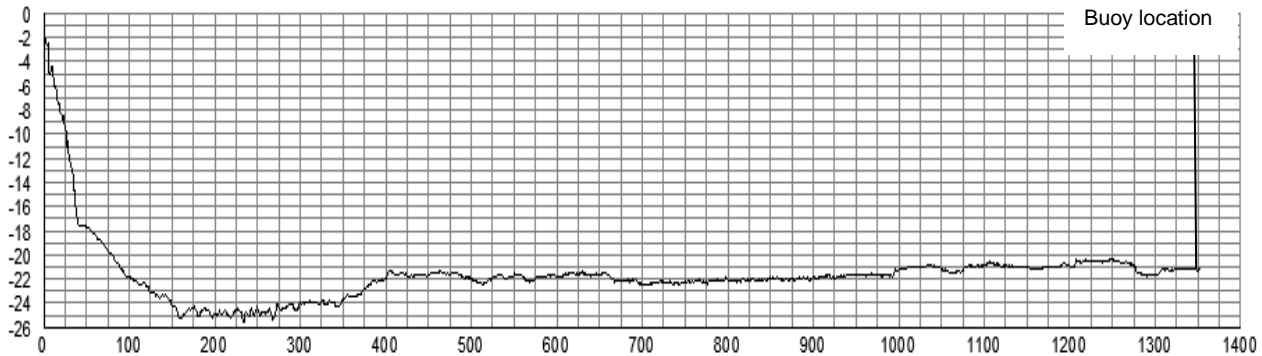


Figure 5.2 – Seabed profile from the breakwater to the buoy location

5.2.2. Design storm

The design storm comprises the estimation of the extreme significant wave height and its wave period for a given return period. The extreme wave heights were estimated using an extreme statistical analysis coupled to the Peak-over-Threshold method onto the available time series measured in Richards Bay buoy [VERHAGEN ET AL., 2009], [GODA, 2000] and [HOLTHUIJSEN, 2007], while the extreme wave period is related to the design wave heights. Several extreme functions were fitted to the data (see Appendix A.1); however, Weibull distribution provided the best fit. Therefore, this distribution was used to estimate the design wave height for each return period.

Figure 5.3 and Figure 5.4 show the results of the extreme statistical analysis applied to the collected wave data at the buoy of Richards Bay since 1979 for the design wave heights and wave periods, respectively.

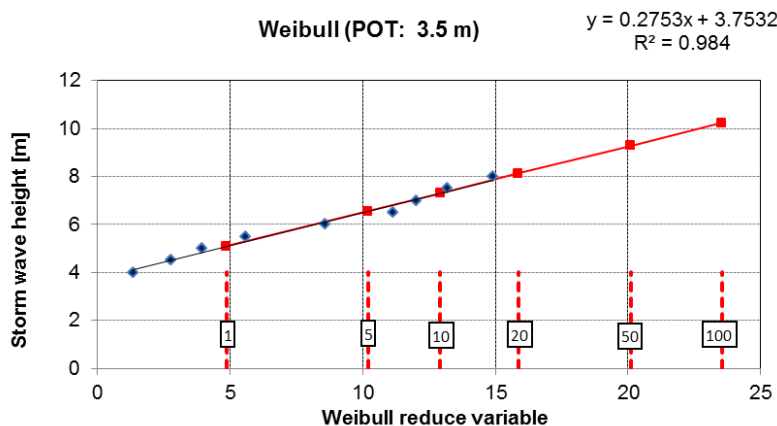


Figure 5.3 – Design storm. Wave heights

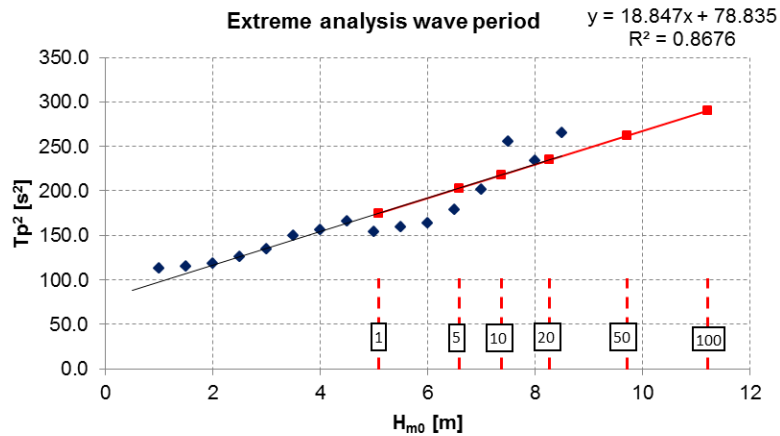


Figure 5.4 – Design storm. Wave periods

Wave characteristics are expected to be affected by Climate change. Therefore, the determination of long-term changes on waves is important for the design of any coastal project. Several researchers have observed an increase of extreme events from wave data recorded during these last 30 years. This trend can be interpreted in two ways: (1) the current extreme events are happening more frequently and (2) higher extreme conditions can occur in the future due to climate change.

Recently, wave heights measured by satellite have been used to quantify the increasing rate of mean and extreme wave heights observed. A global increase of extreme wave height has been estimated for a data series of the past 23 years, resulting in 0.25% increase of wave height in equatorial latitudes and 0.5% in middle latitudes [YOUNG ET AL., 2011]. However, no projections of wave climate scenarios have been performed to give global rates of wave height increase yet. An increase factor of 10% has been considered for the 100-years return period and it has been linearly interpolated for other return periods (see Table 5.2).

Table 5.2 summarizes the design storm obtained for various return periods at the buoy location.

Table 5.2 – Design storms

T	H_{m0}	f_{cc}^1	H_{m0}^{CC} ($f_{cc} \cdot H_{m0}$)	T_p	DNV (1977)	
					Lower T_p	Upper T_p
[yr]	[m]	[-]	[m]	[s]	[s]	[s]
1	5.1	1.000	5.1	13.6	8.5	13.0
5	6.6	1.004	7.2	14.7	9.7	14.8
10	7.3	1.009	8.0	15.2	10.2	15.6
20	8.1	1.019	8.9	15.7	10.8	16.4
50	9.2	1.049	10.2	16.5	11.5	17.6
100	10.2	1.100	11.2	17.0	12.1	18.4

¹ This factor is applied as a result of the climate change.

According to the test results conducted during the initial design of this structure in the 1970s, the wave energy was concentrated in the surroundings of the South Breakwater Head. Such behaviour is related to the bathymetry and the entrance channel characteristics, both refracting the incoming waves towards the roundhead. This phenomenon was also observed in various runs of Richards Bay model in SWAN using the depth data provided by the bathymetry survey. Figure 5.5 shows the behaviour of the waves approaching towards the breakwater considering various angles of incidence.

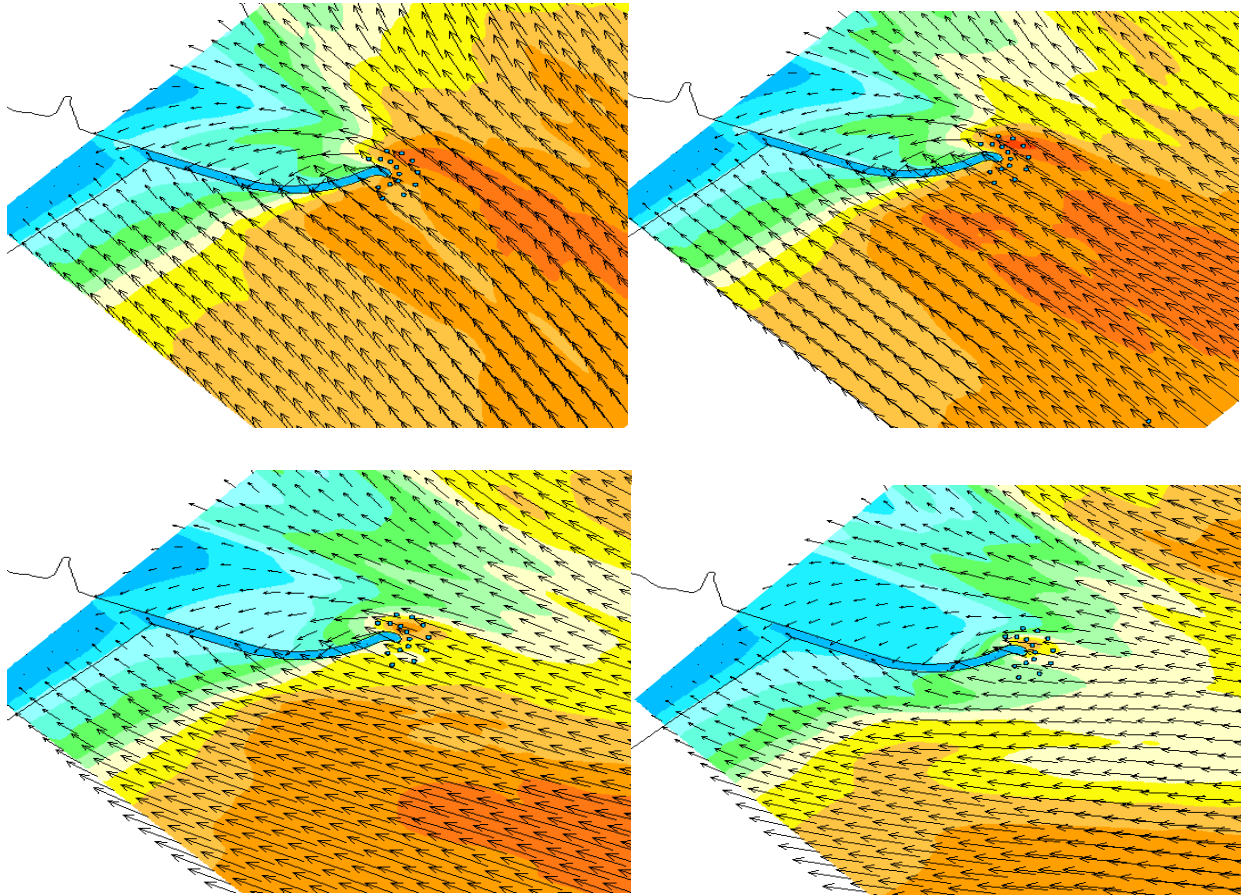


Figure 5.5 – Wave propagation in the surroundings of South Breakwater Head

The wave height has been computed in several locations around the roundhead of the South Breakwater, see Figure 5.6. These results have been used to define the wave characteristics at the location of the roundhead. Table 5.3 presents the design storm for a return period of 100 years.

Table 5.3 – Design storm at breakwater's location

T	H _{m0}	T _p	ϕ
[yr]	[m]	[s]	[°]
100	10.5	17.0	135

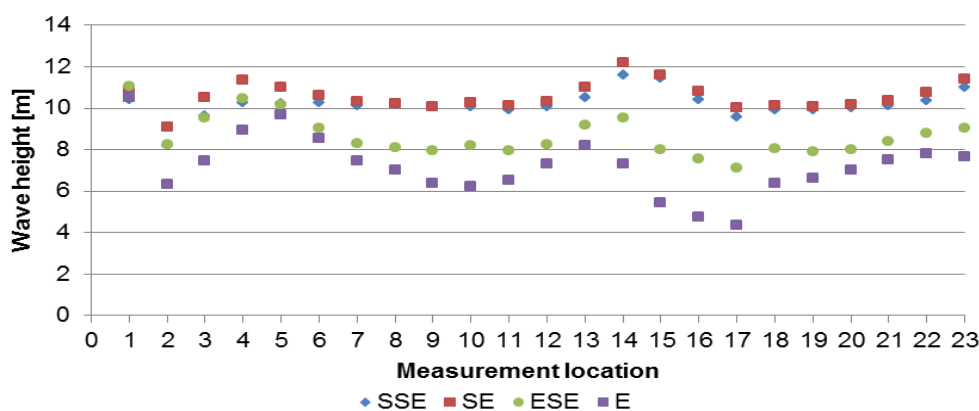
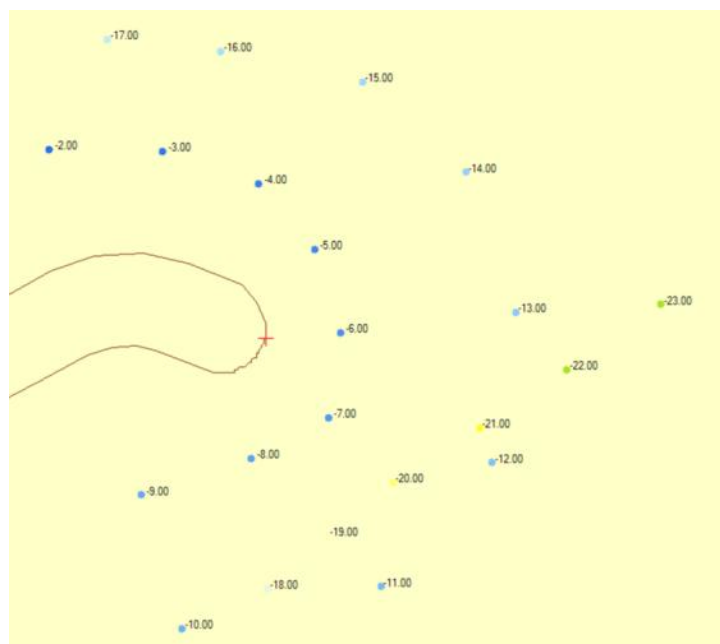


Figure 5.6 – Estimated wave heights in various locations near the roundhead

5.2.3. Design water levels

The design water level in the near shore is estimated by adding to the height of the astronomical tide the effect of sea level rise and storm surge. However, since the design of the repair works considered an extreme event with an occurrence probability of 63%, the design storm can occur with the actual water levels (without sea level rise effect). Therefore, the design water levels are determined in both scenarios: with and without the sea level rise effect.

Moreover, due to the cyclic character of the tides, the extreme storm event can occur either with spring tide or neap tide. Nevertheless, the design of the repair works would be determined for the worst case scenario. This means that the storm surge coincides with the spring tide and sea level rise effect, even though the joint probability of both phenomena occurring at the same time is small. As a result future repair works would not be undertaken so often.

Table 5.4 presents the calculated design water levels relative to Chart Datum without the effect of sea level rise, while in Table 5.5 the effect of sea level is taken into account. The next sections describe the followed process to determine each component of the design water level.

Table 5.4 – Design water levels relative to Chart Datum

T	HAT	H _{storm surge}	DWL _{HW}	LAT	H _{storm surge}	DWL _{LW}
[yr]	[m]	[m]	[m]	[m]	[m]	[m]
1	2.25	1.22	3.47	0.00	1.22	1.22
5	2.25	1.48	3.73	0.00	1.48	1.48
10	2.25	1.60	3.85	0.00	1.60	1.60
20	2.25	1.75	4.00	0.00	1.75	1.75
50	2.25	1.99	4.24	0.00	1.99	1.99
100	2.25	2.23	4.48	0.00	2.23	2.23

Table 5.5 – Design water levels relative to Chart Datum with Sea Level Rise

T	HAT	H _{storm surge}	SLR	DWL _{HW}	LAT	H _{storm surge}	SLR	DWL _{LW}
[yr]	[m]	[m]	[m]	[m]	[m]	[m]	[m]	[m]
1	2.25	1.22	0.003	3.47	0.00	1.22	0.003	1.22
5	2.25	1.48	0.043	3.77	0.00	1.48	0.043	1.52
10	2.25	1.60	0.094	3.95	0.00	1.60	0.094	1.70
20	2.25	1.75	0.194	4.20	0.00	1.75	0.194	1.95
50	2.25	1.99	0.496	4.73	0.00	1.99	0.496	2.48
100	2.25	2.23	1.000	5.48	0.00	2.23	1.000	3.23

5.2.3.1. Tides

The water level data at Durban, which is located a few km southwards of Richards Bay Port, is applied to estimate the elevations at the breakwaters location. Due to the proximity between the two places the tidal behaviour between both can be considered similar. Therefore, the water level data from Durban can be used in this research. These data was obtained from the website <http://tbone.biol.sc.edu/tide/tideshow.cgi?site=Durban%2C+South+Africa>. Figure 5.7 shows results of the water level measurement at Durban.

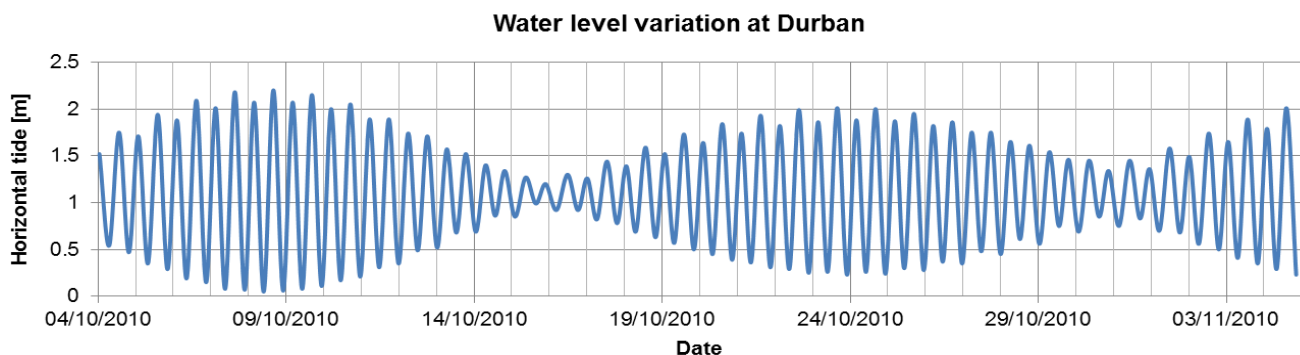


Figure 5.7 – Water level variation at Durban. Semidiurnal tide

From Figure 5.7 it can be drawn that the tidal behaviour in this part of the coast is semidiurnal. This means that there will be two high water levels and two low water levels per day. To identify the water levels that comprise a tidal chart, the higher and lower components are separated and they are presented in Figure 5.8.

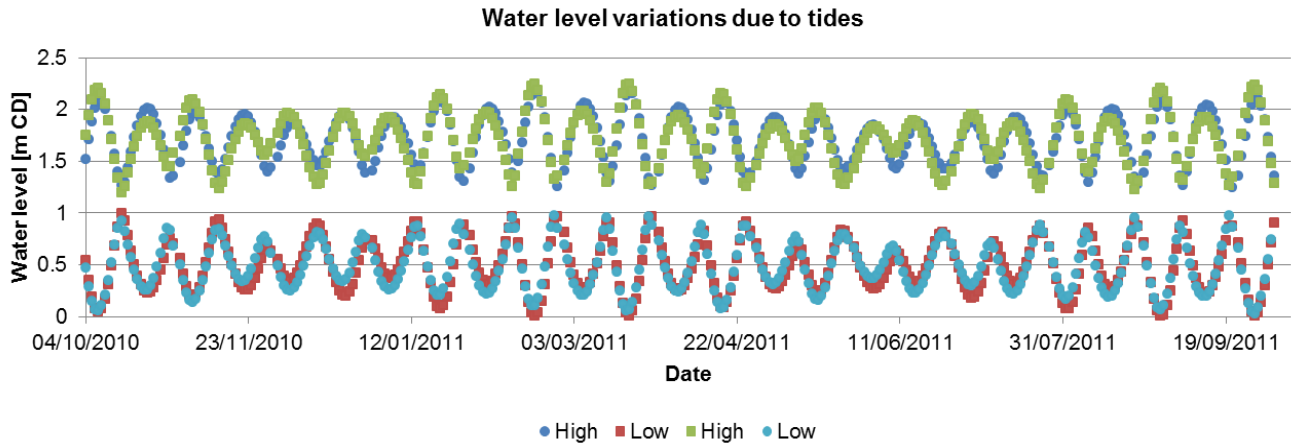


Figure 5.8 – Water level components variation at Durban

Table 5.6 presents the tidal chart of water levels that apply in Richards Bay.

Table 5.6 – Tidal chart at Richards Bay

HAT	2.25	[m]
MHHW	1.75	[m]
MHW	1.70	[m]
MSL	1.13	[m]
MLW	0.50	[m]
MLLW	0.46	[m]
LAT	0.00	[m]

5.2.3.2. Storm surge

Any storm surge consists of three components, which can separately be determined by applying simple equations:

- **Wave set-up:** describes the effect of water level variation as a result of waves approaching the shore. Goda developed a method to estimate the increase of water level due to wave set-up [GODA, 2000]. The expression derived by Goda can be simplified as:

$$H_{\text{wave}} = W_s \cdot H_0 = W_s \cdot K_r \cdot H_s^{\text{dw}+\text{CC}} \quad \text{Wave set-up approach by Goda} \quad [5.1]$$

Here, H_{wave} is the increase in water level due to wave set-up; W_s represents the wave set-up factor, which depends on the wave height, period and direction; K_r is the refraction coefficient and $H_s^{\text{dw}+\text{CC}}$ stands for the significant wave height in deep water modified according to climate change predictions.

Table 5.7 summarizes the estimation of wave set-up for various return periods.

Table 5.7 – Wave set-up estimation [GODA, 2000]

T	K_r	H_s^{buoy}	H_s^{dw} (H_s^{buoy}/K_r)	H_s^{dw+CC} ($f_{cc} \cdot H_s^{dw}$)	H_0' ($K_r \cdot H_s^{dw+CC}$)	W_s	H_{wave}
[yr]	[-]	[m]	[m]	[m]	[m]	[-]	[m]
1	0.91	5.1	5.68	5.68	5.51	0.14	0.77
5	0.91	6.6	7.30	7.33	7.11	0.14	1.00
10	0.91	7.3	8.12	8.19	7.95	0.14	1.11
20	0.91	8.1	9.00	9.17	8.90	0.14	1.25
50	0.91	9.2	10.26	10.77	10.44	0.14	1.46
100	0.91	10.2	11.28	12.41	12.04	0.14	1.69

- **Pressure set-up:** takes into account the effect of local atmospheric pressure on the water level. The pressure set-up is determined by using the inverse barometer approximation which relates for every 1hPa (mbar) decrease in the atmospheric pressure to an increase of about 1cm [CIRIA, 2007].

$$H_{pressure} = \frac{(P_{ave} - P_{obs}) \cdot C}{100} \quad \text{Pressure set-up} \quad [5.2]$$

Here, $H_{pressure}$ represents the increase in water level due to pressure set-up; P_{ave} is the average sea pressure; P_{obs} stands for the observed sea pressure and C is a pressure constant that equals to 1.

The results for pressure set-up are presented in Table 5.8.

Table 5.8 – Pressure set-up estimation

T	P_{ave}	P_{obs}	$H_{pressure}$
[yr]	[mbar]	[mbar]	[m]
1	1013	980	0.33
5	1013	980	0.33
10	1013	980	0.33
20	1013	980	0.33
50	1013	980	0.33
100	1013	980	0.33

- **Wind set-up:** considers how the local wind affects the water elevation. Wind set-up is caused by the shear stress that the wind blowing exerts on the sea surface. The following expression is used to determine the wind set-up [CIRIA, 2007].

$$H_{wind} = f \cdot C_D \cdot \frac{\rho_{air}}{\rho_w} \cdot \frac{u_w^2}{g \cdot h} \cdot F \cdot \cos(\phi) \quad \text{Wind set-up} \quad [5.3]$$

Here, H_{wind} is the increase in water level due to wind set-up; f stands for the type of coast factor (0.5 for open coast and 1 for closed coast); C_D represents the air/water drag coefficient (varies between $0.8 \cdot 10^{-3}$ and $3 \cdot 10^{-3}$, the value of $2 \cdot 10^{-3}$ is taken in this research); ρ_{air} and ρ_{water} are the air and water densities, respectively; u is the wind velocity, which was obtained from an

extreme statistical analysis of wind speed data (see Appendix A.2); h represents the water depth; F stands for the fetch length, which is limited to 300km due to the cutoff lows characteristics in the region; and ϕ is the approach angle to the coast.

The wind set-up calculations are summarized in Table 5.9.

Table 5.9 – Wind set-up estimation

T	U_w	U_w^{CC}	H_{wind}
[yr]	[m/s]	[m/s]	[m]
1	27.3	30.1	0.12
5	30.7	33.8	0.15
10	31.7	34.9	0.16
20	33.3	36.6	0.18
50	35.1	38.6	0.20
100	36.5	40.1	0.21

The storm surge is therefore the sum of the water levels obtained for the wave set-up, pressure set-up and wind set-up. Table 5.10 shows the storm surge water levels for each return period considered.

Table 5.10 – Storm surge

T	H_{wave}	$H_{pressure}$	H_{wind}	$H_{storm\ surge}$
[yr]	[m]	[m]	[m]	[m]
1	0.77	0.33	0.12	1.22
5	1.00	0.33	0.15	1.48
10	1.11	0.33	0.16	1.60
20	1.25	0.33	0.18	1.75
50	1.46	0.33	0.20	1.99
100	1.69	0.33	0.21	2.23

5.2.3.3. Sea Level Rise

Climate change is affecting the inshore water levels amongst other features, the phenomenon associated to the increasing water levels is known as Sea Level Rise (SLR). Recent observations from satellites, have set that the global SLR rate over the last decade has been $+3.3 \pm 0.4$ mm/year. Comparisons between 30 years of South African tide records show that the local SLR is in agreement with the global rate. For instance, the SLR is $+2.74$ mm/year for the South African East Coast, where Richards Bay is located [THERON, 2011].

Several researchers have provided various SLR scenarios for the water levels in 2100. Their SLR projections comprise a wide range of values, which are found between 0.5m and 2m. In this research, a value of 1m is considered for the SLR by 2100. The water levels predicted according to the SLR rates and this particular projection are summarized in Table 5.11.

Table 5.11 – Sea Level Rise

T	SLR
[yr]	[m]
1	0.003
5	0.043
10	0.094
20	0.194
50	0.496
100	1.000

Moreover, due to the uncertainties of these predictions, there is a considerable risk that any of the projected scenarios occurs in the future. Therefore, the design of the repair works should be carried out to be easily adapted to any future scenario.

5.3. Design of the repair alternatives

The design of the repair works involves the analysis of the current state of the breakwater roundhead and the proposal of various repair alternatives. Since this section is fairly damaged, two different repair methods will be considered to restore its initial state. The first method comprises the superposition of a new armour layer above the existing layers (covering alternative) while the second method will replace the damaged armour layer with a new armour layer (replacing alternative). Several concrete armour units are taken into account for the repair designs, such as dolos, antifer cubes, Core-Loc and Xbloc, whose size is estimated according to the new design conditions defined in section 5.2 for a return period of 100 years.

The equations applied to determine the armour unit dimensions were discussed in section 3.3. Hudson stability formula (equation [3.3]) has been used to calculate the required size of dolos, Core-Loc and Xbloc. The stability factor K_D corresponds to the head section and Table 3.10 shows the appropriate K_D -values for each armour unit. The antifer cube size was estimated using the equation [3.8].

Table 5.12 summarizes the required armour unit sizes for the repair works.

Table 5.12 – Armour unit sizes

Armour unit	Design formula	Stability number	Nominal diameter	Unit size
		[-]	[m]	[ton]
Dolos	Hudson	3.1748	2.47	36.0
Antifer cubes	Chegini et al.	2.9792	2.63	43.5
Core-Loc	Hudson	2.9625	2.64	44.3
Xbloc	Hudson	2.9625	2.64	44.3

The two generations of Accropode have not been chosen as possible repair armour units because (1) they cannot interlock with the remaining dolosse (covering alternative case) and (2) their placement is not as easy as other single-layer armour units (Core-Loc and Xbloc).

Due to the increase in size of the armour units and the width of the cross-section, the construction of a new toe is required. Equations [3.12] and [3.13] are used to estimate the new toe protection.

Table 5.13 presents the results of the new toe protection size considering the worst design water level that corresponds to the lowest tide.

Table 5.13 – Toe design for the covering alternative

DWL _{LW}	Bed level	h	Toe level	h _t	h _t /h	H _s	h _t /H _s	N _s	D _{n50}	h _t /D _{n50}	W ₅₀
[m]	[m]	[m]	[m]	[m]	[-]	[m]	[-]	[-]	[m]	[-]	[ton]
3.23	-18.5	21.73	-12.5	15.73	0.72	10.5	1.498	5.0942	1.30	12.10	5.8

The underlayer may require a new design to accommodate and ensure the stability of the new armour layer. However, this will depend on the considered repair method.

Other features to take into account during the design stage are the layer thickness and the required number of units or total volume of units per layer, which must be quantified to assess the costs of the repair works. The layer thickness is related to the number of layers in which the units are placed, the size of the unit itself and the layer coefficient, while the required number of units is based on the placement packing density, the number of layers and the geometry of the roundhead. The following expressions are applied to estimate the layer thickness, packing density and number of units per surface of cross-sectional area [CHL, 2006]:

$$r = n \cdot k_{\Delta} \cdot D_{n50} = n \cdot k_{\Delta} \cdot \left(\frac{W_a}{\rho_a}\right)^{1/3} \quad \text{Layer thickness} \quad [5.4]$$

$$\phi = n \cdot k_{\Delta} \cdot \left(1 - \frac{P}{100}\right) \quad \text{Packing density} \quad [5.5]$$

$$\frac{Nr}{A} = \frac{\phi}{D_{n50}^2} = n \cdot k_{\Delta} \cdot \left(1 - \frac{P}{100}\right) \cdot \left(\frac{\rho_a}{W_a}\right)^{2/3} \quad \text{Number of units per cross-sectional area} \quad [5.6]$$

Here, n represents the number of layers, k_Δ is the layer coefficient, Φ is the packing density, P is the cover layer average porosity.

Table 5.14 summarizes the obtained values of layer thickness, packing density and number of units per surface of cross-sectional area for each armour unit.

Table 5.14 – Layer thickness, packing density and number of units per area

Armour unit	n	k _Δ	P	Φ	W _a	ρ _a	r	Nr/A	m ³ concrete / m ² breakwater
[-]	[-]	[-]	[%]	[-]	[ton]	[t/m ³]	[m]	[units/m ²]	
Dolos	2	0.94	56.00	0.83	36	2.4	4.64	0.136	2.04
Antifer cubes	2	1.10	47.00	1.17	44	2.4	5.80	0.168	3.08
Core-Loc	1	1.51	60.15	0.60	45	2.4	4.01	0.085	1.59
Xbloc	1	1.40	58.70	0.58	45	2.4	3.72	0.082	1.54

5.3.1. Covering alternative

This design option consists of covering the remaining 30-tonne dolosse with a double layer of 36-tonne dolosse, a double-layer of 44-tonne antifer cubes or a single-layer of 45-tonne Core-Loc. The first option involves the placement of larger dolos that should be stable enough to withstand the new design loads. This repair alternative follows the repair works applied in the past at the very same location. The second option is similar to the repair works carried out in the rehabilitation of Durban's port, where the dolosse were smashed to create an appropriate slope before the placement of antifer cubes. In the third option, the Core-Loc units are directly placed on top of the dolosse layer to ensure a good interlocking between both units. The remaining dolos layer will act as an underlayer for the new armour layer, leading to a reduction in construction costs compared to other alternatives.

Besides, Xbloc is not considered in this repair alternative because (1) it cannot interlock easily with the remaining dolosse due to its shape and (2) requires a flat slope to ensure an appropriate placement.

Figure 5.9, Figure 5.10 and Figure 5.11 show a sketch of the covering repair alternatives taking into account the geometric design guidelines [CHL, 2006].

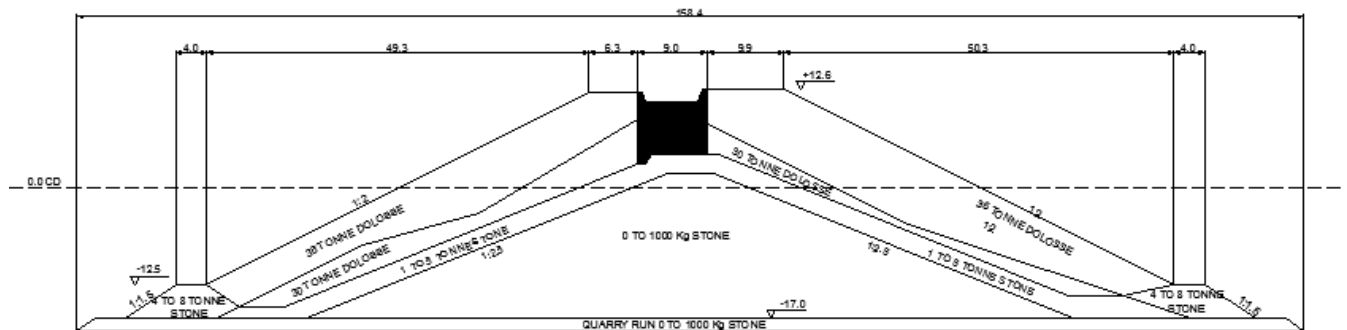


Figure 5.9 – Dolos cover layer alternative

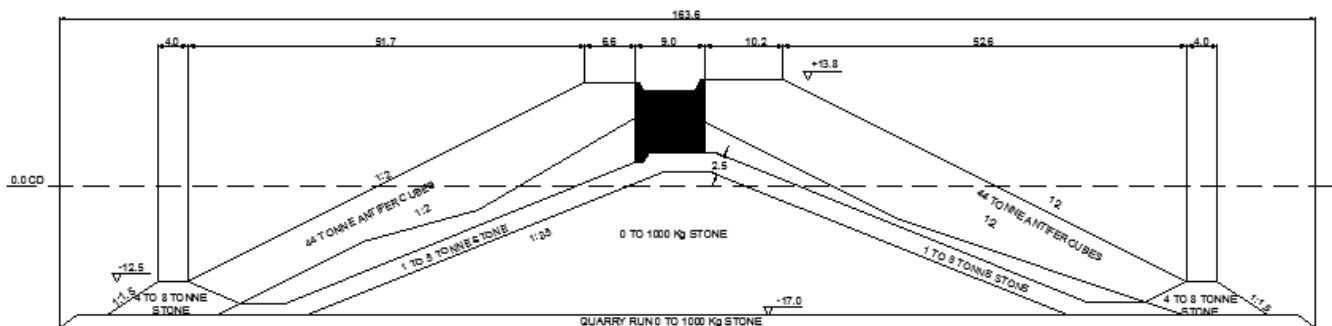


Figure 5.10 – Antifer cubes cover layer alternative

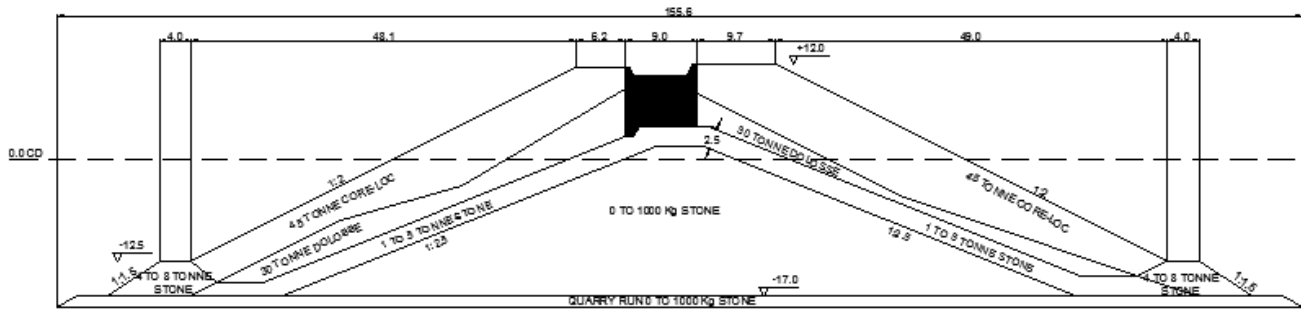


Figure 5.11 – Core-Loc cover layer alternative

The total number of required units for this repair alternative is presented in Table 5.15.

Table 5.15 – Required number of antifer cubes and Core-Loc for the covering alternative

Armour unit [-]	r [m]	Nr/A [units/m ²]	A [m ²]	Nr [units]
Dolos	4.64	0.136	6007	2034
Antifer cubes	5.80	0.168	6634	2625
Core-Loc	4.01	0.085	5808	695

It should be noticed that the covering surfaces vary between types of armour unit due to the required layer thickness (r) of each unit, even though the damage area is identical for each alternative. This phenomenon occurs in all the considered repair alternatives, see next sections as well.

5.3.2. Replacement alternative

This repair alternative consists of removing the remaining 30-tonne dolosse from the roundhead and placing a new armour layer, which can involve the same or different types of armour units. Therefore, different design options can be compared in this section, including both single- and double-layer armouring. Larger dolos, antifer cubes, Core-Loc and Xbloc are considered as armour units for the repair works.

5.3.2.1. Double-layer option

This option comprises the replacement of the damaged 30-tonne dolosse by either 36-tonne dolosse or 44-tonne antifer cubes, both placed in a double-layer. The first armour unit should behave identically to the lighter dolosse, however should be stable enough to withstand the new wave conditions. The second armour unit provides a large structural ability and is stable because of its own weight. Both units are subjected to more rocking, which results in a higher risk of impact loads and breakage. This alternative is less economical than other options due to higher construction costs derived from the large amount of armour units to build and the removal of the initial armour layer.

Since the size of the armour units has increased, the existing underlayer cannot fulfil the filter requirements and a new underlayer should be constructed. Equation [3.10] is applied to estimate the size of the new underlayer. Table 5.16 shows the results for the underlayer.

Table 5.16 – Stone size for the underlayer for the double-layer armouring

Armour unit		Underlayer			
Type	W_a	$W_a/15$	$W_a/10$	W_u	Rock-class
[-]	[ton]	[ton]	[ton]	[ton]	[-]
Dolos	36	2.4	3.6	3.0	3-6 ton
Antifer cube	44	2.93	4.4	3.7	3-6 ton

The sketches of the double-layer armour repair alternative with 36-tonne dolosse and 44-tonne antifer cubes are presented in Figure 5.12 and Figure 5.13, respectively. It should be noted that the underlayer rock class have been modified to reduce the required number of material classes and its corresponding costs of stock.

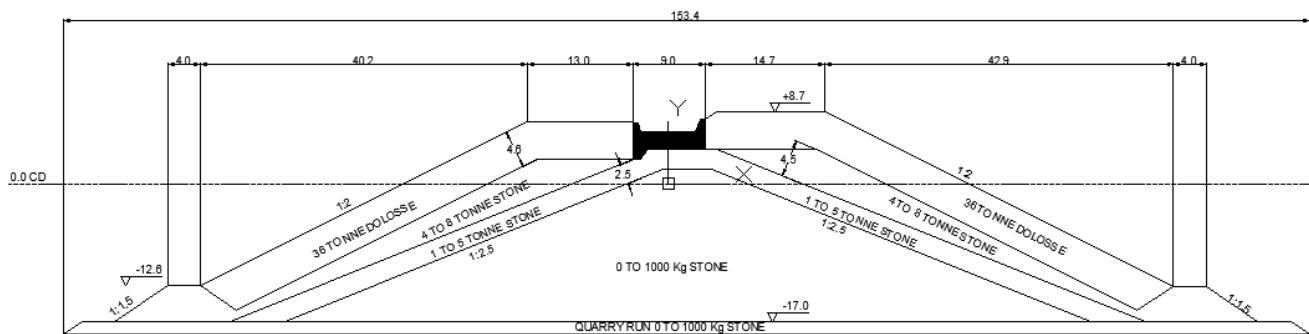


Figure 5.12 – Double-layer of 36-tonne dolosse for the replacing alternative

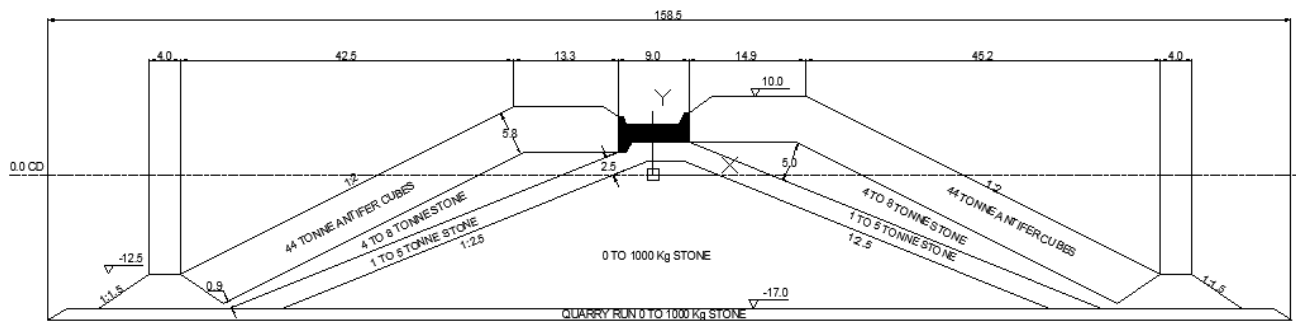


Figure 5.13 – Double-layer of 44-tonne antifer cubes for the replacing alternative

The total number of required armour units for this repair option is summarized in Table 5.17

Table 5.17 – Required number of armour units for the double-layer replacement alternative

Armour unit	r	Nr/A	A	Nr
[-]	[m]	[units/m ²]	[m ²]	[units]
Dolos	4.64	0.136	6239	2097
Antifer cubes	5.80	0.168	6785	2676

5.3.2.2. *Single-layer option*

This option consists of the replacement of the damaged 30-tonne dolosse by either 45-tonne Core-Loc or 45-tonne Xbloc, both placed in a single-layer. Both units have a bulky shape that provides not only good interlocking but also structural strength. However, rocking between units is expected leading to higher risk of breakage. This alternative is less economical than the cover option due to higher construction costs derived from the large amount of armour units to build and the chosen repair method.

The existing underlayer cannot fulfil the filter requirements due to the increase of the armour unit size. Thus a new underlayer should be constructed. Equation [3.10] is applied to estimate the size of the new underlayer. Table 5.18 shows the results for the underlayer.

Table 5.18 – Stone size for the underlayer for the single-layer armouring

Armour unit		Underlayer			
Type	W_a	$W_a/15$	$W_a/10$	W_u	Rock-class
[-]	[ton]	[ton]	[ton]	[ton]	[-]
Core-Loc	45	3	4.5	3.75	3-6 ton
Xbloc	45	3	4.5	3.75	3-6 ton

The sketches of the single-layer armour repair alternative with 45-tonne Core-Loc and 45-tonne Xbloc are presented in Figure 5.14 and Figure 5.15, respectively. It should be noted that the rock class for the underlayer has been modified to reduce the required number of material classes and its corresponding costs of stock.

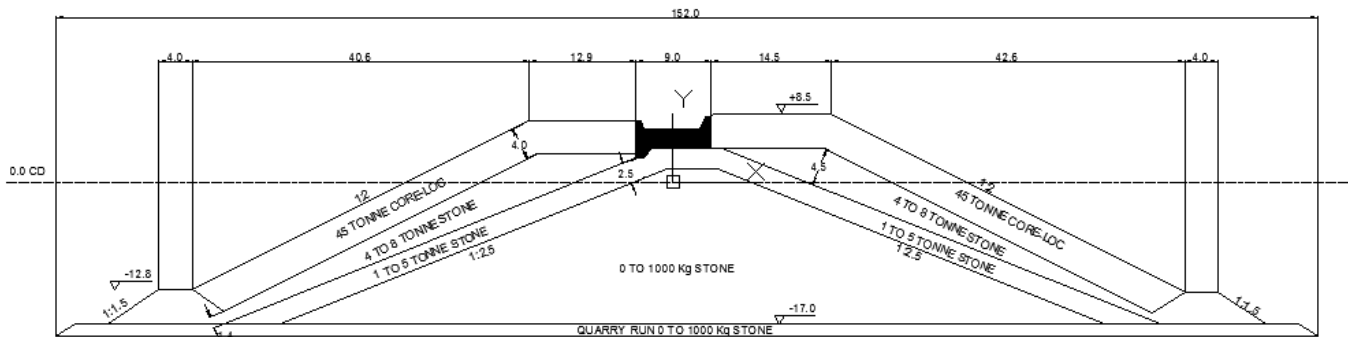


Figure 5.14 – Single-layer of 45-tonne Core-Loc for the replacing alternative

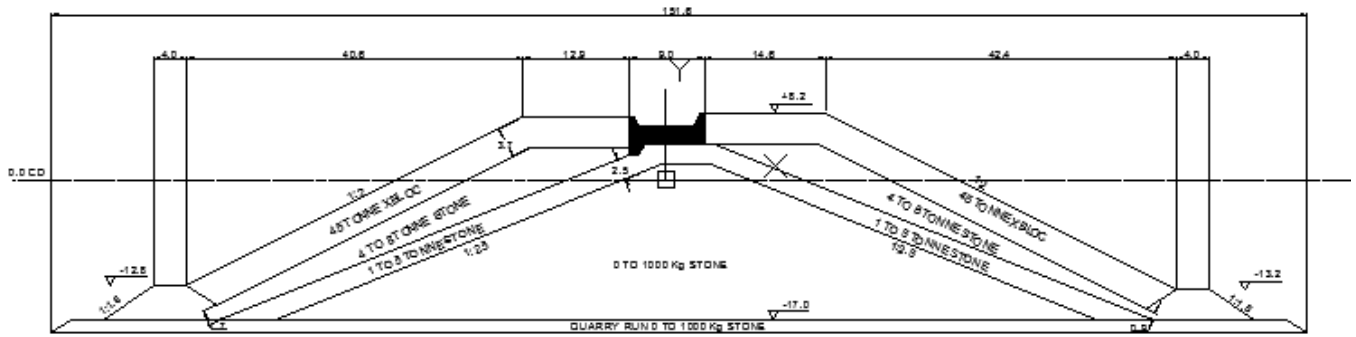


Figure 5.15 – Single-layer of 45-tonne Xbloc for the replacing alternative

The total number of required armour units for this repair option is summarized in Table 5.19

Table 5.19 – Required number of armour units for the single-layer replacement alternative

Armour unit	r	Nr/A	A	Nr
[-]	[m]	[units/m ²]	[m ²]	[units]
Core-Loc	4.01	0.085	6219	730
Xbloc	3.72	0.082	6208	709

6. Model set-up

This chapter focuses on the required theory to design and operate any scaled physical model of a hydraulic structure. Hence, the principles of physical modelling will be discussed, so as the advantages and disadvantages of such models (section 6.1). In section 6.2, the model dimensions of the breakwaters of Richards Bay Port and its design conditions will be scaled according to the explained principles of physical modelling.

6.1. Principles of physical modelling

Physical modelling is based on the idea that the model behaves in a similar way to the prototype that intends to represent. Thus, a validated physical model can be used to predict the prototype's behaviour under a specified set of conditions. However, there is a possibility that the physical model may not represent the prototype behaviour due to scale effects and laboratory effects. To minimize the scale effects, the modeller should understand and apply the adequate similarity relationships, while the laboratory effects are reduced by a careful operation of the model [HUGHES, 2008].

6.1.1. Principle of similitude

Similitude between the real world and small-scale models is achieved when all major influential factors are in proportion between the two systems, while those factors that are not in proportion are so small as to be negligible to the process. The requirements of similitude vary with the problem to be studied and the necessary accuracy in the model to reproduce the prototype's behaviour. For coastal projects with short waves, the similitude is reached when three general conditions are met:

- Geometric similarity: ratios of all corresponding linear dimensions between prototype and model are equal. This relationship is independent of any kind of motion and involves only similarity in form.
- Kinematic similarity: indicates a similarity of motion between particles in the model and prototype. It is achieved when the ratio between the components of all vectorial motions in the two systems is the same for all particles at all times.
- Dynamic similarity: ratios of all masses and vectorial forces in model and prototype are the same. To understand the implication of this similarity, Newton's second law of motion is applied. Newton's Second law equates the vectorial sum of external forces acting on an element to the element's mass reaction to those forces. This similitude is required when the structure capability to resist water velocities and accelerations is studied.

Generally, the requirements for physical modelling similitude are expressed in terms of scaled ratios as:

$$N_X = \frac{X_p}{X_m} = \frac{\text{Value of X in prototype}}{\text{Value of X in model}} \quad [6.1]$$

Here, N_x represents the prototype-to-model scale ratio of the parameter X.

In practice, it is impossible to obtain a perfect similitude, i.e. all the prototype-to-model ratios are identical. Fortunately, in many coastal projects, inertial, viscous and gravitational forces dominate the processes and therefore, the model should be scaled to ensure the similarity of these forces in both systems. This leads to a similitude criterion based on the following dimensionless products:

- **Froude number:** represents the relative influence of inertial and gravity hydraulic flow.

$$F_r = \left(\frac{U}{\sqrt{g \cdot L}} \right)_p = \left(\frac{U}{\sqrt{g \cdot L}} \right)_m \quad [6.2]$$

With $N_U = U_p/U_m$, $N_L = L_p/L_m$ and $N_g = g_p/g_m = 1$, equation [6.2] reduces to:

$$N_U = \sqrt{N_g \cdot N_L} = \sqrt{N_L} \quad [6.3]$$

- **Reynolds number:** expresses the relative importance of the inertial force on a fluid particle to the viscous force on the particle.

$$Re = \left(\frac{\rho \cdot U \cdot L}{\mu} \right)_p = \left(\frac{\rho \cdot U \cdot L}{\mu} \right)_m \quad [6.4]$$

With $N_U = U_p/U_m$, $N_L = L_p/L_m$, $N_\rho = \rho_p/\rho_m = 1$ and $N_\mu = \mu_p/\mu_m = 1$, equation [6.4] is written as:

$$N_U = \frac{N_\mu}{N_\rho \cdot N_L} = \frac{1}{N_L} \quad [6.5]$$

- **Strouhal number:** it is an important dimensionless number in unsteady, oscillating flows where the period of oscillation is given in the temporal variable. The similarity is achieved when the period of oscillation is related to the flow. In case of wave motion, the oscillating period is related to the wave period.

$$\left(\frac{L}{U \cdot t} \right)_p = \left(\frac{L}{U \cdot t} \right)_m \quad [6.6]$$

Gravity forces predominate in free surface flows and, thus most hydraulic models can be designed using the Froude criterion, see section 6.1.3.1. Therefore, the model created for the roundhead of the South Breakwater at Richards Bay Port is Froude-scaled. Moreover, the modeller should reduce the viscosity effects in the model to avoid scale effects by either reducing the length along waves propagate or considering a larger wave height to counteract friction losses.

6.1.2. Advantages of physical modelling

Physical modelling allows faithful reproduction of nonlinearities and complex physical interactions between fluid and structures only if the model has been properly scaled and the laboratory effects are controlled. It also provides an excellent tool to examine processes that still not well understood or cannot adequately be represented by simplified mathematical models.

A list of the physical modelling advantages is presented in [HUGHES, 2008]:

- Physical models incorporate and integrate the fully nonlinear governing equations of the modelled processes without simplifications.
- Complex boundaries and bathymetry can be included.
- Easy data collection.
- Model forcing conditions can easily be simulated.
- Similitude requirements are well understood and easily implemented.

- Visual feedback that allows considering physical process aspects that were previously rejected and understand how changes in the forcing conditions affect the model.
- Optimization of engineering solutions
- Cost-effective option with respect to alternate study methods.

6.1.3. Disadvantages of physical modelling

The physical modelling disadvantages are related to scale effects or laboratory effects. Scale effects occur in reduced models where it is impossible to simulate all relevant variables with adequate prototype-to-model relationships (see section 6.1.3.1). Laboratory effects are caused by an inappropriate operation of the model where all the prototype conditions cannot be properly simulated (see section 6.1.3.2).

6.1.3.1. Scale effects in physical model

When a physical model is scaled using Froude number, gravity is considered as the dominant physical force that balances inertial forces. The other forces (viscosity, elasticity, surface tension, friction, etc.) are incorrectly scaled and may lead to scale effects unless their contribution to the processes is small. These scale effects can be seen as a loss in accuracy in the results obtain through physical modelling. The following scale effects can occur:

- Viscous scale effect. The linear geometric scaling of material diameters that follows from Froude scaling may lead to too large viscous forces corresponding to too small Reynolds numbers. This means that the flow regime around the breakwater armour units of the changes from turbulent in the prototype to laminar in the model. However, this scale effect can be neglected if the Reynolds number relative to the armour unit stability number is greater than $3 \cdot 10^4$ [HUGHES, 1993].

$$R_N = \frac{\sqrt{g \cdot h} \cdot l_a}{\nu} \quad \text{Reynolds number relative to the armour unit stability number} \quad [6.7]$$

The related increase in flow resistance reduces the flow in and out of filter layers and core. This causes relatively larger up-rush and down-rush velocities. As a result run-up levels will be too high and armour stability too low, which leads to safer stability coefficients [BURCHARTH ET AL., 1999]. This is corrected by means of increasing the size of core material than the estimated from geometric length scale. After scaling Reynolds number is calculated to check if the flow in the structure is turbulent, as occurs in the prototype. The viscous scale effects are insignificant when Reynolds number in the core is larger than $2 \cdot 10^3$ [HUGHES, 1993].

- Surface tension scale effect. Surface tension becomes important when the water waves are very short or water depth is very shallow. Le Méhauté presented in 1976 some rules of thumbs to define whether the surface tension is important in physical modelling. These conditions are: (1) wave periods smaller than 0.35 seconds and (2) water depth smaller than 2 cm. The restoring force of surface tension begins to be significant for these parameter values and the model will experience wave motion dampening that does not occur in the prototype [HUGHES, 1993]. Both parameters are considerably large in this research so that the scale effects due to surface tension forces are negligible.

- Friction scale effect. This scale effect is related to bottom friction and internal friction. Bottom friction scale effects are possible in coastal structure models when the wave propagates long distances. However, in most rubble mound breakwater models is not considered because of the relative large length scales used.
Internal friction arises from the contact between adjacent armour units. This type of friction is negligible in prototype rubble mound breakwaters if compared to dominant forces affecting the structure response to wave action. Nevertheless, the frictional forces between units may not be in similitude with the prototype due to differences in armour unit surface roughness between the two systems. To reduce this scale effect, a standard practice is to smooth the model units by painting them, which also helps in the damage assessment.
- Aeration scale effect. This scale effect was studied by Hall in 1990. He conducted several experiments to examine the entrainment and movement of air bubbles pushed into the voids of rubble mound structure models by waves breaking on the structure and by flow separation due to rapid movement of water through armour units. The entrained air bubbles are not in similitude between both systems, which leads to larger energy dissipation in the model. Wave run-up will also be affected by this scale effect.

6.1.3.2. *Laboratory effects in physical model*

Laboratory effects in physical models are caused by an inappropriate operation of the model due to [HUGHES, 2008]:

- Physical constraints on flow caused by the need of representing a portion of the prototype in a finite amount of space. Therefore, the flume walls and wavemaker paddles create model boundaries that do not exist in the prototype. This results in waves reflecting from the boundaries and introducing wave trains into the simulated wave field.
- Mechanical means of wave and current generation may introduce unintentional nonlinear effects. The model engineer should be able to produce mechanical waves as similar as the waves observed in nature.
- Simplification of forcing conditions, where only a subset of all possible conditions is chosen for testing. Generation of unidirectional waves and simulation of storms by using a constant water level are examples of this type of laboratory effect.

6.2. Physical model design

This section deals with the design of the roundhead model for the south breakwater of Richards Bay Port. Descriptions of the modelling facilities, the scale selection and details of the model design are included.

6.2.1. Facilities

6.2.1.1. Wave basin

The physical model experiment programme was conducted in the Hydraulic Laboratory of the Centre of Scientific and Industrial Research at Stellenbosch, South Africa. The basin has a length of 32m; a width of 4m and an available height of 1m (see Figure 6.1).

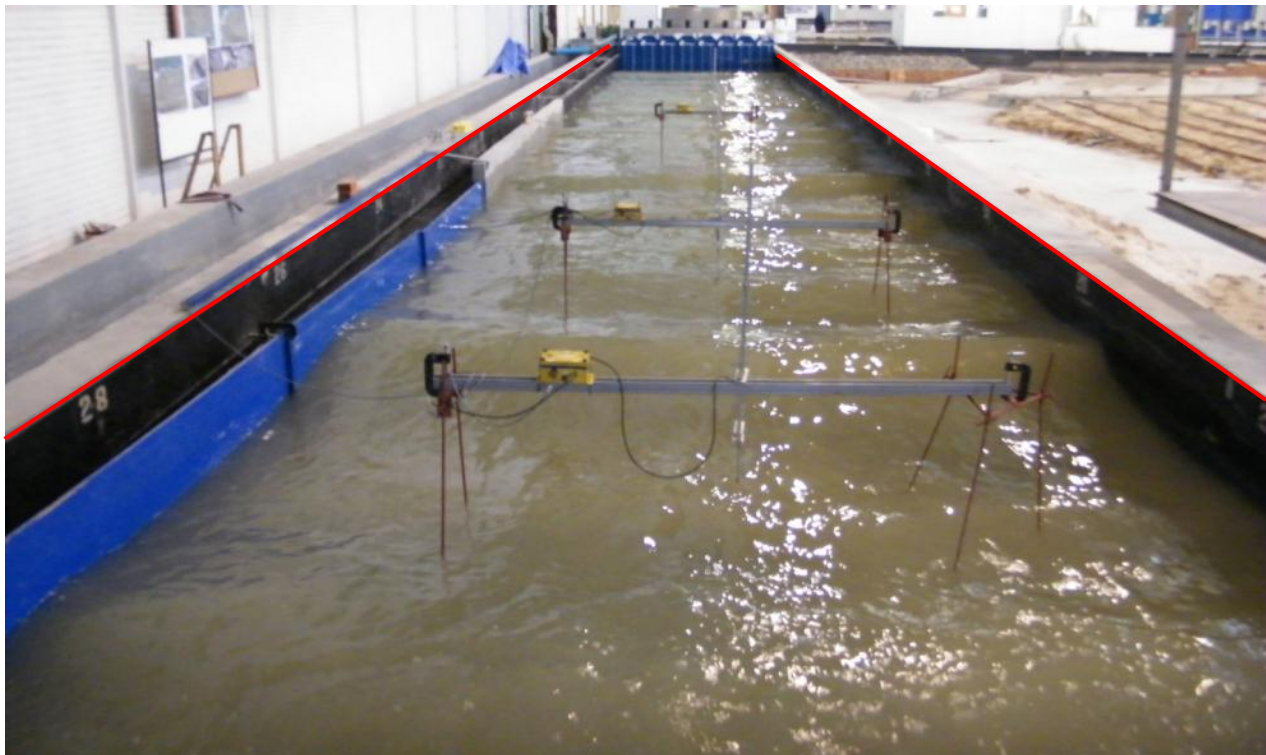


Figure 6.1 – Wave basin

6.2.1.2. Wavemaker

The basin has a multi-element system of wave generation with dynamic wave absorption capabilities. This wavemaker consists of a 4.0m wide module with eight paddles (0.5m wide each) that move horizontally forwards and backwards to generate waves in the basin (see Figure 6.2).

The wavemaker program can generate sinusoidal waves and irregular waves at normal or oblique angles. The wave direction is established by varying the phase between adjacent paddles. The frequency and width of the paddle determine the possible range of wave angles to be generated.

The irregular waves produced by the wavemaker are adjusted to one of the standard spectral shapes, JONSWAP and Pierson-Moskowitz. However, users can establish other spectral definitions by using series of spectral densities separated by a constant frequency increment.

At the South African East coast, the cutoff lows are the main wave generation mechanism. These low pressure systems are time limited, which are related to a fetch limitation. As a result, JONSWAP spectrum can be applied to represent the wave data measured at Richards Bay [ROSSOUW, 2012]. This spectrum allows also the application of directional spreading. However, due to the dimensions of the basin (4m wide), this feature was not applied in this research (see section 6.1.3.2).



Figure 6.2 – Wavemaker

6.2.1.3. *Capacitance wave measurement probes*

The waves in the model were measured with capacitance probes. As the water level varies around the probes, so does the voltage reading. By calibration, the voltage readings are translated into the corresponding water level and simultaneously captured. As a result of the probe output analysis, a time-series of the variation in water surface elevation is provided, from which the wave parameters are estimated.

To record the wave conditions in the model, three single probes were used in the basin. The first probe was located at 6.75m (model distance) from the structure toe. This probe was used as the wave control point. The second probe was placed at 0.35m (model distance) in front of the roundhead toe to measure the wave heights at the sea-side. The last probe was located 0.25m (model distance) behind the roundhead toe to measure the wave heights at the lee-side. The recorded wave data was spectrally analysed by in-house software and the relevant parameters such as significant wave height (H_{m0}), maximum wave height (H_{max}) and peak period (T_p) were derived. The wave probe setup can be seen in Figure 6.3.



Figure 6.3 – Wave probes

6.2.1.4. *Camera equipment*

A total of three digital cameras were used to capture video footage of every test and take pictures before and after of each test condition. These cameras were mounted on tripods at fixed locations to ensure that the video footages were captured at the same positions, see Figure 6.4. Additionally, a digital camera was used to take pictures during the tests from various positions.



Figure 6.4 – Camera equipment

6.2.2. Model scale selection

Several factors are considered in the scale selection for physical models that vary from one modelling application to another. Those factors are [HUGHES, 1993]:

- Size of the facility and wavemakers capability.
- Flow Reynolds number for the proposed scale.
- Experience with similar physical models.
- Parameters to be considered in the model.
- Costs.

In general, large scales are considered uneconomical, while small scales are most likely to suffer larger scale effects. This leads to a compromise solution between costs and technical requirements for similitude. The scale used to analyse the roundhead stability is 1:75, which was determined to avoid the viscous scale effects according to equation [6.7] and to be able to reuse the existing model units at the laboratory.

6.2.3. Model design

The design of the model involves the downscaling of all the design features according to the discussed similitude theory in section 6.1 to ensure its construction. This paragraph presents the downscaling results for the seabed profile, breakwater geometry, construction materials and wave climate and water level conditions.

6.2.3.1. Seabed profile

A transitional slope of 1:15, which extends a length of about 4.5m, is built inside the basin to connect deep water with shallower water close to Richards Bay breakwaters. Thereafter, the provided bathymetry is downscaled and constructed along the next 20m of the basin. The last 3m are used to construct a gravel beach that will absorb the remaining wave energy.

Figure 6.5 shows a sketch of the seabed profile to be constructed in the basin related to the basin floor.

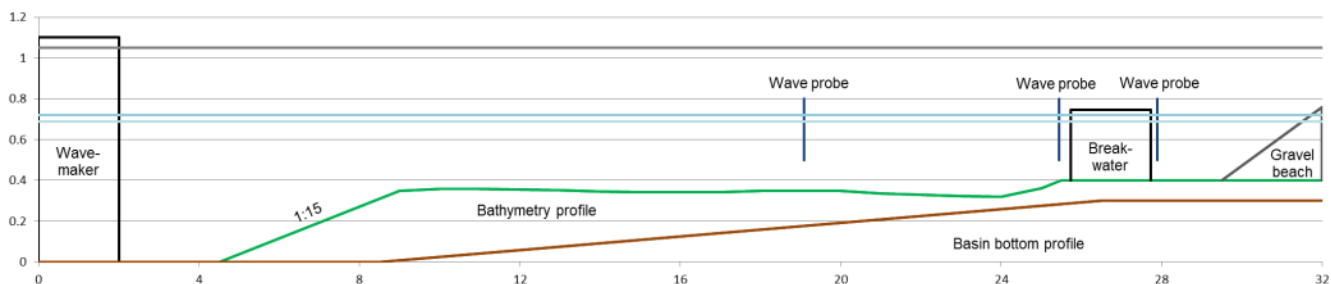


Figure 6.5 – Seabed profile in the basin

6.2.3.3. Construction material of the breakwater

The material used in the construction of the breakwater is scaled according to Froude criterion, which assures that the gravity forces are properly scaled.

Since the design of the units is based on their hydraulic stability, the stability number $H_s/(\Delta \cdot D_{n50})$ is applied in the scaling of the material. This number should be the same in both prototype and model. Thus, the scaling of the unit sizes in the model is adjusted with respect to deviations in the relative density between model and prototype. A scale length $\lambda=1:75$ has been applied for the breakwater model, and the unit sizes can be determined by:

$$D_{n50,m} = \lambda \cdot D_{n50,p} \cdot \frac{\Delta_p}{\Delta_m} \tag{6.8}$$

By using the relation between unit mass and unit size, $W = \rho_a \cdot \Pi \cdot D_{n50}^3$, the previous equation is simplified as:

$$W_m = \lambda^3 \cdot \frac{\rho_m}{\rho_p} \cdot W_p \cdot \left(\frac{\Delta_p}{\Delta_m}\right)^3 \tag{6.9}$$

The indices m and p refer to model and prototype, respectively.

Equation [6.9] has been applied to scale the materials used in the breakwater construction except the core. The armour layer is built using concrete units whereas graded rock is applied in the construction of the underlayers and toe protection (see Appendix B. Material properties).

- **Armour layer:** concrete units have been used in the construction of the breakwater armour layer. The considered mass density of the armour units and the water in the prototype structure is 2400 kg/m³ and 1025 kg/m³, respectively. Such densities are 2350 kg/m³ and 1000 kg/m³ in the model case. Therefore, the relative density for prototype and model is 1.34 and 1.35, respectively. This leads to a total scale factor for the armour unit size of $\lambda=1:77.08$. Table 6.1 lists the required armour unit characteristics for the construction of the various models including the available number of units in the laboratory.

Table 6.1 – Armour unit specifications for the model

Armour unit	Material	Number units	Nominal size	Mass	Density
[-]	[-]	[-]	[mm]	[g]	[kg/m ³]
Dolos	Polypropylene, barium sulphate and Sasol	2163	32.7	82	2350
Antifer cubes		2224	34.9	100	2350
Core-Loc	wax	800	35.2	102	2350

- **Underlayer:** graded rock has been applied in the construction of the breakwater underlayer. The considered mass density of the rock is 2650 kg/m³ in both prototype and model, while the mass density of the water is 1025 kg/m³ and 1000 kg/m³ in prototype and model, respectively.

Hence, the relative density for prototype and model is 1.59 and 1.65, respectively. As a result, the total scale factor for the graded rock of the underlayer is $\lambda=1:78.06$.

The graded rock specifications are summarized in Table 6.2.

Table 6.2 – Graded rock specifications for the underlayer

Graded rock (1 to 5 tonnes)		ELL	NLL	M50	NUL	EUL
Prototype	Weight [kg]	700	1000	2300	5000	6500
Model	Weight [g]	1.5	2.1	4.8	10.5	13.7

- Toe protection: graded rock has been applied in the construction of the breakwater toe protection. The considered mass density of the rock is 2650 kg/m^3 in both prototype and model, while the mass density of the water is 1025 kg/m^3 and 1000 kg/m^3 in prototype and model, respectively. Thus, the relative density for prototype and model is 1.59 and 1.65, respectively. As a result, the total scale factor for the graded rock of the toe protection is $\lambda=1:78.06$.

The graded rock specifications are summarized in Table 6.3.

Table 6.3 – Graded rock specifications for the toe protection

Graded rock (4 to 8 tonnes)		ELL	NLL	M50	NUL	EUL
Prototype	Weight [kg]	2500	4000	5800	8000	10000
Model	Weight [g]	5.3	8.4	12.2	16.8	21.0

Quarry run with grading 200 to 1000 kg is used as core material. The required rock grading has been estimated using the Burcharth scaling method for the core [BURCHARTH ET AL., 1999]. This scaling method takes into account the flow within the breakwater layers. As a result, larger core material is applied in the model than using Froude criterion. Detailed information about the rock grading is provided in Table 6.4.

Table 6.4 – Graded rock specifications for the core

Graded rock (300 to 1000 kg)		ELL	NLL	M50	NUL	EUL
Prototype	Weight [kg]	200	300	600	1000	1500
Model	Weight [g]	1.4	2.1	4.2	6.9	10.4

6.2.3.4. *Wave climate conditions*

The experiments were performed with irregular waves based on the observed wave field at Richards Bay buoy during 30 years. The South Easterly direction of wave incidence was considered because it provided the most severe condition for the stability of the structure, see section 5.2.2.

The wave characteristics at the buoy location were used as the target conditions because the model control point was placed in an identical depth as the buoy. Therefore, those values were downscaled according to Froude similitude criterion using a scale factor of 1:75.

Test durations were estimated taking into account the number of waves that attack the structure, the time that the wavemaker needs to generate the specified wave conditions and the time that the waves require to reach the control point. Since the lapse of time between wave observations at Richards Bay buoy is 3 hours, the storm duration was set as 3 hours to provide a good representation of the measured waves during the tests. Then, the number of incident waves reaching the structure for such storm duration is approximated to 1000 waves. Moreover, the wavemaker requires 20 seconds (model scale) to generate the specified wave conditions and the wave travelling time is about 60 seconds (model scale) to reach the control point.

Table 6.5 presents the downscaled wave characteristics at the model control point, considering only those return periods that were tested.

Table 6.5 – Design storms at the model control point

T	H_{m0}	T_p	T_z	T_{storm}	T_{waves}	T_{measurement}	T_{measurement}
[yr]	[mm]	[s]	[s]	[s]	[s]	[s]	[min]
1	68	1.57	1.26	1256	1336	1516	25.3
10	107	1.76	1.40	1404	1484	1664	28.0
50	136	1.91	1.52	1524	1784	1784	30.0
100	149	1.96	1.57	1570	1830	1830	31.0
Overload¹	179	1.96	1.57	1570	1830	1830	31.0

¹ The overload consists of increasing the 100-year return period significant wave height by a 20%. This significant wave height belongs to a 375-year return period and is only feasible with high design water levels.

Since the wave data recorded by the buoy at Richards Bay location belongs to an irregular wave field, the best way to describe such data is by means of a variance-density spectrum. This spectrum provides a statistical description of the wave height variation caused by wind. A lot of research has been carried out to predict and generate realistic wave fields. During the 1970s, a large field experiment conducted in the North Sea resulted in the JONSWAP-spectrum definition. Such a spectrum represents a non-fully developed sea, which has a fetch limitation of about 100km (see section 6.2.1.2). The JONSWAP-spectrum is commonly used for all sorts of laboratory tests, allowing an easy access and comparison of the obtained data. Its expression was generated by modifying the Pierson-Moskowitz spectrum with a peak-enhancement function, resulting in the equation [6.10] [HOLTHUIJSEN, 2007]:

$$E_{\text{JONSWAP}}(f) = \alpha \cdot H_s^2 \cdot f_{\text{peak}}^4 \cdot f^5 \cdot \exp\left\{\frac{5}{4} \cdot \left(\frac{f}{f_{\text{peak}}}\right)^{-4}\right\} \cdot \gamma \cdot \exp\left\{\frac{1}{2} \cdot \left(\frac{f-f_{\text{peak}}}{\sigma \cdot f_{\text{peak}}}\right)^2\right\} \quad [6.10]$$

Where α is the energy scale parameter, γ and σ are shape parameters and f_{peak} is the frequency scale parameter. The values for the JONSWAP-spectrum parameters used in this research were: $\alpha=0.229$; $\gamma=2.5$; and $\sigma=0.07$ for $f \leq f_{\text{peak}}$ and $\sigma=0.09$ for $f > f_{\text{peak}}$.

6.2.3.5. *Water level conditions*

Two water level conditions were set up for each considered storm. One related to low water levels whereas the other is related to high water levels. By conducting such experiments, it is intended to analyse the effects of the storms in both sides of the breakwater head (sea- and lee-side). The water levels were downscaled according to Froude similitude criterion by a scale factor of 1:75.

Table 6.6 presents the water levels at the structure to be applied in the model, considering only those return periods to be tested.

Table 6.6 – Design water levels for the model in front of the structure

T	DWL_{HW}	DWL_{LW}
[yr]	[mm]	[mm]
1	293	263
10	299	269
50	310	280
100	320	290
Overload	320	-

7. Experimental process

The experimental process comprises four phases: (1) calibrating the probes and wavemaker, (2) constructing the models, (3) testing each model and (4) analysing the measured data. All these parts will be discussed in the following sections.

7.1. Probe and wavemaker calibration

The probe calibration was used to set up the relationship between the water surface elevation and the voltage signals read by the equipment. Thereafter, every time the water level was modified, the capacitance probes were readjusted and their voltage readings were reset.

The wave conditions and water levels for the tests were specified in section 6.2.3.4 and 6.2.3.5. The irregular wave field was described with a JONSWAP spectrum and was used as the input signal for wave generation. The water level and wave parameters, which were calibrated in prototype values, are summarized in Table 7.1.

Table 7.1 – Wave calibration

Test	Calibration	Water level at wavemaker DWL [m CD]	Target wave		JONSWAP	Wavemaker	Measured waves without structure	
			H_s [m]	T_p [s]	γ [-]	Gain [-]	H_s [m]	T_p [s]
RB-A1	Cal 01	51.975	5.10	13.60	2.5	1.00	4.292	13.82
	Cal 02	51.975	5.10	13.60	2.5	1.26	5.408	13.93
	Cal 03	51.975	5.10	13.60	2.5	1.26	5.408	13.94
	Cal 04	51.975	5.10	13.60	2.5	1.19	5.100	13.96
RB-B1	Cal 05	49.725	5.10	13.60	2.5	1.20	5.099	14.09
RB-B2	Cal 06	50.175	8.00	15.20	2.5	1.22	8.232	16.09
RB-B3	Cal 07	51.000	10.2	16.50	2.5	1.21	10.175	16.65
RB-B4	Cal 08	51.750	11.2	17.00	2.5	1.21	10.946	16.71
	Cal 09	51.750	11.2	17.00	2.5	1.22	11.300	17.25
RB-A2	Cal 10	52.425	8.00	15.20	2.5	1.21	8.453	16.5
	Cal 11	52.425	8.00	15.20	2.5	1.18	8.279	16.65
RB-A3	Cal 12	53.250	10.2	16.50	2.5	1.21	10.35	16.51
RB-A4	Cal 13	54.000	11.2	17.00	2.5	1.23	11.31	17.91
RB-A5	Cal 14	54.000	13.4	17.00	2.5	1.26	12.558	17.90
	Cal 15	54.000	13.4	17.00	2.5	1.37	13.056	17.97

The wave calibration runs were conducted using a modified JONSWAP long crested sea state. As a result, the spectrum peak was raised by changing the wavemaker gain until the designed wave height and the wave height measured in the target probe were similar. During the calibration process, waves were noticed to be breaking between 10 and 14m from the paddles. Moreover, wave energy was enhanced near the structure due to the existence of the sand trap.

7.2. Model construction

The model drawings were printed to create templates of the breakwater sections. These templates were placed at the specified model locations to guide the construction of the breakwater head and part of its trunk. Thereafter, the available stones were sieved to ensure the correct dimensions and grading of the material that would be used in the construction of the core, underlayer and toe protection. Besides, the stones were washed before their placement to make sure that the water remained clear during the test duration.

The breakwater was built following the real construction process. This means that the core material, underlayer and toe protection were placed in this sequence without compaction and within the limits marked for each layer in the templates. This procedure replicates the high porosity obtained in the real construction.

The existing armour layer (30-tonne dolosse) presented large amount of both broken and displaced dolos. Available dolos units and stones were used to build this layer. To simulate the effect of the broken pieces, stones of about half the dolos weight were placed in between the non-broken dolos. As a result, no dolos units were broken for the construction of the model.

The described breakwater construction covers the model base. Figure 7.1 illustrates the followed sequence to build the current roundhead. The considered repair alternatives were constructed on top of this structure to perform a series of tests to each one, see Figure 7.2 to Figure 7.4. The new armour units, consisting of dolosse, antifer cubes or Core-Locs, were placed one by one to obtain the required placement packing density. Finally the armour units were painted in different colours to facilitate the damage assessment.





Figure 7.1 – Construction sequence of the roundhead model



Figure 7.2 – Roundhead model of the covering alternative with 36-tonne dolosse



Figure 7.3 – Roundhead model of the covering alternative with 45-tonne Core-Loc



Figure 7.4 – Roundhead model of the covering alternative with 44-tonne Antifer cubes

7.3. Test program

The same experiments were conducted to the three repair alternatives. The significant wave heights were determined as described in section 6.2.3.4. With these values and the calibration results, the required input files for the wavemaker were created. Table 7.2 summarizes the input characteristics for the wave generator.

Table 7.2 – Wave characteristics

Test	Return period	Water level at wavemaker	Target wave		JONSWAP	Wavemaker
	T [yr]	DWL [m]	H _s [m]	T _p [s]	γ [-]	Gain [-]
RB-B1	1	49.725	5.10	13.60	2.5	1.20
RB-A1	1	51.975	5.10	13.60	2.5	1.19
RB-B2	10	50.175	8.00	15.20	2.5	1.22
RB-A2	10	52.425	8.00	15.20	2.5	1.18
RB-B3	50	51.000	10.2	16.50	2.5	1.21
RB-A3	50	53.250	10.2	16.50	2.5	1.21
RB-B4	100	51.750	11.2	17.00	2.5	1.22
RB-A4	100	54.000	11.2	17.00	2.5	1.23
RB-A5	Overload	54.000	13.4	17.00	2.5	1.37

A standard procedure was followed during all the tests, which consisted of:

- Setting the water level.
- Adjusting and resetting the capacitance probes.
- Preparation of the files for the wavemaker and for the measuring software.
- Taking the before test pictures from all the fixed cameras.
- Turning the video cameras on for filming the whole test.
- Starting the measurement programme.
- After 20 seconds, the wavemaker is started.
- Observation of the breakwater performance, focusing on the movements of the armour units.
- Taking the after test pictures from the fixed cameras after turning the video off.

7.4. Data analysis

This section describes the followed process to analyse the gathered information during the tests. Such information comprises the data measured from the capacitance probes and visual information based on notes, pictures and videos taken during the experiments.

For every test, the wave characteristics were estimated from the data measured at the capacitance probes by applying Matlab routines (identical to the analysing process carried out during the calibration of the wavemaker). As a result, the time series, spectrum, significant wave height and peak period were computed for each probe location. By comparing the results between calibration and

tests, the reflection coefficient was determined, which allowed the estimation of the incident wave height and its associated stability number N_s .

As it was described in section 3.4.2.1, the damage of a breakwater can be characterized by two different methods: (1) counting the number of displaced units or (2) measuring the eroded surface profile of the armour slope. In this analysis, the counting method is applied to assess the damage of the roundhead.

The relative displacement, which is defined as the ratio between the number of displaced units and the total number of units within a specific area was applied to measure the damage. In the relative displacement definition, the movements of the armour units and the reference area should be specified. The Coastal Engineering Manual provides the classification of movements, the specific area for various armour units and the damage level expressed in terms of relative displacement, see Table 3.13.

To analyse the movements within the armour layer, the image superposition method was applied. The armour track software was used to estimate the damage level of each test. This software was developed by CSIR to assess the damage in structures built with dolos. It overlays the before- and after-test pictures and allows the visual comparison of the armour unit positions because of the constant flickering of both images. Therefore, all movements were identified and quantified due to the possibility of drawing lines connecting the original and final positions of the moving units.

8. Test results

This section presents and discusses the obtained results for each of the considered repair alternatives. The experiments were carried out to determine the hydraulic stability of each design.

Section 8.1 focuses on the tests conducted on the covering alternative using 36-tonne dolosse, whereas the performance of the 45-tonne Core-Loc repair option is discussed in section 8.2. Finally, section 8.3 deals with the results of the experiments carried out on the covering alternative consisting of 44-tonne antifer cubes.

8.1. Experiment 1: Covering alternative using 36-tonne dolosse

A total of eight tests were carried out with water level varying between +1.22m CD to +5.48m CD at the structure toe. Table 8.1 shows a summary of the obtained results. All tests were run for durations of 1000 waves, as described in section 6.2.3.4.

Table 8.1 – Measurements with covering alternative using 36-tonne dolosse

Test	Water level	Target wave		Measured wave				Incident wave		Reflected wave		Stability number
	(toe)	(buoy)		(buoy)		(toe)		(buoy)	(toe)	(buoy)	(toe)	
	DWL [m CD]	H _s [m]	T _p [s]	H _{m0} [m]	T _p [s]	H _{m0} [m]	T _p [s]	H _{m0} [m]	H _{m0} [m]	H _{m0} [m]	H _{m0} [m]	
RB-B1	+1.22	5.10	13.60	5.11	13.81	5.18	13.46	5.10	5.01	0.27	0.13	1.51
RB-A1	+3.47	5.10	13.60	5.02	13.51	5.17	13.41	4.93	4.96	0.92	0.46	1.50
RB-B2	+1.70	8.00	15.20	8.26	15.99	8.18	14.85	8.23	7.84	0.69	0.32	2.37
RB-A2	+3.95	8.00	15.20	8.47	16.06	8.27	16.78	8.28	7.77	1.77	0.84	2.35
RB-B3	+2.48	10.20	16.50	10.37	16.17	9.94	17.00	10.18	9.38	2.00	0.92	2.84
RB-A3	+4.73	10.20	16.50	10.59	17.65	10.35	16.84	10.35	9.66	1.05	1.13	2.92
RB-B4	+3.23	11.20	17.00	11.02	18.10	10.64	17.20	10.95	10.03	1.20	0.55	3.03
RB-A4	+5.48	11.20	17.00	11.40	17.65	11.21	17.20	11.31	10.45	1.45	0.66	3.16

The armour track software developed by CSIR was applied to estimate the damage level of each test. All movements were identified and quantified. The relative displacement for dolos was calculated by the following expression [PHELP ET AL., 1999]:

$$D = \frac{0.5 \cdot \text{Number units displaced less than 1 dolos height} + \text{Number units displaced more than 1 dolos height}}{\text{Total number of units within a specified zone}} \cdot 100 \quad [8.1]$$

The small movements of dolos, less than one dolos height, are related to broken dolos; while the larger movements define the units that are displaced from their original position. Table 8.2 presents the results of the damage using equation [8.1] for the first experiment.

Table 8.2 – Damage of the covering alternative using 36-tonne dolosse

Displacements	Tests							
	RB-B1	RB-A1	RB-B2	RB-A2	RB-B3	RB-A3	RB-B4	RB-A4
0.1C - 0.5C	15	19	55	88	65	47	55	84
0.5C - 1C	3	1	13	8	19	20	18	15
1C – 2C	0	0	7	0	0	2	5	4
> 2C	0	0	2	7	22	40	38	59
Number of units considered as damage	9	10	43	55	64	76	80	113
Number of units within specific zone	2163							
Relative displacement D [%]	0.4	0.5	2.0	2.5	3.0	3.5	3.7	5.2

8.1.1. Test RB-B1

The first test began with a water level of +1.22m CD, an input wave height of 5.10m and wave period of 13.6s. The generated waves were not depth limited and broke onto the structure. During the test, minor movements of dolos were noticed along the water line and there was no overtopping. Figure 8.1 presents two images of waves approaching the structure during this test.

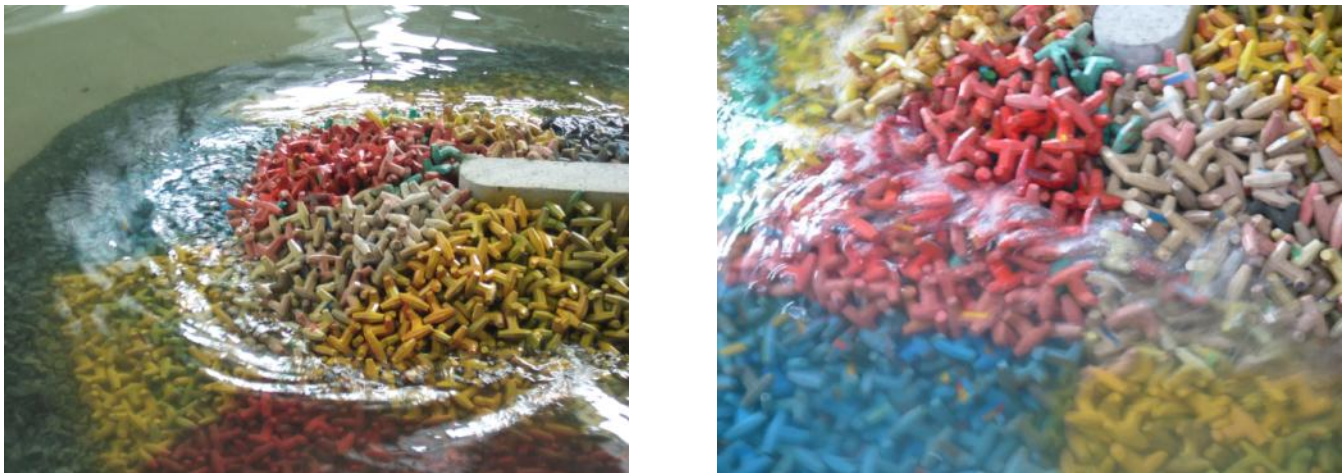


Figure 8.1 – Images of the roundhead with dolos during test RB-B1

8.1.2. Test RB-A1

For this test, the input wave conditions were identical to the previous test, but the water level was raised to +3.47m CD. The waves were not depth limited and most of their energy was released when impacting the structure. During this test, no overtopping was observed and minor movements of dolos were noticed along the water line. Images taken during this test are presented in Figure 8.2.

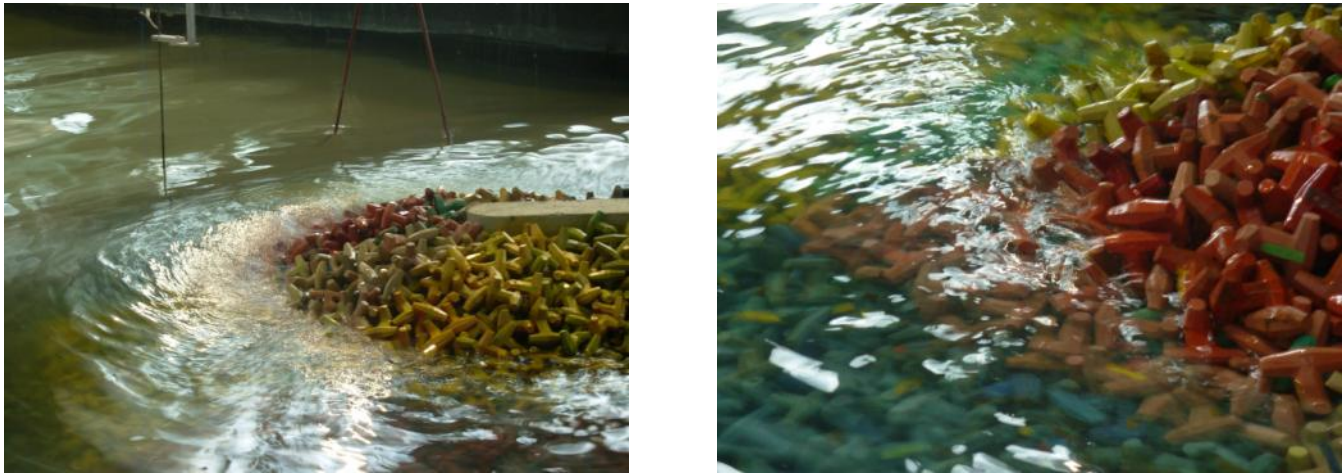


Figure 8.2 – Images of the roundhead with dolos during test RB-A1

8.1.3. Test RB-B2

For this test, the water level was lowered until reaching +1.70m CD. The input wave characteristics belonged to the 10-year return period, which corresponds to 8.0m of wave height and 15.2s of wave period. The generated waves were not depth limited and broke onto the structure. During the test, some movements of dolos were noticed along the water line and minor overtopping was also observed. Figure 8.3 illustrates the wave climate at the structure during test RB-B2.



Figure 8.3 – Images of the roundhead with dolos during test RB-B2

8.1.4. Test RB-A2

In this test the wave characteristics remained identical to the previous test, whereas the water level was raised until +3.95m CD. The waves were not depth limited and they broke onto the structure. During test RB-A2, minor overtopping was appreciated and some dolos moved along the water line. Images taken during this test are shown in Figure 8.4.



Figure 8.4 – Images of the roundhead with dolos during test RB-A2

8.1.5. Test RB-B3

This test began with a water level of +2.48m CD, an input wave height of 10.2m and wave period of 16.5s. The waves were depth limited and breaking occurred at -21.0m CD (close to the buoy location). Although the waves were broken, some overtopping was observed during this test. Movement of dolos was noticed along the water line, mainly at the lee side. Images of waves approaching the roundhead are presented in Figure 8.5.

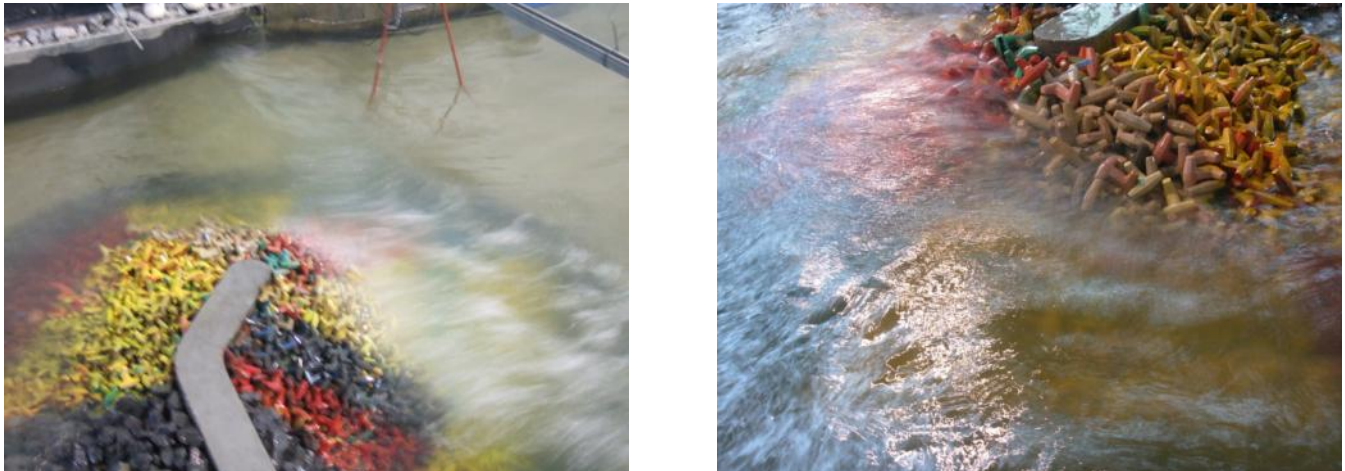


Figure 8.5 – Images of the roundhead with dolos during test RB-B3

8.1.6. Test RB-A3

For this test, the wave characteristics were kept identical as for test RB-B3 while the water level was raised until reaching +4.73m CD. The waves broke at a depth of -21.0m CD because of the depth limitation. Various units were displaced along the water line, especially at the lee side and some overtopping was noticed. Figure 8.6 shows waves approaching and overtopping the structure.

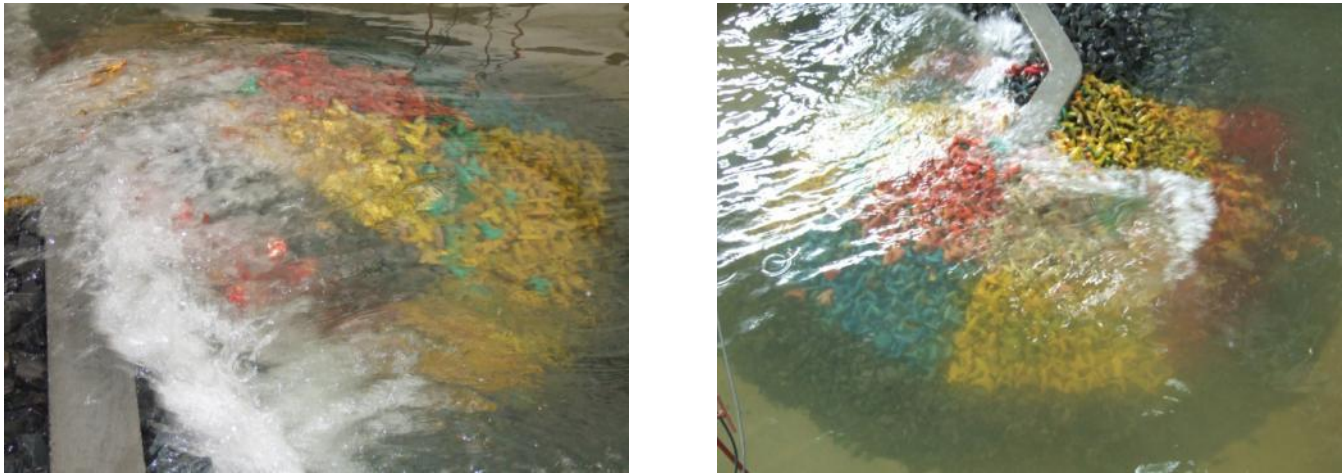


Figure 8.6 – Images of the roundhead with dolos during test RB-A3

8.1.7. Test RB-A4

In this test the water level was raised to +5.48m CD and the input wave characteristics were 11.2m for the significant wave height and 17.0s for the peak period. Breaking of waves was noticed at a depth of -21.0m CD due to the depth limitation. Severe overtopping was observed during this test and large amount of dolos were displaced along the water line at the lee side. However, the underlayer consisting of 30-tonne dolos was not visible and thus the failure state was not reached. Figure 8.7 illustrates waves approaching and overtopping the roundhead.



Figure 8.7 – Images of the roundhead with dolos during test RB-A4

8.1.8. Test RB-B4

Prior to this test the armour layer was repaired in the spots where damage was concentrated. Thereafter, the water level was set to +3.23m CD and the input wave characteristics were identical to Test RB-A4 (11.2m and 17.0s for wave height and peak period, respectively). During this test, waves were depth limited and the breaking occurred at -21.0m CD. Severe overtopping was noticed during

this test. As a result, large quantity of units was displaced at the lee side along the water line, although the underlayer was not visible at the end of the test. Images taken during test RB-B4 are presented in Figure 8.8.



Figure 8.8 – Images of the roundhead with dolos during test RB-B4

8.2. Experiment 2: Covering alternative using 45-tonne Core-Loc

For this experiment, nine tests were undertaken with water level varying between +1.22m CD to +5.48m CD at the structure toe. Table 8.3 shows a summary of the obtained results. All tests were run for durations of 1000 waves, as described in section 6.2.3.4.

Table 8.3 – Measurements with covering alternative using 45-tonne Core-Loc

Test	Water level	Target wave		Measured wave				Incident wave		Reflected wave		Stability number
	(toe)	(buoy)		(buoy)		(toe)		(buoy)	(toe)	(buoy)	(toe)	
	DWL [m CD]	H _s [m]	T _p [s]	H _{m0} [m]	T _p [s]	H _{m0} [m]	T _p [s]	H _{m0} [m]	H _{m0} [m]	H _{m0} [m]	H _{m0} [m]	
RB-B1	+1.22	5.10	13.60	5.06	13.55	5.13	14.35	5.00	4.95	0.76	0.37	1.50
RB-A1	+3.47	5.10	13.60	5.01	13.48	5.12	14.20	4.95	4.86	0.79	0.39	1.47
RB-B2	+1.70	8.00	15.20	8.31	16.03	8.37	15.08	8.23	8.00	1.14	0.55	2.42
RB-A2	+3.95	8.00	15.20	8.25	16.16	8.34	16.95	8.17	7.83	1.16	0.56	2.37
RB-B3	+2.48	10.20	16.50	10.31	16.26	10.06	17.04	10.18	9.52	1.66	0.78	2.88
RB-A3	+4.73	10.20	16.50	10.41	16.24	10.50	17.56	10.35	9.84	1.12	0.53	2.97
RB-B4	+3.23	11.20	17.00	10.97	18.19	10.91	19.67	10.87	10.25	1.49	0.70	3.10
RB-A4	+5.48	11.20	17.00	11.30	17.89	11.45	17.62	11.21	10.67	1.41	0.67	3.23
RB-A5	+5.48	13.20	17.00	12.84	17.93	12.83	18.26	12.79	12.33	1.15	0.55	3.73

All movements were identified and quantified using the armour track software developed by CSIR. The relative displacement for Core-Loc was estimated applying the following expression [TULSI, 2012]:

$$D = \frac{0.5 \cdot \text{Number units displaced less than 1 Core-loc height} + \text{Number units displaced more than 1 Core-loc height}}{\text{Total number of units within a specified zone}} \cdot 100 \quad [8.2]$$

The damage results using equation [8.2] are shown in Table 8.4.

Table 8.4 – Damage of the covering alternative using 45-tonne Core-Loc

Displacements	Test								
	RB-B1	RB-A1	RB-B2	RB-A2	RB-B3	RB-A3	RB-B4	RB-A4	RB-A5
0.1C - 0.5C	37	14	73	39	64	35	54	37	0
0.5C - 1C	0	2	6	4	4	2	1	1	0
1C – 2C	0	0	0	0	1	1	0	0	0
> 2C	0	0	1	2	5	3	2	4	45
Number of units considered as damage	19	8	41	24	40	23	30	23	45
Number of units within specific zone	800								
Relative displacement D [%]	2.3	1.0	5.1	2.9	5.0	2.8	3.7	2.9	5.6

It should be noted that an appropriate placement of the Core-Loc units is required to avoid large displacements of the armour units. However the placement of these units is not easy at Richards Bay due to the local wave climate. Therefore, the required packing density is difficult to ensure. This placement conditions have been replicate in the model to obtain representative results.

8.2.1. Test RB-B1

For this first test the water level was set to +1.22m CD and the input wave characteristics were 5.10m for the significant wave height and 13.6s for the peak period. The generated waves were not depth limited and broke onto the structure. During this test minor movements of Core-Loc were noticed along the water line during this test and no overtopping was observed. Figure 8.9 presents images of the roundhead performance during test RB-B1.



Figure 8.9 – Images of the roundhead with Core-loc during test RB-B1

8.2.2. Test RB-A1

In this test the water level was raised to +3.47m CD, whereas the input wave conditions remained identical to the previous test. Waves were not depth limited and they reached the structure before breaking. During this test, no overtopping was observed and minor movements were appreciated along the water line. Images taken during this test are presented in Figure 8.10.

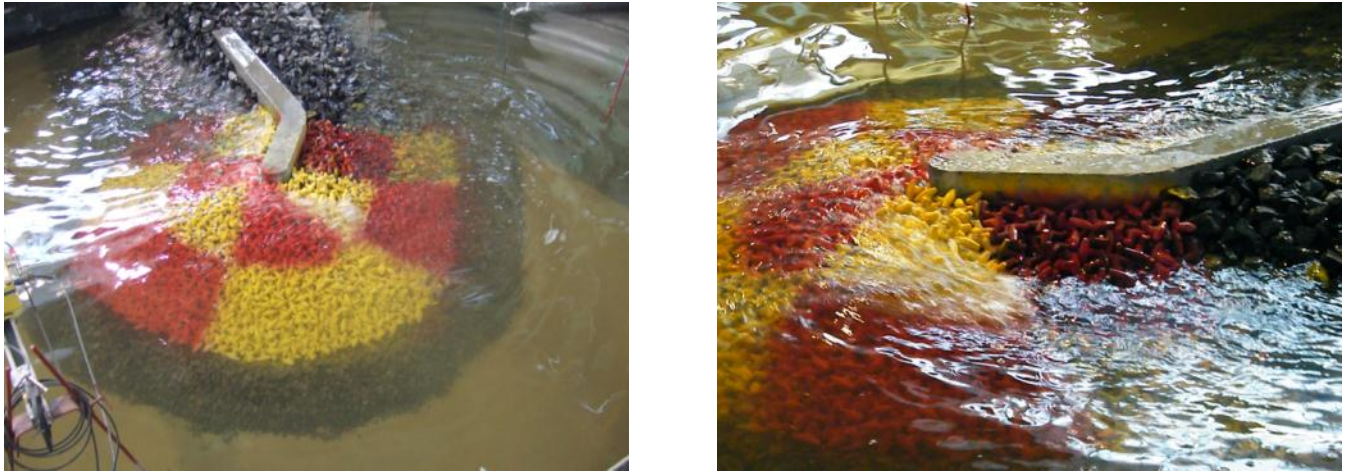


Figure 8.10 – Images of the roundhead with Core-loc during test RB-A1

8.2.3. Test RB-B2

This test began with the water level set to +1.70m CD and the input wave characteristics belonged to the 10-year return period (8.0m of wave height and 15.2s of peak period). Waves were not depth limited and broke onto the structure. Various Core-Loc units were rocking along the water line and one Core-Loc was washed away. For armour units placed in a single-layer failure occurs when any unit is displaced. Minor overtopping was also observed during this test. Figure 8.11 illustrates the wave climate at the structure during test RB-B2.



Figure 8.11 – Images of the roundhead with Core-loc during test RB-B2

8.2.4. Test RB-A2

For this test the wave characteristics remained identical to the previous test, while the water level was raised to +3.95m CD. The generated waves were not depth limited and they broke onto the structure. During test RB-A2, minor overtopping was appreciated, some Core-Loc units were rocking along the water line and two units moved from their position. Images taken during this test are shown in Figure 8.12.



Figure 8.12 – Images of the roundhead with Core-loc during test RB-A2

8.2.5. Test RB-B3

This test began with a water level of +2.48m CD, an input wave height of 10.2m and wave period of 16.5s. Some waves were depth limited and breaking occurred at -21.0m CD (close to the buoy location). Although waves were broken, some overtopping was observed during this test. Six Core-Loc units were washed away at the roundhead lee side where the underlayer consisting of 30-tonne dolos was visible. Some other units along the water line presented small movements. Figure 8.13 shows images of waves approaching the roundhead during this test.

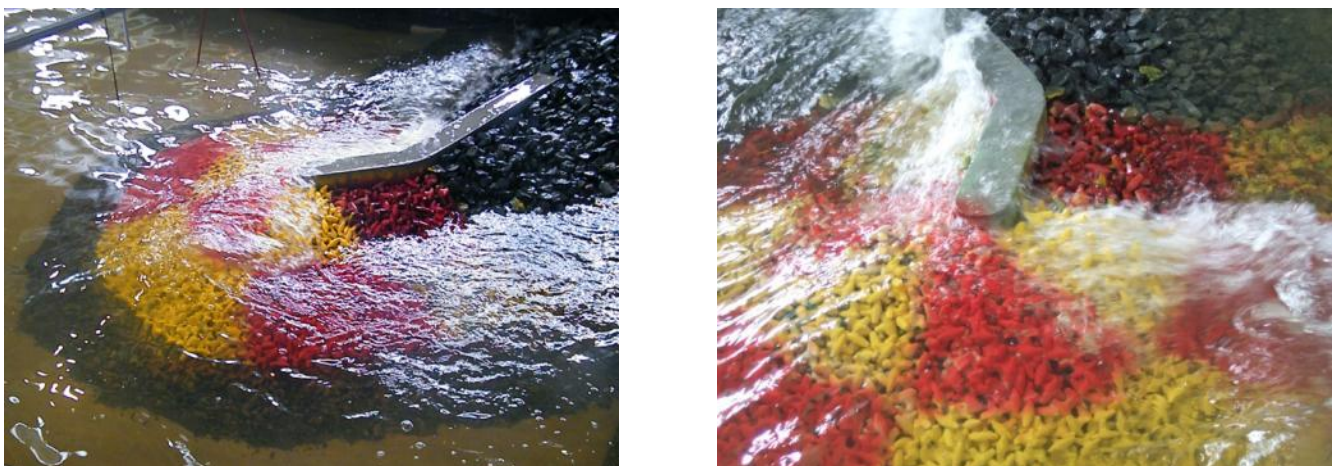


Figure 8.13 – Images of the roundhead with Core-loc during test RB-B3

8.2.6. Test RB-A3

Prior to this test, the armour layer at the lee side of the roundhead was repaired keeping in mind that the local wave conditions difficult the placement of Core-Loc. The input wave characteristics remained identical as for test RB-B3 while the water level was set to +4.73m CD. Some waves broke at a depth of -21.0m CD because of the depth limitation. During this test, various units were rocking along the water line and four Core-Loc units were displaced from different locations of the structure. Some overtopping was also noticed, as it is illustrated in Figure 8.14.



Figure 8.14 – Images of the roundhead with Core-loc during test RB-A3

8.2.7. Test RB-B4

In this test, the water level was lowered until +3.23m CD. The input wave height was 11.2m and its wave period was 17.0s. During this test, some waves were depth limited and breaking occurred at -21.0m CD. Severe overtopping was noticed during this test. As a result, various units were rocking along the water line and two Core-Loc units were washed away from different structure positions. Images taken during test RB-B4 are presented in Figure 8.15.



Figure 8.15 – Images of the roundhead with Core-loc during test RB-B4

8.2.8. Test RB-A4

The water level was raised to +5.48m CD for this test, whereas the wave characteristics remained identical to the previous test. Breaking of waves was noticed at a depth of -21.0m CD due to the depth limitation. Severe overtopping was observed during this test. Various Core-Loc units were rocking along the water line and four units were displaced from different locations of the structure. Figure 8.16 illustrates waves approaching and overtopping the roundhead.



Figure 8.16 – Images of the roundhead with Core-loc during test RB-A4

8.2.9. Test RB-A5

For the last test, the water level remained in +5.48m CD whereas the wave characteristics were 13.4m for the wave height and 17.0s for the peak period. Breaking of waves was noticed at a depth of -21.0m CD due to the depth limitation. Severe overtopping was observed during this test and large amount of Core-Loc were displaced, especially at the lee side between the crest and water line. Figure 8.17 illustrates waves approaching and overtopping the roundhead.

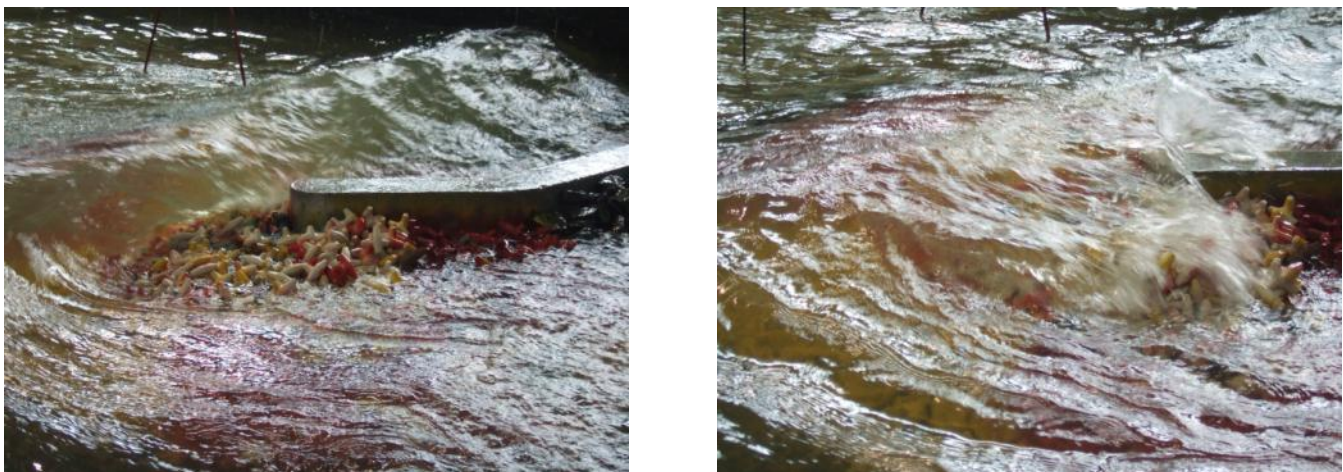


Figure 8.17 – Images of the roundhead with Core-loc during test RB-A5

8.3. Experiment 3: Covering alternative using 44-tonne antifer cubes

A total of nine tests were undertaken for this experiment, where the water level varied between +1.22m CD to +5.48m CD at the structure toe. Table 8.5 shows a summary of the obtained results. All tests were run for durations of 1000 waves, as described in section 6.2.3.4.

Table 8.5 – Measurements with covering alternative using 44-tonne antifer cube

Test	Water level	Target wave		Measured wave				Incident wave		Reflected wave		Stability number
	(toe)	(buoy)		(buoy)		(toe)		(buoy)	(toe)	(buoy)	(toe)	
	DWL [m CD]	H _s [m]	T _p [s]	H _{m0} [m]	T _p [s]	H _{m0} [m]	T _p [s]	H _{m0} [m]	H _{m0} [m]	H _{m0} [m]	H _{m0} [m]	
RB-B1	+1.22	5.10	13.60	5.19	13.87	5.24	14.30	5.10	5.12	0.99	0.56	1.55
RB-A1	+3.47	5.10	13.60	5.09	13.55	5.28	13.57	5.00	5.10	0.95	0.55	1.54
RB-B2	+1.70	8.00	15.20	8.54	17.84	8.24	16.68	8.23	7.94	2.27	1.23	2.40
RB-A2	+3.95	8.00	15.20	8.43	15.97	7.99	14.76	8.28	7.65	1.60	0.84	2.31
RB-B3	+2.48	10.20	16.50	10.46	16.13	9.64	16.89	10.18	9.23	2.43	1.24	2.79
RB-A3	+4.73	10.20	16.50	10.55	17.74	10.03	16.66	10.35	9.55	2.04	1.06	2.87
RB-B4	+3.23	11.20	17.00	11.04	18.15	10.45	17.19	10.89	9.98	1.85	0.97	3.02
RB-A4	+5.48	11.20	17.00	11.40	17.71	10.93	16.96	11.31	10.41	1.38	0.73	3.15
RB-A5	+5.48	13.20	17.00	12.80	17.77	12.27	21.37	12.75	11.62	1.15	0.60	3.51

All movements were identified and quantified using the armour track software developed by CSIR. The relative displacement for the antifer cube alternative was estimated applying the following expression:

$$D = \frac{\text{Number units displaced more than the antifer cube nominal diameter}}{\text{Total number of units within a specified zone}} \cdot 100 \quad [8.3]$$

Table 8.6 presents the damage results for this experiment using equation [8.3].

Table 8.6 – Damage of the covering alternative using 45-tonne Core-Loc

	Test									
	RB-B1	RB-A1	RB-B2	RB-A2	RB-B3	RB-A3	RB-B4	RB-A4	RB-A5	
Number of units considered as damage	0	0	16	9	21	38	47	54	94	
Number of units within specific zone	2224	2224	2224	2224	2224	2224	2224	2224	2224	2224
Relative displacement D [%]	0.0	0.0	0.7	0.4	0.9	1.7	2.1	2.4	4.2	

Due to Richards Bay wave climate, the random placement method was applied in the construction of this repair alternative.

8.3.1. Test RB-B1

This first test began with a water level of +1.22m CD, an input wave height of 5.10m and wave period of 13.6s. The generated waves were not depth limited and broke onto the structure. During the test, no overtopping was observed and a few number of antifer cubes were rocking along the water line. Figure 8.18 presents two images of waves approaching the structure during this test.



Figure 8.18 – Images of the roundhead with antifer cubes during test RB-B1

8.3.2. Test RB-A1

For this test, the input wave conditions were identical to the previous test, whereas the water level was raised to +3.47m CD. Waves were not depth limited and they reached the structure before breaking. Minor movements of antifer cubes were noticed along the water line. There was no overtopping during this test. Images taken during test RB-A1 are presented in Figure 8.19.



Figure 8.19 – Images of the roundhead with antifer cubes during test RB-A1

8.3.3. Test RB-B2

In this test the water level was lowered to +1.70m CD. The input wave characteristics were 8.0m for the wave height and 15.2s for the wave period. Few waves were depth limited and breaking occurred at -21.0m CD (close to the buoy location). Some antifer cubes located along the water line moved and some overtopping was also observed during this test. Figure 8.20 illustrates the wave climate at the structure during test RB-B2.



Figure 8.20 – Images of the roundhead with antifer cubes during test RB-B2

8.3.4. Test RB-A2

This test began with a water level +3.95m CD, while the input wave characteristics remained identical to test RB-B2. Waves were not depth limited and they broke onto the structure. During this test, some overtopping was appreciated and some antifer cubes were washed away along the water line. Images taken during this test are shown in Figure 8.21.



Figure 8.21 – Images of the roundhead with antifer cubes during test RB-A2

8.3.5. Test RB-B3

In this test, the water level was lowered to +2.48m CD. The wave characteristics were 10.2m for the wave height and 16.5s for the wave period, which belonged to 50-year return period. Waves were depth limited and breaking occurred at -21.0m CD. Some overtopping was observed during this test and some units at the water line were displaced. Images of waves approaching the roundhead are presented in Figure 8.22.

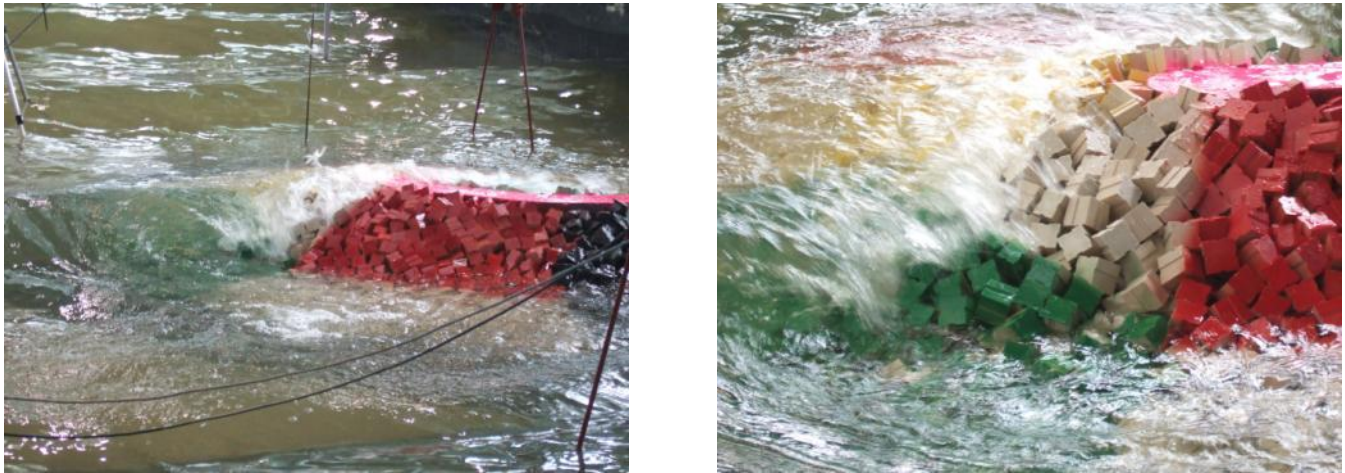


Figure 8.22 – Images of the roundhead with antifer cubes during test RB-B3

8.3.6. Test RB-A3

For this test, the wave characteristics were kept identical as for test RB-B3 while the water level was raised to +4.73m CD. Some waves were breaking at a depth of -21.0m CD because of the depth limitation. Some antifer cubes placed at the crest were rocking during this test. Various units located along the water line were washed away and overtopping was also noticed. Figure 8.23 shows waves approaching and overtopping the structure.



Figure 8.23 – Images of the roundhead with antifer cubes during test RB-A3

8.3.7. Test RB-B4

Prior to this test, repairs of the armour layer were undertaken. The water level was set to +3.23m CD and the input wave height was 11.2m and its wave period was 17.0s. During this test, waves were depth limited and the breaking occurred at -21.0m CD. Severe overtopping was noticed during this test, which resulted in the displacement of various units along the water line. The underlayer was not visible and thus the structure did not fail. Images taken during test RB-B4 are presented in Figure 8.24.



Figure 8.24 – Images of the roundhead with antifer cubes during test RB-B4

8.3.8. Test RB-A4

For this test wave conditions remained identical to previous test, while the water level was +5.48m CD. Breaking of waves was noticed at a depth of -21.0m CD due to the depth limitation. Severe overtopping was observed during this test and various antifer cubes located along the water line were washed away. The underlayer consisting of 30-tonne dolos was not visible and thus the failure state was not reached. Figure 8.25 shows waves approaching to the roundhead.



Figure 8.25 – Images of the roundhead with antifer cubes during test RB-A4

8.3.9. Test RB-A5

For the last test, the water level remained at +5.48m CD whereas the wave characteristics were 13.4m for the wave height and 17.0s for the peak period. Waves were depth limited and breaking occurred at -21.0m CD. Severe overtopping was observed during this test and large amount of antifer cubes were washed away at the lee side along the water line. The underlayer consisting of 30-tonne dolos was visible at the lee side and thus the structure failed. Images taken during this overload test are presented in Figure 8.26.



Figure 8.26 – Images of the roundhead with antifer cubes during test RB-A5

9. Evaluation of the test results

This chapter focuses on the evaluation of the test results by comparing them not only with each other but also with some criteria that will be used to determine how appropriate each repair alternative is. This evaluation method is described in section 9.1. Thereafter, section 9.2 deals with the evaluation of each experiment according to the criteria. Finally, a qualitative description of the construction feasibility of each repair alternative is provided in section 9.3.

9.1. Evaluation method

The evaluation method is based on three criteria. These are divided in (1) stability performance of the structure and (2) wave transformation at the roundhead.

The first criterion is based on the stability performance of the structure that is described by the stability number N_s and the measured damage D . This damage is defined by the relative displacement determined by the equations [8.1] to [8.3]. These results are compared to the values provided by the Coastal Engineering Manual (see Table 3.13). As it occurs in the analysis of the photographic surveys, for each test the damage is linked to the stability number. Moreover, when the relative displacement is below 5%, the Hudson's damage level coefficient K_D is estimated through the stability number using equation [9.1]. This allows the comparison between both K_D -values, the one applied in the design of the armour unit sizes (see Table 3.10) and the estimated value after each test. As a result, the goodness of the design parameter can be proven for the armour units designed using Hudson equation.

$$K_D = \frac{N_s^3}{\cot \alpha} \quad [9.1]$$

At the breakwater roundhead several processes transform the waves propagation. The observed processes are absorption, diffraction, reflection, wave run-up and overtopping. When a wave attacks the roundhead, part of its energy is absorbed by the structure and the remaining energy either reflects, overtops or diffracts. From the measured wave characteristics, the reflection coefficient is estimated for each armour unit as the ratio between the reflected and incident wave. The overtopping is estimated according to the methods presented in the Rock Manual. All these processes provide an explanation of what causes the damage development in the breakwater roundhead.

9.2. Evaluation of the experiments

In this section the results presented in chapter 8 are compiled to provide an overview of all the conducted experiments and facilitate their comparison. Three repair alternatives have been tested in the basin. The aim of these experiments is to understand the behaviour of each armour unit and determine the most appropriate repair option taking into account the evaluation method described in section 9.1.

The various armour units were randomly placed during the construction of the roundhead model. Due to the structure shape and the difficulty of applying a regular placement grid, the required interlocking

between units was more difficult to achieve. This leads to a reduction in the designed packing density of the armour layer.

The stability performance of each repair alternative is described in Table 9.1.

Table 9.1 – Comparison of stability parameters

Armour units		Test								
		RB-B1	RB-A1	RB-B2	RB-A2	RB-B3	RB-A3	RB-B4	RB-A4	RB-A5
Dolos	N_s [-]	1.51	1.50	2.37	2.35	2.84	2.92	3.03	3.16	-
	D [%]	0.4	0.5	2.0	2.5	3.0	3.5	3.7	5.2	-
	K_D [-]	1.74	1.68	6.65	6.48	11.40	12.45	13.93	15.76	-
Core-Loc	N_s [-]	1.50	1.47	2.42	2.37	2.88	2.97	3.10	3.23	3.73
	D [%]	2.3	1.0	5.1	2.9	5.0	2.8	3.7	2.9	5.6
	K_D [-]	1.67	1.58	7.07	6.63	11.91	13.15	14.87	16.77	-
Antifer cubes	N_s [-]	1.55	1.54	2.40	2.31	2.79	2.87	3.02	3.15	3.51
	D [%]	0.0	0.0	0.7	0.4	0.9	1.7	2.1	2.4	4.2
	K_D [-]	1.85	1.83	6.91	6.18	10.86	12.03	13.73	15.58	-

It should be noticed that the estimated values of the Hudson damage level coefficient for dolos and Core-Loc can be compared with the applied K_D -value in the design of the armour units. According to Table 3.10, the K_D -value used in the design of dolos and Core-Loc units at the head is 16 and 13, respectively. From the results shown in Table 9.1, the following conclusions can be drawn:

- The dolos unit has been designed using a Hudson damage level coefficient of 16; while the estimated values for the design storm are slightly lower (14 and 16, respectively). This results in an armour unit size that is strong enough to withstand the wave action without failing.
- The Core-Loc unit was designed applying a K_D value of 13. However, this value is far below the estimated values for the design storm (15 and 17). As a result, the estimated Core-Loc size for this design is not heavy enough to resist the expected wave loads, which has been observed during the test runs because of the difficulty of ensuring the correct interlocking between units.

Since the antifer cube unit was designed using Chegini formula, the comparison between the test results and the design should be carried out taking into account their stability numbers. The stability number used in the design of the armour unit was 2.979. This value is slightly overpassed by the design storm tested in the flume (see Table 9.1). Therefore the damage observed in the structure is slightly larger than the one expected in reality. Although some antifer cubes are displaced, the structure did not reach the failure state. This means that these units were strong enough to withstand the wave loads imposed by the design storm runs at the flume. Moreover, failure occurred during the overload test where the displacement of units was concentrated in a limited area at the lee side.

Figure 9.1 shows the relative displacement of units linked to the stability number.

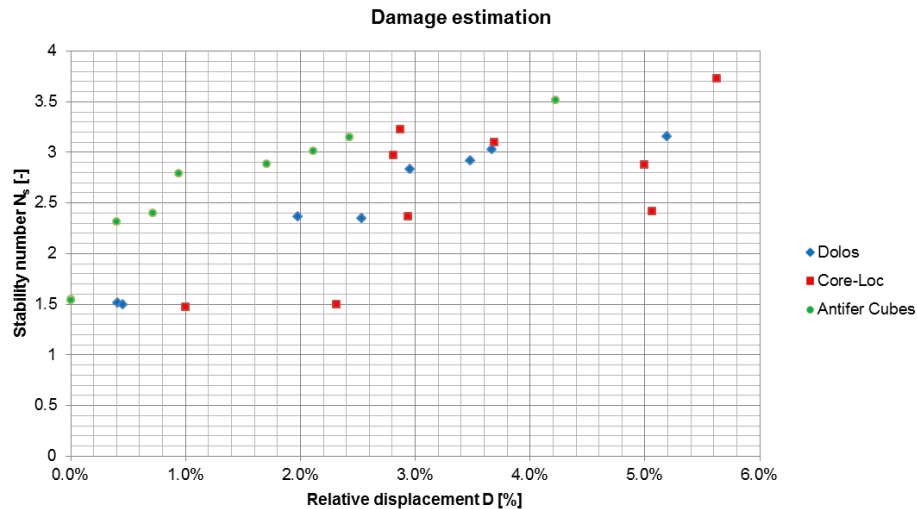


Figure 9.1 – Relative displacement

From Figure 9.1 it follows that the measured damage is larger when the stability number is higher. Core-Loc presents an erratic behaviour compared to other units due to difficulties in ensuring a good interlocking between the units. Since the Core-Loc units were not properly interlocked, the resistance mechanisms to withstand the wave action were not totally achieved. As a result, larger instabilities were introduced to these units leading to higher damage levels. Besides, large differences are noticed between damage levels with similar stability number (see red squares in Figure 9.1). They are caused by the considered water level and the variation of interlocking between units placed at the lower and upper parts of the breakwater slope. A larger rearrangement of units was noticed at the lower part of the slope resulting in a larger amount of units displaced during the low water level tests. Even though these displacements were relatively small (less than one nominal diameter), higher damage levels were computed because these displacements are related to the amount of broken pieces. However the packing density achieved during the Core-Loc placement played an important role in the stability of this layer (see results of section 8.2).

Moreover, according to Figure 9.1, the antifer cubes are more stable than other units because they show smaller values of relative displacement for similar stability numbers. This phenomenon is explained by the different resistance mechanisms of antifer cubes and dolos. The first unit withstands the wave loads and water flow mainly due to its mass, whilst dolos resists them by the interlocking between units. Therefore, the small displacements (less than one nominal diameter) have more impact on slender units than massive, leading to higher damage levels in dolos than antifer cubes. As a result, the estimated damage for dolos is shifted to higher relative displacement values compared to the antifer cubes estimation (see Figure 9.1).

In the three experiments, the damage was concentrated along the water line, mainly at the lee side in an area located between 120 and 150 degrees from the incident wave direction. This damage was caused by the wave breaking on the structure. At this particular section of the breakwater the incident wave splits in two. The first part breaks directly on the sea side and exerts a force that is directed up-slope. This force is counteracted by the friction between units and the gravity forces. However, some of these waves overtop the structure and impact at the rear side close to the water line. This impact

exerts a force on the units that is directed down-slope and should be added to the turbulent forces of the waves propagating into the lee side. These forces are only counteracted by the friction between units because the gravity force component is also directed down-slope. Therefore, the units at this particular location are less stable due to the relationship between forces.

Figure 9.2 presents the reflection coefficients for the different experiments related to the overtopping and the water level analysed.

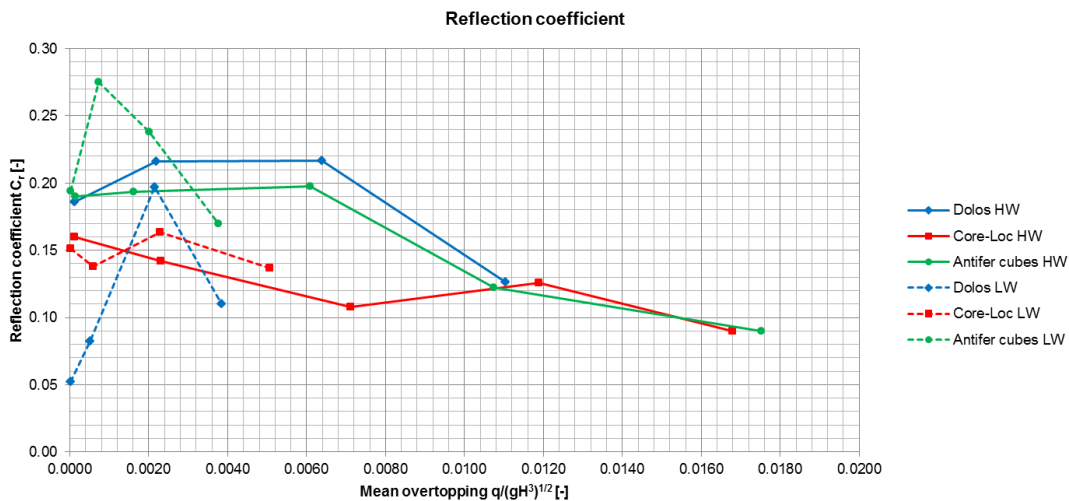


Figure 9.2 – Reflection coefficient

According to Figure 9.2 the Core-Loc alternative presents the lowest reflection coefficient, which is linked to the permeability of the structure. In the Core-Loc case, this structure is the most permeable because has been constructed with the lowest packing density value, see Table 5.14. Therefore, more wave energy is absorbed by this structure, which reduces the wave reflection. However the behaviour of the reflection coefficient is fairly similar between high water levels and low water levels.

Besides, from Figure 9.2 it follows that the behaviour of the reflection coefficient is similar between the antifer cubes and dolos despite their different properties. For the low water level tests, the structure built with antifer cubes presents the largest reflection coefficient. This phenomenon is explained by the interaction between the waves and structure. Since the antifer cube structure is the most impermeable one, this structure absorbs less wave energy, and thus higher wave reflection is measured. Finally, when the overtopping is fairly large, the reflection coefficient drops due to the transfer of wave energy to the rear side. However, the point where the change in the trend is noticed depends on the water level, the structure permeability and the number of waves that actually overtop the structure.

From these experiments, it can be concluded that rubble mound breakwaters constructed with double armour layers will perform better in harsh environments because a certain damage level is allowed without compromising the structure stability. Therefore, this reduces the costs during the preliminary design stage because the choice between armour unit types is limited to only consider those units placed in double armour layers. On the contrary, armour units placed in single layer become the best repair option in milder wave climates where the placement requirements are more easily met.

9.3. Construction feasibility

This section describes the construction feasibility of each repair alternative qualitatively. The application of any repair option is determined according to the environmental conditions of the site and the construction costs. The environmental conditions of the site are related to the wave climate, the stability of the toe and irregularities in the existing slope of the roundhead and toe. The state of the existing toe and slope are described by the comparison of the profile surveys and the as-built cross-sections, which has been analysed prior to the new repair works design. The construction costs depend on the required number of units, the transport costs, the storage costs, placement costs and available equipment.

For the three repair alternatives, the environmental conditions are identical. The wave climate along the year is analysed to determine the calm season, where the storm events are more unlikely. Therefore, the repair works are easier to be undertaken. Figure 9.3 shows the annual wave climate at Richards Bay [Rossouw, 2012].

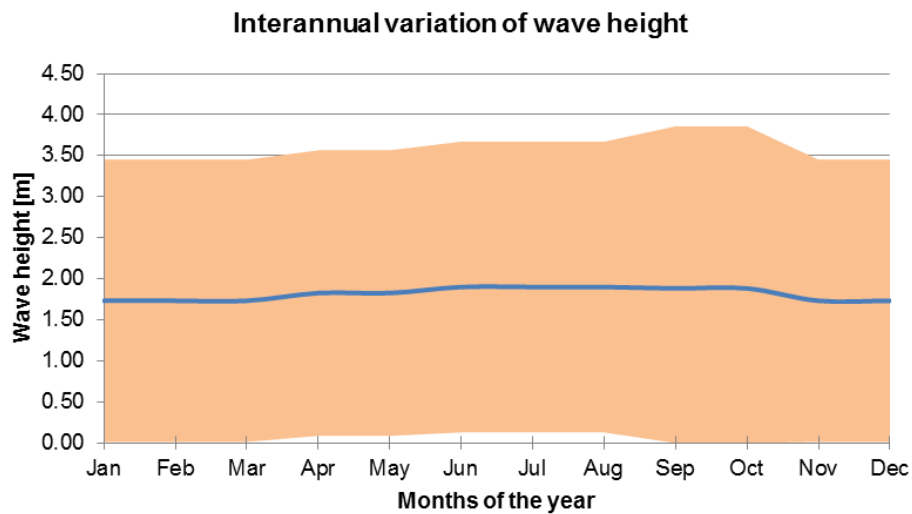


Figure 9.3 – Interannual variation of wave height at Richards Bay

From Figure 9.3 it follows that the repair works should be carried out during the summer months, between November and March. The usual wave height is about 1.7m at Richards Bay, which makes it difficult to place the new armour units. Therefore, the armour units that require good interlocking between units, such as Core-Loc and Dolos, are less appropriate in a location with such wave climate, due to the difficulties to ensure their correct placement. From this point of view, antifer cubes are the most suitable units to carry out the repair works, because they are placed randomly and they require meeting fewer specifications during their placement.

The construction costs of the repair alternatives, as has been mentioned above, are related to the required number of units to be produced, the transport costs from the production site to the construction site, the storage costs of the units before their placement at the structure, the placement costs and the available equipment to undertake the repair works.

The required volume of concrete per unit, the costs of producing the moulds and the total number of units required to carry out the repair works should be taken into account to quantify the manufacturing costs of each unit. Table 9.2 provides information about the required number of units and the total volume of concrete needed to construct the structure.

Table 9.2 – Required number of units and total volume of concrete

Armour unit	n	W_a	ρ_a	V_a	Φ	r	Nr/A	A	Nr	V_{total}
[-]	[-]	[ton]	[t/m ³]	[m ³]	[-]	[m]	[units/m ²]	[m ²]	[units]	[m ³]
Dolos	2	36	2.4	15.0	0.83	4.64	0.136	6007	2034	30510
Antifer cubes	2	44	2.4	18.3	1.17	5.80	0.168	6634	2625	48125
Core-Loc	1	45	2.4	18.8	0.60	4.01	0.085	5808	695	13035

According to Table 9.2 the structure built with Core-Loc requires the lowest amount of units, and thus the smallest total volume of concrete. Besides, the construction of one Core-Loc mould is more expensive due to the complexity of its geometrical shape. However, since the required total number of units and moulds is the smallest, this leads to the cheapest manufacturing option. Moreover, the storage space and transport costs are also related to the required number of units. Therefore, the smaller the quantity of units to be produced the smaller the costs of storage and transport.

The costs of constructing the dolos moulds are larger due to the complexity of its geometrical shape compared to the antifer cubes. However, since the total amount of dolos and its concrete volume are smaller compared to the antifer cubes (see Table 9.2); similar manufacturing costs between both units are expected.

To reduce the repair works costs, the available equipment at the breakwater should be used to carry out the repairs. Therefore, the existing crane should be able to handle the units and place them in their corresponding position. If that is not possible, an appropriate crane should be built to undertake such a job, which will increase the construction costs.

Finally, the placement costs are based on the required specifications of each armour unit to be placed on a structure. Hence, the more complex the placement is, the more time is needed to place one unit. As a result, the costs of placement will increase with the required time to carry out the repair works. This means that the interlocking units will be more expensive to be placed than the antifer cubes due to their positioning requirements. However, in the case of placing antifer cubes, the construction of a new toe is required. This adds a new cost component in the construction costs of the antifer cube repair alternative.

10. Conclusions and recommendations

10.1. Conclusions

The main objective of this thesis is to assess the most appropriate design for the repair works that should be applied in the roundhead of the South breakwater at Richards Bay Port through a Quasi Three-Dimensional (3D) model testing. This was achieved by reproducing the observed damage at the structure's roundhead in one of CSIR's hydraulic laboratory flumes and testing three repair alternatives.

The repair alternatives consisted of covering the damaged structure with new armour units. Three different armour units were used in this research, such as dolos, Core-Loc and antifer cubes.

Each armour unit was tested considering two water levels (low and high astronomical tide) and five different wave conditions, which correspond to the design storms for different return periods. Before and after each test, pictures were taken to be compared by the superposition technique. In this way the movements of the armour units within the corresponding reference area are distinguished and quantified to establish the stability of the structure. Besides, the reflection coefficient per test and armour unit was estimated.

General conclusions

- The main failure mechanism of the three repair alternatives is the displacement of units along the water line.
- In the roundhead the damage was concentrated along the water line, mainly at the lee side in a critical area located between 120 and 150 degrees from the incident wave direction.
- The impact of the overtopping waves and the turbulent flow caused by the waves propagating at the lee side of the roundhead exert forces onto the armour units directed down-slope that are only counteracted by the friction between units. The units located in this critical area are less stable because the gravity forces of the units do not add up to the resistance force.
- At the sea side some units are displaced due to wave action. The forces exerted by the waves due to the impact and the turbulent flow are directed up-slope. These forces are counteracted by the friction forces between units and the gravity forces of the units. This phenomenon is identical to what the trunk sections withstand.
- In the design of the roundhead armour units, the stability formulae applied are the same as for the trunk. However a lower value of the damage level coefficient K_D is considered. As a result, the required armour unit size is larger for this specific location.
- The placement of units at the roundhead is more complicated than in the other sections of the breakwaters because of the convex shape of this section. Therefore, the specified packing densities are not that easy to be achieved during the construction of the repair works, even though a regular grid is used to assist the placement of units.

Conclusions for the dolos repair alternative

- To ensure the stability of the roundhead, it should be constructed with dolos units twice heavier than the dolosse placed at the trunk. However, in the actual roundhead construction, the placed dolosse are just 1.5 times heavier than the units at the trunk, resulting in a structure not strong enough to resist the wave conditions.
- Although there are many parts of broken dolos at the roundhead (see Table 8.2), this is not the main structural failure mechanism. However, the broken pieces should be taken into account in future storms because they can act as projectiles and increase the future damage of the structure.
- At the roundhead the dolosse are less interlocked due to the convex shape of this section. Therefore, the armour layer will be more vulnerable to wave action.
- From the point of view of unit stability, the construction of 36-tonne dolosse with a density of 2.4t/m^3 is not feasible because of its slenderness. This means that the unit size is limited to avoid too much breakage of units. Therefore, the heavier dolos than can be constructed in reality with a density of 2.4t/m^3 have a weight of 30-tonne. As a result, this alternative is not applicable unless the shape of the 30-tonne dolos is kept during the manufacturing and the concrete density is increased to achieve the required weight.

Conclusions for the Core-Loc repair alternative

- At the roundhead the Core-Loc units placement is more complex than at the trunk due to the convex shape of this section. Therefore, the appropriate interlocking between units is more difficult to be achieved. This leads to a less stable armour layer.
- Since the Core-Loc units are placed in a single armour layer, any displacement results in the structure failure (see Table 8.4). Therefore, this alternative is not an appropriate repair option because various Core-Loc units have been displaced during the tests and this will require constant maintenance.
- It has been seen that the Core-Loc interlocks very well with the existing dolos. However, at the roundhead due to placement difficulties and wave conditions, their performance is not as good as expected.
- The Core-Loc armour layer presents the lowest reflection coefficients, see Figure 9.2. This is inversely linked to the permeability of the Core-Loc structure. Since this structure is constructed with the lowest packing density, more space between units is noticed resulting in a more permeable structure. Therefore, it absorbs more wave energy and reduces the wave reflection and wave overtopping.

Conclusions for the antifer cube repair alternative

- The antifer cube size has been determined using Chegini formula, see equation [3.8]. This formula includes larger number of relevant parameters to estimate the unit size. As a result the same armour unit size can be used for the whole structure.
- The antifer cubes are randomly placed at the roundhead. This placement is not as difficult as for the interlocking units because it requires fewer specifications to be met. Therefore, due to the wave conditions expected at Richards Bay this repair alternative is the most suitable.

However, the required packing density is difficult to achieve due to the convex shape of the roundhead, which leads to a more vulnerable structure.

- The largest wave overtopping was noticed in the structure built with antifer cubes. This is related to the highest reflection coefficient computed from the wave measurements, see Figure 9.2. Besides, the reflection coefficient depends on the permeability of the structure. For this armour unit, the resulting structure is the most impermeable due to it is built using the largest packing density value.
- A new toe protection must be built in front of the first row of antifer cubes to ensure their stability. This may increase the total constructions costs of the repair alternative.
- From the point of view of unit stability, massive armour units such as antifer cubes are not size limited. Therefore, the construction of 44-tonne antifer cube with a density of 2.4t/m^3 is feasible.

10.2. Recommendations

- It has been found that the armour units placed at the roundhead of a breakwater behave differently than when they are placed at the trunk. Generally, these armour units are designed using the trunk section formulae and multiplying its result by a safety factor. This safety factor is included in the damage level coefficient applied in the Hudson formula, which is different for the trunk and head sections, see Table 3.10. Therefore, more research must be carried out to determine the formulae that should be applied in the design of the armour units at the roundhead.
- From the damage observed during the tests, the critical area located between 120 and 150 degrees from the incident wave direction should be redesigned to reduce its damage. Thus two measures can be applied, which consist of:
 - Changing the slope from the cross-section located at 120 degrees to a steeper slope. This will change the flow propagation at the rear side of the breakwater (separating the flow from the structure) and the impact of the wave overtopping will occur on the water. As a result the forces exerted onto the units will be reduced.
 - Placing heavier armour units in the critical area. This can be achieved by either placing bigger units or denser units. The placement of bigger units is related to the increase of the armour unit size while the density of the concrete remains as 2.4t/m^3 . The main disadvantage of this option is how to interlock these bigger units with the smaller ones. The second option comprises the use of denser units, which might be more appropriate because the size remains identical while the concrete density is increased by adding heavier aggregates to the mix. This will simplify the placement between units.
- The dolos units have a limitation in size due to their slenderness. If a dolos unit heavier than 30-tonne is required to withstand the wave action, the only feasible approach right now is the increase of the concrete density mix by adding heavier aggregates. Hence it is recommended to carry out more research to modify the dolos shape so that heavier units can be manufactured.
- Although the design of the whole model has been performed in such a way that the viscous scale effects are avoided, the core scaling is close to the limit. This might result in the measurement of slightly larger damage in the model due to the flow at the core is not fully turbulent. Therefore it is recommended to conduct more tests with a larger scale.

References

- [1] BAKKER, P.; VAN DEN BERGE, A.; HAKENBERG, R.; KLABBERS, M.; MUTTRAY, M.; REEDIJK, B.; ROVERS, I. (2003): 'Development of Concrete Breakwater Armour Units', Delta Marine Consultants, Gouda, The Netherlands.
- [2] BAKKER, P.; KLABBERS, M.; REEDIJK, J.S. (2004): 'Introduction of the Xbloc Breakwater Armour Unit', Delta Marine Consultants, Gouda, The Netherlands.
- [3] BURCHARTH, H.F.; LIU, Z.; TROCH, P. (1999): 'Scaling of Core Material in Rubble Mound Breakwater Model Test', Proceedings of the COPEDEC V, Cape Town, South Africa.
- [4] CHEGINI, V.; AGHTOUMAN, P.; SHIRIAN, N. (2005): 'Experimental Studies of Rubble Mound Breakwaters', International Coastal Symposium 2005, Hofn, Iceland.
- [5] CSIR (2007): 'Port of Richards Bay: Photographic Monitoring of the North and South Breakwaters, May 2007', Council for Scientific Research and Industrial Research (CSIR), Stellenbosch, South Africa.
- [6] CSIR (2011): 'Port of Richards Bay: Photographic Monitoring of the North and South Breakwaters, May 2011', Council for Scientific Research and Industrial Research (CSIR), Stellenbosch, South Africa.
- [7] DENECHERE, M. (2011): 'Technology, experience and cost-effectiveness in a single concrete unit for breakwater armouring: The Accropode II unit', Concrete Layer Innovations (CLI), France.
- [8] FRENS, A.B. (2007): 'The Impact of Placement Method on Antifer-block Stability', MSc-Thesis, Delft University of Technology, Delft, The Netherlands.
- [9] GODA, Y. (2000): 'Random Seas and Design of Maritime Structures', World Scientific Publishing Company, Singapore.
- [10] HILL KAPLAN SCOTT & PARTNERS: 'Report on the Design and Use of the Dolos', Murray & Stewart Centre, East London, South Africa.
- [11] HOLTHUIJSEN, L.H. (2007): 'Waves in Oceanic and Coastal Waters', Cambridge University Press, Cambridge, UK.
- [12] HUGHES, S.A. (1993): 'Physical Models and Laboratory Techniques in Coastal Engineering', Coastal Engineering Research Center (CERC), US Army Corps of Engineers, Vicksburg, Mississippi, USA.
- [13] HUGHES, S.A. (2008): 'Combined Wave and Surge Overtopping of Levees: Flow Hydrodynamics and Articulated Concrete Mat Stability', Engineer Research and Development Center, US Army Corps of Engineers, Vicksburg, Mississippi, USA.
- [14] MELBY, J.A. (1993): 'Dolos Design Procedure Based on Crescent City Prototype Data', Coastal Engineering Research Center (CERC), US Army Corps of Engineers, Vicksburg, Mississippi, USA.
- [15] MELBY, J.A.; TURK, G.F. (1997): 'Core-Loc Concrete Armour Units', Coastal Engineering Research Center (CERC), US Army Corps of Engineers, Vicksburg, Mississippi, USA.
- [16] MORI, N.; YASUDA, T.; MASE, H.; TOM, T.; OKU, Y. (2010): 'Projection of Extreme Wave Climate Change under Global Warming', Hydrological Research Letters, Japan.
- [17] MUTTRAY, M.; REEDIJK, B.; KLABBERS, M. (2003): 'Development of an Innovative Breakwater Armour Unit', Delta Marine Consultants, Gouda, The Netherlands.

References

- [18] NATIONAL RESEARCH INSTITUTE FOR OCEANOLOGY (1974): 'Design of Richards Bay Harbour Entrance Wave Model Tests on Entrance Layout', Council for Scientific Research and Industrial Research (CSIR), Stellenbosch, South Africa.
- [19] PHELP, D.; HOLTZHAUSEN, S.; HOUGH, G.; BARTELS, A. (1999): 'Digital Image Techniques to Quantify Structure Damage in Physical Models', Proceedings of the COPEDEC V, Cape Town, South Africa.
- [20] REEDIJK, B.; KLABBERS, M.; VAN DEN BERGE, A.; HAKENBERG, R. (2003): 'Development of the Xbloc Breakwater Armour Unit', Delta Marine Consultants, Gouda, The Netherlands.
- [21] REEVE, D.; CHADWICK, A.; FLEMING, C. (2004): 'Coastal Engineering: processes, theory and design practices', SPON Press, New York, USA.
- [22] SCHIERECK, G.J. (2001): 'Introduction to bed, bank and shoreline protection', VSSD, Delft, The Netherlands.
- [23] THERON, A. 2011: 'Extreme Inshore Sea Water Levels and Sea Level Rise', Council for Scientific and Industrial Research (CSIR), Stellenbosch, South Africa
- [24] TURK, G.F.; MELBY, J.A. (1997): 'Core-Loc Concrete Armour Units: Technical Guidelines', Coastal Engineering Research Center (CERC), US Army Corps of Engineers, Vicksburg, Mississippi, USA.
- [25] VAN DER MEER, J.W. (1988): 'Rock slopes and gravel beaches under wave attack', PhD-Thesis, Delft University of Technology, Delft, The Netherlands.
- [26] VAN DER MEER, J.W. (1999): 'Design of Concrete Armour Layers', Proceedings of the International Conference on Coastal Structures, Santander, Spain, 213-221.
- [27] VERHAGEN, H.J.; D'AGREMOND, K.; VAN ROODE, F.C. (2009): 'Breakwaters and closure dams', VSSD, Delft, The Netherlands.
- [28] YAGCI, O.; KAPDASLI, S. (2003): 'Alternative Placement Technique for Antifer Blocks used on Breakwaters', Istanbul Technical University, Istanbul, Turkey.
- [29] YOUNG, I.R.; ZIEGER, S.; BABANIN, A.V. (2011): 'Global Trends in Wind Speed and Wave Height', Science, American Association for the Advancement of Science, Washington, USA.
- [30] ZWAMBORN, J.A. (1976): 'Dolosse for Coastal Works', Council for Scientific and Industrial Research (CSIR), Stellenbosch, South Africa.

Manuals

- [31] CIRIA; CUR; CETMEF (2007): 'The Rock Manual. The use of rock in hydraulic engineering', CIRIA C683, London, UK.
- [32] COASTAL AND HYDRAULICS LABORATORY (2006): 'Coastal Engineering Manual', Coastal Engineering Research Center (CERC), US Army Corps of Engineers; Vicksburg; Mississippi, USA.
- [33] COASTAL AND HYDRAULICS LABORATORY (1984): 'Shore Protection Manual', Coastal Engineering Research Center (CERC), US Army Corps of Engineers; Vicksburg; Mississippi, USA.

Technical brochures

- [34] CLI (2011): 'Abstract of Accropode. Technical Specifications', Concrete Layer Innovations, France.

- [35] CLI (2010): 'Guidelines for design. Core-Loc Design Guide Table', Concrete Layer Innovations, France.
- [36] CLI (2012): 'Guidelines for design. Accropode II - Ecopode Design Guide Table', Concrete Layer Innovations, France.
- [37] DMC (2011): 'Xbloc. Effective Wave Protection for Breakwaters and Shores', Delta Marine Consultants, Gouda, The Netherlands.

Personal communication

- [38] PHELP, D. (2011)
- [39] ROSSOUW, M. (2012)
- [40] TULSI, K. (2012)

Appendix A. Extreme analysis

This appendix deals with the extreme analysis applied to estimate the design storm and the extreme wind speed. Both are required to define the design conditions for the repair alternatives of the breakwater roundhead located at Richards Bay port.

A.1. Design storm

The wave data provided since 1979 by Richards Bay buoy was analysed to estimate the storm design conditions. The extreme wave heights were determined using an extreme statistical analysis coupled to the Peak-over-Threshold method [VERHAGEN, H.J. ET AL., 2009], [GODA, Y., 2000] and [HOLTHUIJSEN, L.H., 2007].

The Peak-over-Threshold method allows the classification of waves into storms and regular waves. Various thresholds have been considered to separate the storms from regular waves, see Figure A.1 and Figure A.2.

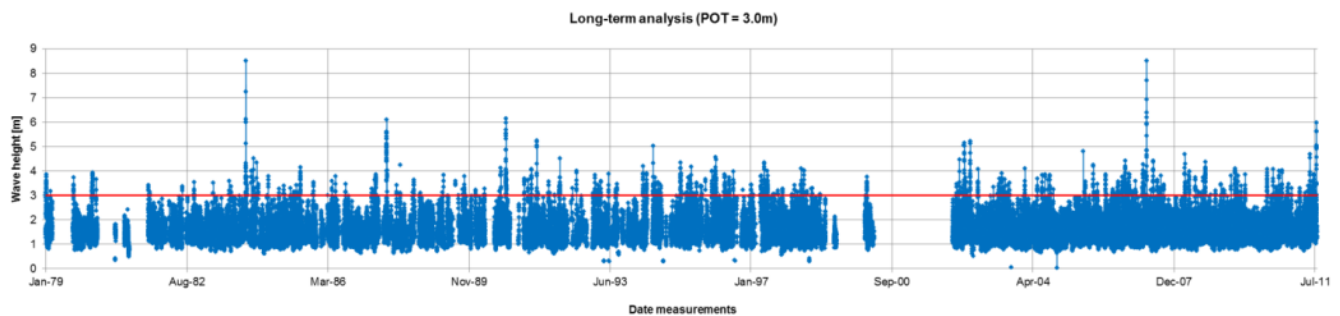


Figure A.1 – Long-term analysis combined with Peak-over-Threshold of 3.0m

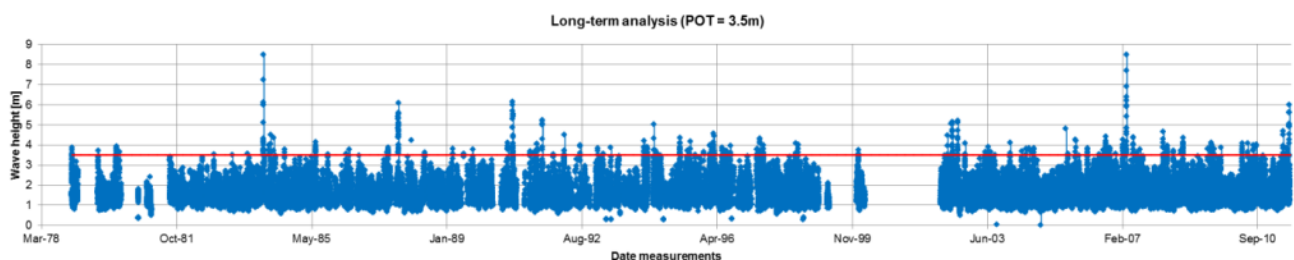


Figure A.2 – Long-term analysis combined with Peak-over-Threshold of 3.5m

Once the waves were classified, the peak value of each storm is taken as the representative storm value. The wave data generated in such way was used to estimate the design wave height by applying an extreme statistical analysis. Gumbel and inverse Weibull distributions were the considered extreme functions to predict the design wave heights for various return periods. Figure A.3 and Figure A.4 and Table A.1 and Table A.2 summarize the obtained results for design wave heights.

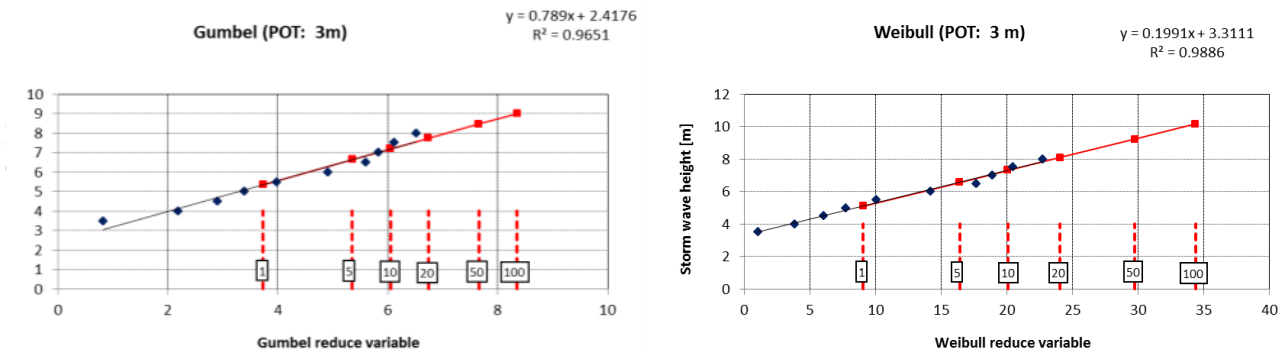


Figure A.3 – Peak-over-Threshold of 3.0m. Gumbel and inverse Weibull extreme analysis

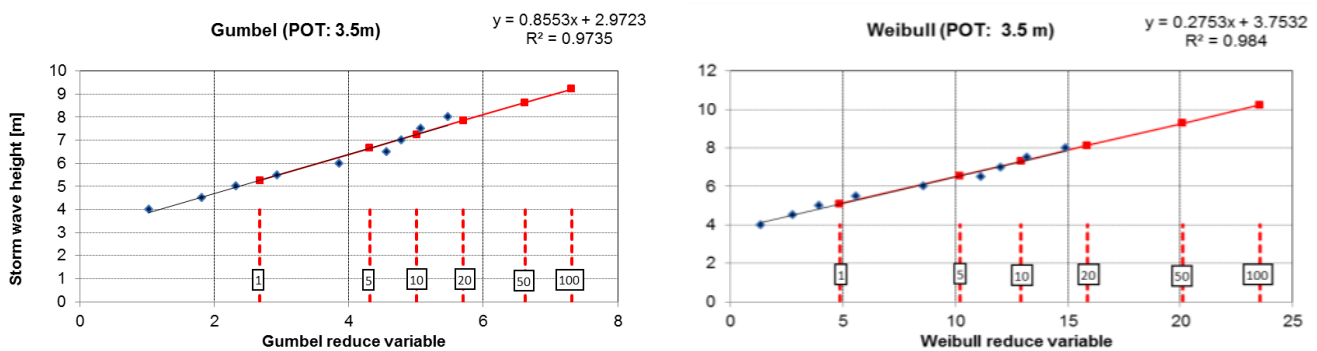


Figure A.4 – Peak-over-Threshold of 3.5m. Gumbel and inverse Weibull extreme analysis

Table A.1 – Gumbel projection

Threshold	Return period (T)						[yr]
	1	5	10	20	50	100	
3.0	5.36	6.64	7.19	7.74	8.46	9.01	[m]
3.5	5.26	6.66	7.26	7.85	8.64	9.23	[m]

Table A.2 – Inverse Weibull projection

Threshold	Return period (T)						[yr]
	1	5	10	20	50	100	
3.0	5.11	6.57	7.31	8.10	9.23	10.15	[m]
3.5	5.09	6.56	7.31	8.12	9.29	10.23	[m]
Average	5.1	6.6	7.3	8.1	9.2	10.2	[m]

From Figure A.3 and Figure A.4, the following conclusions can be drawn: (1) slight differences exist between the considered threshold and (2) inverse Weibull distribution gives more reliable results than Gumbel function, according to the obtained standard deviations values. Hence, the estimated wave heights with the inverse Weibull distribution were used in the design of the repair alternatives for the breakwater roundhead, see Table A.2.

The design wave periods were related to the extreme wave heights. Taking into account the data measured at Richards Bay buoy, an averaged wave period was calculated for each wave height bin. Thereafter, a regression line was fitted to these data allowing the estimation of the wave period that corresponds to each return period. Figure A.5 presents the design wave period estimation.

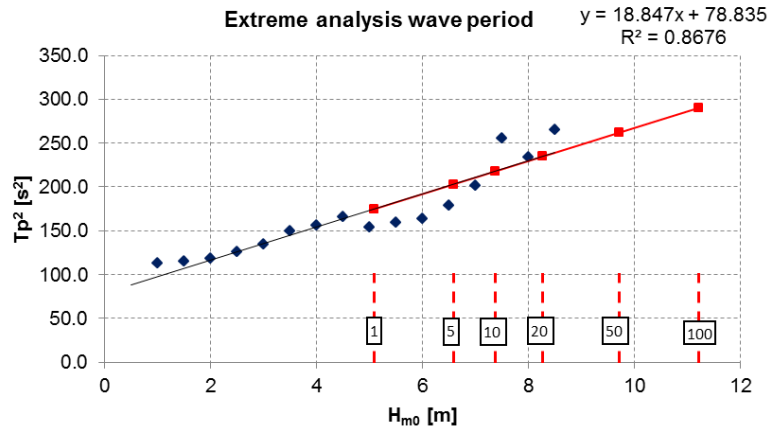


Figure A.5 – Design storm. Wave periods

A.2. Extreme wind

The wind data measured since 1994 in Richards Bay was used to estimate the required extreme winds, which were thereafter applied in the determination of the storm surge wind set-up component. These extreme winds were obtained using an extreme statistical analysis coupled to the Peak-over-Threshold method; identical to the one applied in the estimation of the design wave heights. As for the extreme wave heights, Gumbel and inverse Weibull distribution were applied to estimate the extreme winds. Gumbel distribution provided better fit to the measured data, and therefore was applied to compute the extreme wind speeds for each return period.

Table A.3 summarizes the obtained results for the extreme wind speeds.

Table A.3 – Extreme wind speeds

Threshold	Return period (T)						[yr]
	1	5	10	20	50	100	
10	27.36	30.62	32.03	33.44	35.29	36.7	[m/s]
12	27.28	31.84	30.47	33.21	35.03	36.4	[m/s]
14	27.28	30.44	31.80	33.16	34.96	36.32	[m/s]
16	27.27	30.39	31.74	33.08	34.85	36.2	[m/s]
18	27.27	30.35	31.68	33.00	34.75	36.07	[m/s]
20	27.37	30.59	31.97	33.35	35.17	36.55	[m/s]
22	27.45	30.81	32.24	33.67	35.54	36.97	[m/s]
Average	27.3	30.7	31.7	33.3	35.1	36.5	[m/s]

Appendix B. Material properties

A description of the rock material used in the construction of Richards Bay breakwater is presented in this appendix. The rock grading specifications presented in Table B.1 to Table B.2 should be obtained using the available material in the laboratory.

Table B.1 – Graded rock specifications for the toe protection

Graded rock (4 to 8 tonnes)		ELL	NLL	M50	NUL	EUL
Prototype	Weight [kg]	2500	4000	5800	8000	10000
Model	Weight [g]	5.3	8.4	12.2	16.8	21.0

Table B.2 – Graded rock specifications for the underlayer

Graded rock (1 to 5 tonnes)		ELL	NLL	M50	NUL	EUL
Prototype	Weight [kg]	700	1000	2300	5000	6500
Model	Weight [g]	1.5	2.1	4.8	10.5	13.7

Table B.3 – Graded rock specifications for the core

Graded rock (300 to 1000 kg)		ELL	NLL	M50	NUL	EUL
Prototype	Weight [kg]	200	300	600	1000	1500
Model	Weight [g]	1.4	2.1	4.2	6.9	10.4

The followed process to achieve such rock grading specifications involved the comparison between the theoretical grading and various material size combinations, which were available in the laboratory. The theoretical size distributions were estimated using the Rosin-Rammler curves, whose expressions are defined in the Rock Manual [CIRIA ET AL., 2007].

$$y=1-\exp\left\{\ln\left(\frac{1}{2}\right)\cdot\left(\frac{M_y}{M_{50}}\right)^{n_{RRM}}\right\} \quad [B.1]$$

$$n_{RRM}=\frac{\log\left(\frac{\ln(1-y_{NUL})}{\ln(1-y_{NLL})}\right)}{\log\left(\frac{NUL}{NLL}\right)} \quad [B.2]$$

$$M_y=M_{50}\cdot\left(\frac{\ln(1-y)}{\ln(0.5)}\right)^{1/n_{RRM}} \quad [B.3]$$

Here, y represents the fraction passing value in percentage, M_y corresponds to the mass passing the y value, M_{50} is the mass corresponding to 50% passing, n_{RRM} is the uniformity index, NUL stands for the Nominal Upper Limit mass (M_{85}) and NLL is the Nominal Lower Limit mass (M_{15}).

Figure B.1, Figure B.2 and Figure B.3 show the theoretical grading and the best rock grading approximation that was obtained using the available material sizes in prototype values. The required percentages of available rock sizes to obtain the best fit are presented in Table B.4, Table B.5 and Table B.6.

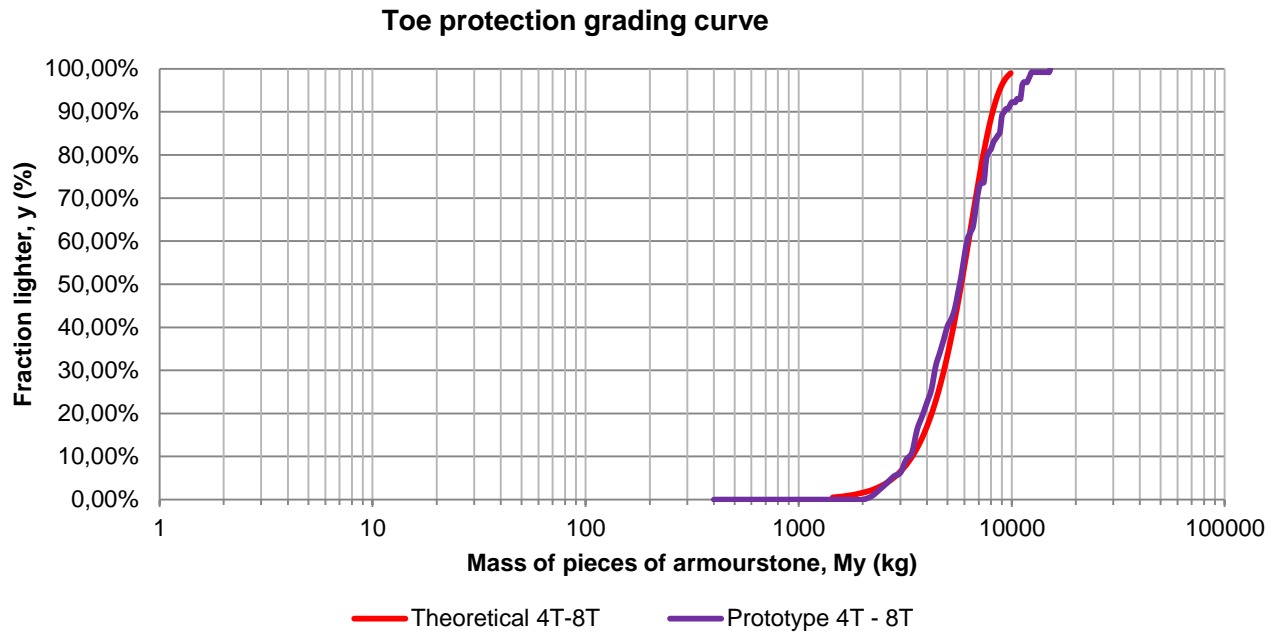


Figure B.1 – Toe protection grading curve

Table B.4 – Percentage of required rock size for the toe protection

Rock size (4 to 8 tonnes)	%
26mm	69.0
5-12mm	31.0

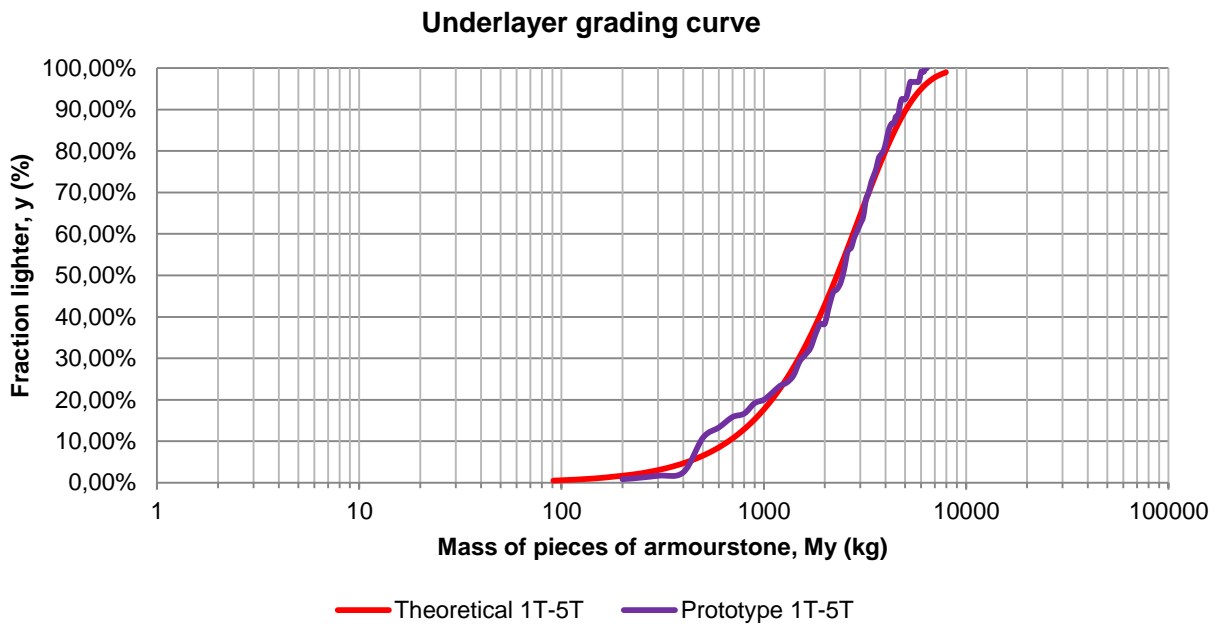


Figure B.2 – Underlayer grading curve

Table B.5 – Percentage of required rock size for the underlayer

Rock size (1 to 5 tonnes)	%
11-13mm	83.3
5-12mm	16.7

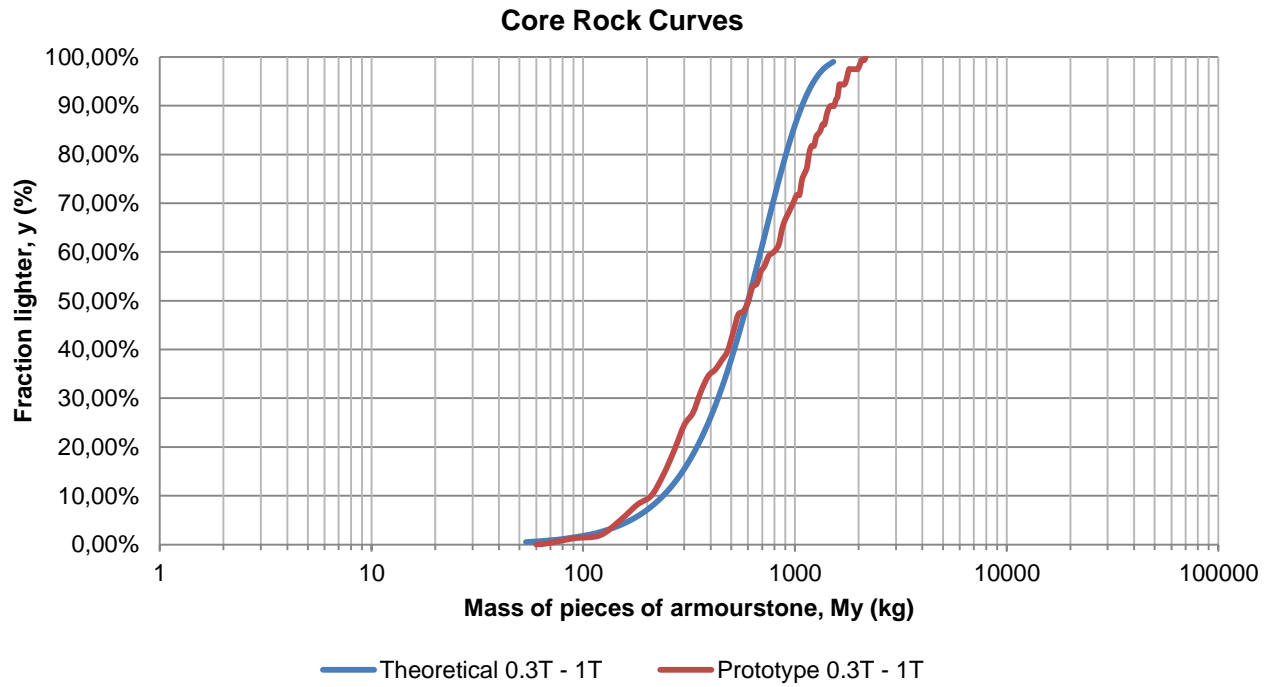


Figure B.3 – Core grading curve

Table B.6 – Percentage of required rock size for the core

Rock size (300 to 1000 kg)	%
11-13mm	83.3
5-12mm	16.7

Appendix C. Pictures of the experiments

Experiment 1: Covering alternative with 36-tonne dolosse

Before Test RB-B1



Lee side

After Test RB-B1



Lee side



Normal to roundhead axis



Normal to roundhead axis



Sea side



Sea side

Appendix C. Pictures of the experiments

Before Test RB-A1



Lee side

After Test RB-A1



Lee side



Normal to roundhead axis



Normal to roundhead axis



Sea side



Sea side

Before Test RB-B2

After Test RB-B2



Lee side



Lee side



Normal to roundhead axis



Normal to roundhead axis



Sea side



Sea side

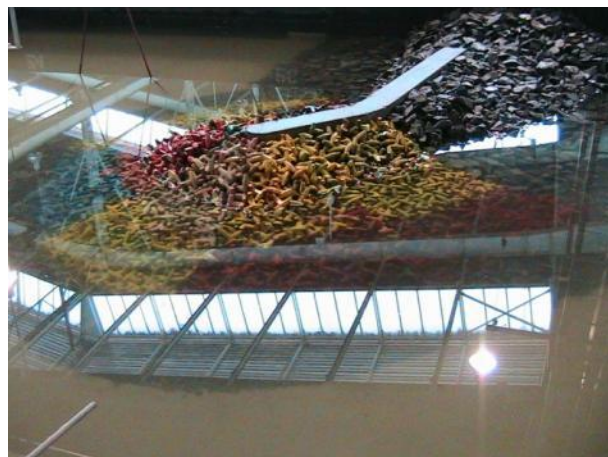
Appendix C. Pictures of the experiments

Before Test RB-A2

After Test RB-A2



Lee side



Lee side



Normal to roundhead axis



Normal to roundhead axis



Sea side



Sea side

Before Test RB-B3



Lee side

After Test RB-B3



Lee side



Normal to roundhead axis



Normal to roundhead axis



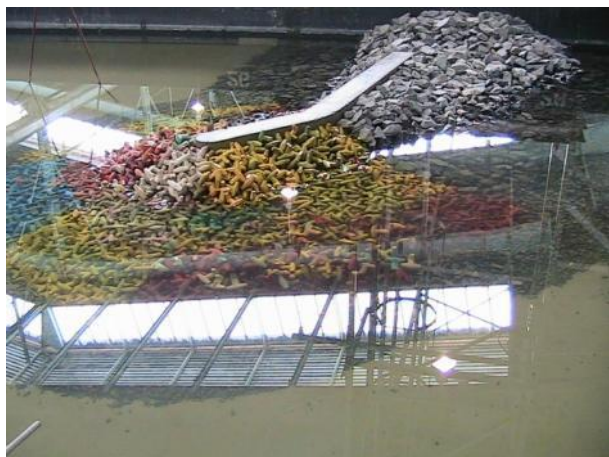
Sea side



Sea side

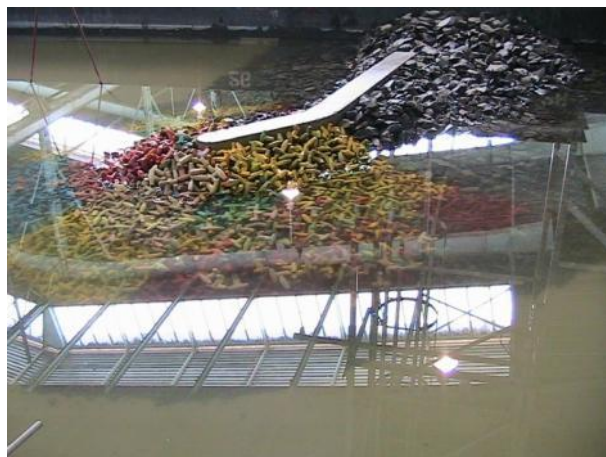
Appendix C. Pictures of the experiments

Before Test RB-A3



Lee side

After Test RB-A3



Lee side



Normal to roundhead axis



Normal to roundhead axis



Sea side



Sea side

Before Test RB-A4

After Test RB-A4



Lee side

Lee side



Normal to roundhead axis

Normal to roundhead axis



Sea side

Sea side

Appendix C. Pictures of the experiments

Before Test RB-B4



Lee side

After Test RB-B4



Lee side



Normal to roundhead axis



Normal to roundhead axis



Sea side



Sea side

Experiment 2: Covering alternative with 45-tonne Core-Loc

Before Test RB-B1

After Test RB-B1



Lee side



Lee side



Normal to roundhead axis



Normal to roundhead axis



Sea side



Sea side

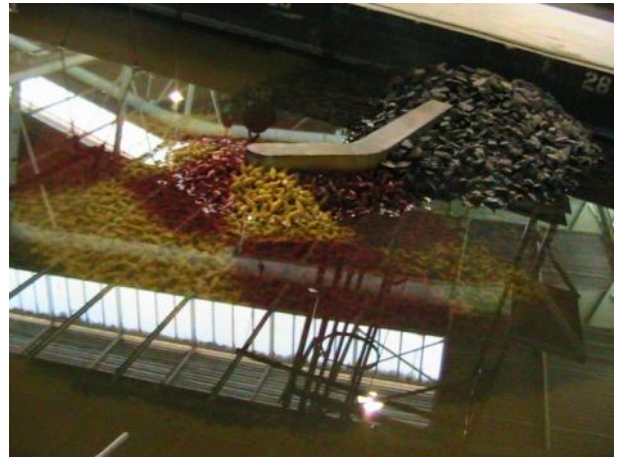
Appendix C. Pictures of the experiments

Before Test RB-A1

After Test RB-A1



Lee side



Lee side



Normal to roundhead axis



Normal to roundhead axis



Sea side



Sea side

Before Test RB-B2

After Test RB-B2



Lee side



Lee side



Normal to roundhead axis



Normal to roundhead axis



Sea side



Sea side

Before Test RB-A2

After Test RB-A2



Lee side

Lee side



Normal to roundhead axis

Normal to roundhead axis



Sea side

Sea side

Before Test RB-B3

After Test RB-B3



Lee side

Lee side



Normal to roundhead axis

Normal to roundhead axis

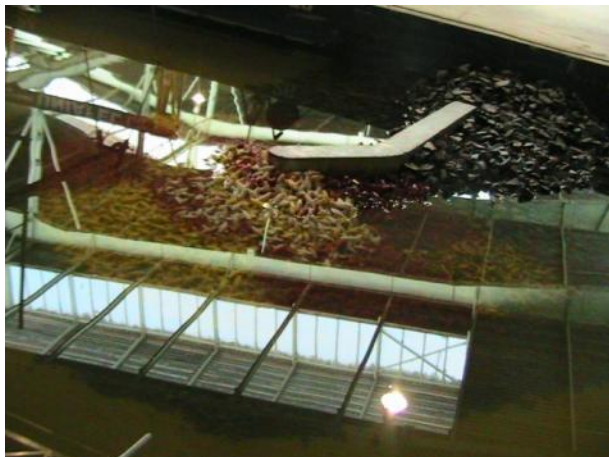


Sea side

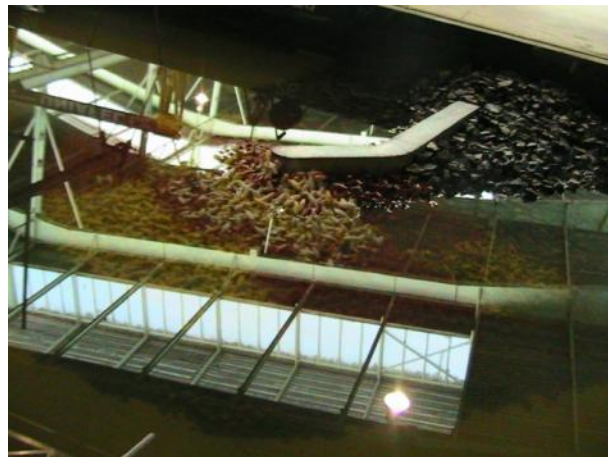
Sea side

Before Test RB-A3

After Test RB-A3



Lee side



Lee side



Normal to roundhead axis



Normal to roundhead axis



Sea side



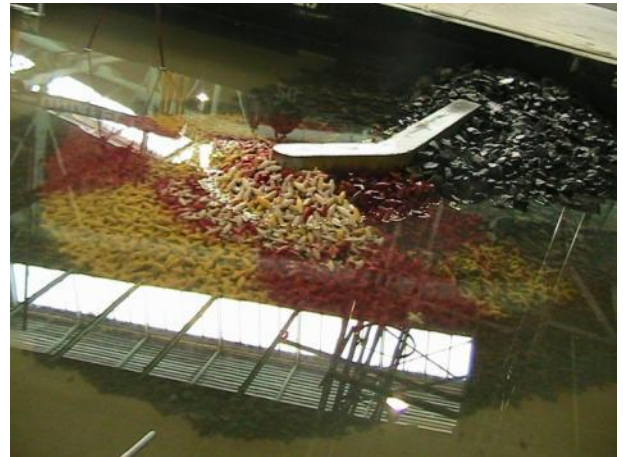
Sea side

Before Test RB-B4

After Test RB-B4



Lee side



Lee side



Normal to roundhead axis



Normal to roundhead axis



Sea side



Sea side

Appendix C. Pictures of the experiments

Before Test RB-A4

After Test RB-A4



Lee side



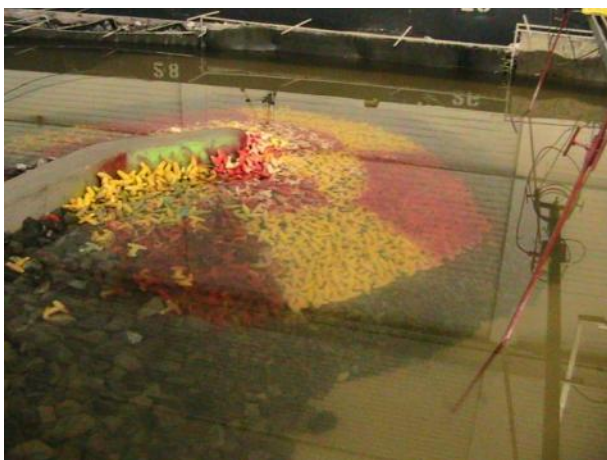
Lee side



Normal to roundhead axis



Normal to roundhead axis



Sea side



Sea side

Before Test RB-A5

After Test RB-A5



Lee side



Lee side



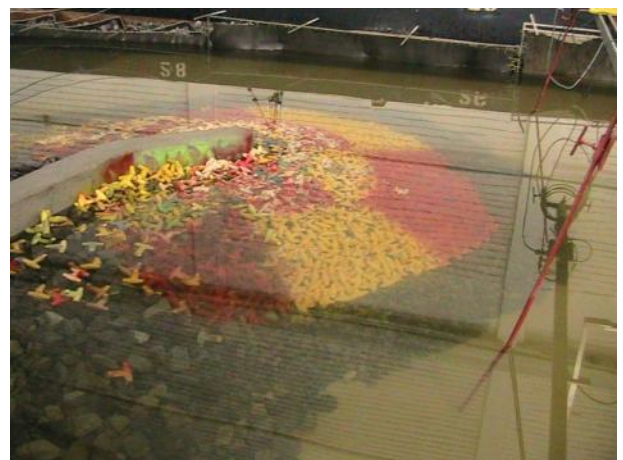
Normal to roundhead axis



Normal to roundhead axis



Sea side



Sea side

Experiment 3: Covering alternative with 44-tonne Antifer cubes

Before Test RB-B1

After Test RB-B1



Lee side

Lee side



Normal to roundhead axis

Normal to roundhead axis

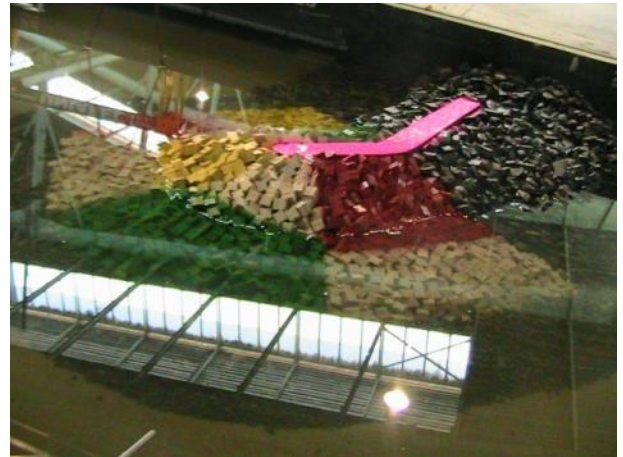


Sea side

Sea side

Before Test RB-A1

After Test RB-A1



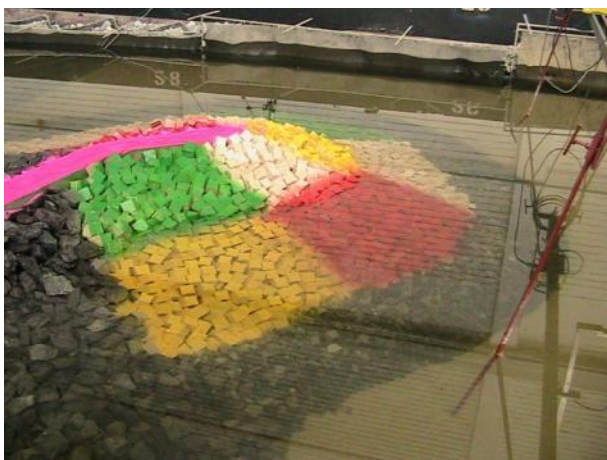
Lee side

Lee side



Normal to roundhead axis

Normal to roundhead axis



Sea side

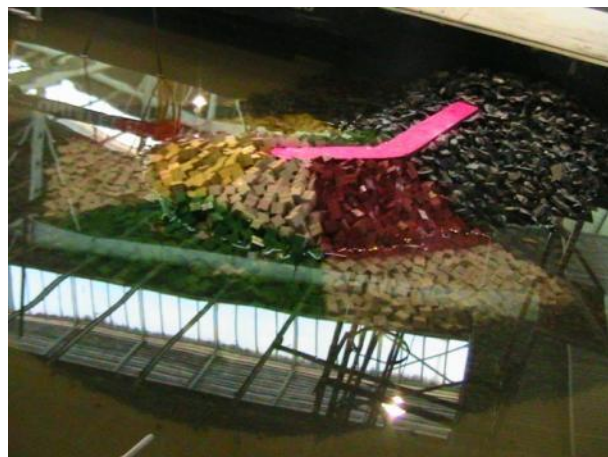
Sea side

Before Test RB-B2

After Test RB-B2



Lee side



Lee side



Normal to roundhead axis



Normal to roundhead axis



Sea side



Sea side

Before Test RB-A2

After Test RB-A2



Lee side



Lee side



Normal to roundhead axis



Normal to roundhead axis



Sea side



Sea side

Before Test RB-B3

After Test RB-B3



Lee side

Lee side



Normal to roundhead axis

Normal to roundhead axis

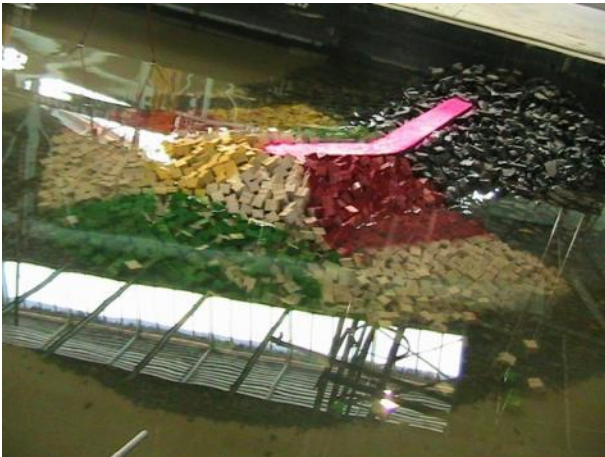


Sea side

Sea side

Before Test RB-A3

After Test RB-A3



Lee side



Lee side



Normal to roundhead axis



Normal to roundhead axis



Sea side



Sea side

Before Test RB-B4

After Test RB-B4



Lee side



Lee side



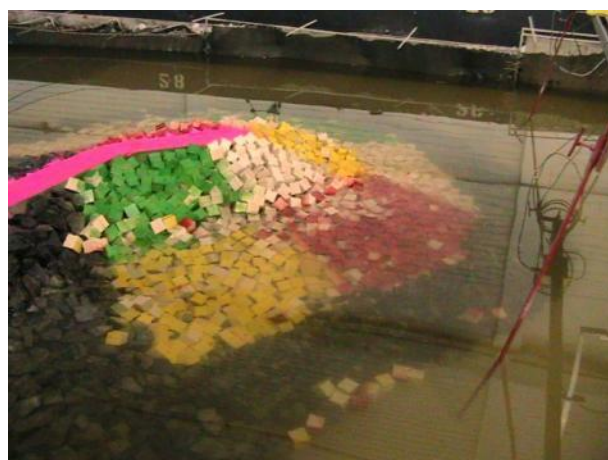
Normal to roundhead axis



Normal to roundhead axis



Sea side



Sea side

Before Test RB-A4

After Test RB-A4



Lee side



Lee side



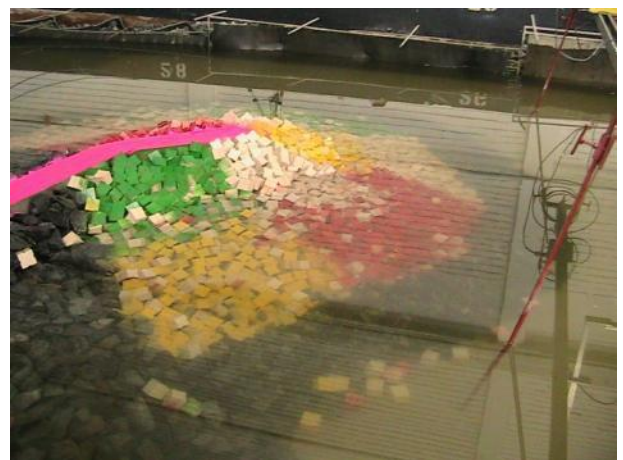
Normal to roundhead axis



Normal to roundhead axis



Sea side



Sea side

Appendix C. Pictures of the experiments

Before Test RB-A5

After Test RB-A5



Lee side



Lee side



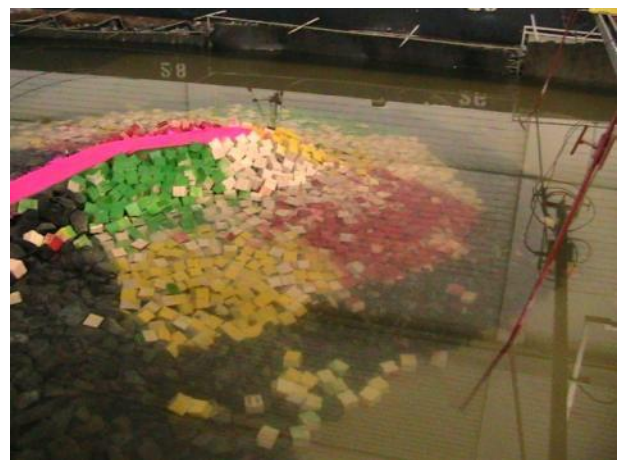
Normal to roundhead axis



Normal to roundhead axis



Sea side



Sea side